IDENTIFICATION AND CHARACTERIZATION OF DRUG TARGETS IN THE PYRIMIDINE AND PURINE PATHWAYS OF TRYPANOSOMA BRUCEI

APPROVED BY SUPERVISORY COMMITTEE

Margaret Phillips, Ph.D.

Richard Bruick, Ph.D.

Benjamin Tu, Ph.D.

Jennifer Kohler, Ph.D.

Michael Reese, Ph.D.

DEDICATION

To my parents Guillermo and Lonnie, and grandparents Luis and Juana, for a lifetime of encouragement and support. My wife Alli, for all the love and support throughout this endeavor.

IDENTIFICATION AND CHARACTERIZATION OF DRUG TARGETS IN THE PYRIMIDINE AND PURINE PATHWAYS OF TRYPANOSOMA BRUCEI

by

CHRISTOPHER LUIS LEIJA

DISSERTATION

Presented to the Faculty of the Graduate School of Biomedical Sciences

The University of Texas Southwestern Medical Center at Dallas

In Partial Fulfillment of the Requirements

For the Degree of

DOCTOR OF PHILOSOPHY

The University of Texas Southwestern Medical Center at Dallas

Dallas, Texas

December, 2016

IDENTIFICATION AND CHARACTERIZATION OF DRUG TARGETS IN THE PYRIMIDINE AND PURINE PATHWAYS OF TRYPANOSOMA BRUCEI

Christopher Luis Leija, Ph.D.

The University of Texas Southwestern Medical Center at Dallas, 2016

Supervising Professor: Margaret A. Phillips, Ph.D.

The single-celled extracellular parasite *Trypanosoma brucei* causes Human African Trypanosomiasis (HAT), which is fatal if untreated. Current therapies result in severe side effects and require complex treatment regimens. In an effort to spur the development of effective, safe, and simple to administer drugs, my work sought to identify and characterize novel drug targets in the parasite pyrimidine and purine pathways. The pyrimidine *de novo* biosynthetic pathway has been well characterized, however little work had been done to evaluate the importance of pyrimidine salvage enzymes. Specifically, my research validates the essentiality two seemingly redundant enzymes: thymidine kinase (TK) and cytidine

deaminase (CDA). Using a combination of genetic and analytical techniques, a novel pathway linking cytosine and thymine nucleotides was discovered. This pathway is composed of the salvage enzymes TK and CDA in addition to a newly discovered 5'-nucleotidase. I demonstrate that the function of this pathway is to convert *de novo* synthesized cytosine deoxynucleotides into the deoxycytidine, which is ultimately converted to thymine deoxynucleotides. The vital role for TK in bridging pyrimidine nucleotide pools may represent a shared vulnerability unique to kinetoplastids, providing an opportunity to target multiple human pathogens.

In contrast to the pyrimidine pathway, the parasite lacks the ability to generate purine nucleotides *de novo*. As a consequence, they are dependent on the salvage of purine nucleosides/bases from the host through a redundant and interconnected network of purine salvage and interconversion enzymes. In theory, any single precursor is capable of sustaining the formation of all purine nucleotides. We demonstrate that strategic inhibition of key metabolic routes circumvents the redundant nature of this pathway. The enzyme guanosine-5'-monophosphate synthase (GMPS) catalyzes the formation of GMP from xanthosine-5'-monophosphate. The generation of a *GMPS* null cell line restricts the parasite to the salvage of guanine to maintain GMP nucleotide pools, which is only viable in supraphysiological concentrations of guanine. Using a similar approach, we also genetically validated the essentiality of adenylosuccinate lyase (ADSL), which catalyzes the formation of AMP and fumarate from adenylosuccinate. In this case, depletion of this enzyme is lethal in all conditions. These two novel drug targets offer a solution to bypassing the redundancy in the purine pathway for the development of anti-trypanosomal therapies.

TABLE OF CONTENTS

PRIOR PUBLICATIONS

Leija C, Rijo-Ferreira F, Kinch LN, Grishin NV, Nischan N, et al. (2016) Pyrimidine Salvage Enzymes Are Essential for *De Novo* Biosynthesis of Deoxypyrimidine Nucleotides in *Trypanosoma brucei*. PLoS Pathog 12(11): e1006010. doi: 10.1371/journal.ppat.1006010

Li, Q.*****, **Leija, C.***, Rijo-Ferreira, F., Chen, J., Cestari, I., Stuart, K., Tu, B. P. and Phillips, M. A. (2015), GMP synthase is essential for viability and infectivity of *Trypanosoma brucei* despite a redundant purine salvage pathway. Molecular Microbiology, 97: 1006–1020. *Equal contribution

Nguyen, S., **Leija, C.**, Kinch, L., Regmi, S., Li, Q., Grishin, N.V., Phillips, M.A. (2015), Deoxyhypusine Modification of Eukaryotic Translation Initiation Factor 5A (eIF5A) Is Essential for *Trypanosoma brucei* Growth and for Expression of Polyprolyl-containing Proteins. Journal of Biological Chemistry, 290(32):199987-98

LIST OF FIGURES

LIST OF TABLES

LIST OF DEFINITIONS

ADSL – adenylosuccinate lyase
ADSS – adenylosuccinate synthase
AK – adenosine kinase
AMP – adenosine-5'-monophosphate
AMP - ampicillin
AMPD – AMP deaminase
APRT – adenine phosphoribosyltransferase
CDA – (deoxy)cytidine deaminase
cDNA – complimentary DNA
c-null – conditional null
dCMP – deoxycytidine-5'-monophosphate
DCTD – dCMP deaminase
dCtd – deoxycytidine
dFBS – dialyzed fetal bovine serum
DKO – double knockout
DNA – deoxyribonucleic acid
dThd – deoxythymidine (thymidine)
dTMP – deoxythymidine-5'-monophosphate
dUMP – deoxyuridine-5'-monophosphate
dUrd – deoxyuridine
E. coli – Escherichia coli
FBS – fetal bovine serum
*g*HAT – *T. brucei gambiense* Human African Trypanosomiasis
GMP – guanosine-5'-monophosphate
GMPR – GMP reductase
GMPS – GMP synthase
HAT – Human African Trypanosomiasis
HGPRT – hypoxanthine-guanine phosphoribosyltransferase
HPLC – high pressure liquid chromatography
Hs – Homo sapiens
Hsv – Herpes simplex virus
IMPDH – IMP dehydrogenase
KAN – kanamycin
LC – liquid chromatography
mRNA – messenger RNA
MS – mass spectrometry
NECT – nifurtimox-eflornithine combination therapy
OD – optical density

PCR – polymerase chain reaction
*r*HAT – *T. brucei rhodesiense*
RNA – ribonucleic acid
RNAi – RNA interference
RT – reverse transcriptase
S-AMP – adenylosuccinate
SDS-PAGE – sodium dodecyl sulfate polyacrylamide gel electrophoresis
SKO – single knockout
SUMO – small ubiquitin-like modifier
Tb – Trypanosoma brucei
TCA – tricarboxylic acid cycle
TERT – telomerase reverse transcriptase
Tet – tetracycline
TK – thymidine kinase
ULP1 – ubiquitin-like specific protease 1
UPRT – uracil phosphoribosyltransferase
UTR – untranslated region
VSG – variant surface glycoprotein
WHO – World Health Organization
WT – wild-type
XPRT – xanthine phosphoribosyltransferase

CHAPTER ONE
Introduction

Human African Trypanosomiasis

The protozoan parasite *Trypanosoma brucei* causes Human African Trypanosomiasis (HAT), also historically known as sleeping sickness. The parasite is transmitted by the Tsetse fly (*Glossina* genus), which is endemic to sub-Saharan Africa. Global efforts to eradicate this debilitating disease led to the creation of an aggressive surveillance program by World Health Organization (WHO)[1]. The WHO reports that the number of human infections have dropped below 10,000 for the first time in 50 years. In 2014, there were about 3,700 reported cases of HAT, representing a continued trajectory of declining infections towards eventual elimination. However, recent data has confirmed the existence of asymptomatic carriers, which will make complete elimination difficult [2]. In addition, *T. brucei* is capable of infecting livestock (Nagana) and wildlife which represent a significant animal reservoir. There always remains the risk resurgence if vigilance is not maintained, putting 70 million people at risk of infection[3].

There are two distinct subspecies that cause disease in humans: *T.b. gambiense* (gHAT) and *T.b. rhodesiense* (rHAT). gHAT is found in western and central regions of Africa, resulting in infection over a period of years to decades before death[4]. These comprise the vast majority of *T. brucei* infections, with the potential to affect 80% of those at risk of infection[3]. rHAT is observed in the Eastern regions of Africa, causing fatalities within weeks to months of infection[5]. *T. brucei* infections are classified into two clinical stages: early and late. It begins during a blood meal when the Tsetse fly transmits the metacyclic trypomastigotes into the skin and which eventually reach the lymphatic system

and bloodstream. At the early haemolymphatic stage, the parasite transforms into bloodstream trypomastigotes continuing to replicate in the bloodstream and lymph eventually resulting in high levels of parasitemia. The early stage of infection begin to manifest into clinical symptoms such as high fever, headaches, and joint pain. At this stage, an infected individual can transmit the parasite to an uninfected Tsetse fly when a blood meal is taken. Within the fly midgut, the parasites transform into procyclic trypomastigotes further maturing into epimastigotes. Epimastigotes migrate to the salivary gland and are primed for transmission during the next blood meal. As the infection continues to progress in the human host from early to late stage, the parasites cross the blood-brain barrier. At this stage infected individuals experience debilitating neurological symptoms including extreme confusion, sleep anomalies, meningoencephalitis, and ultimately most cases lead to death if left untreated.

Current Treatments

The parasite has evolved sophisticated techniques to thrive in an extracellular environment where it faces continuous assault by the host immune system. The basis of parasite immune evasion is mediated by a frequently changing surface coat[6]. The composition of these variant surface glycoproteins (VSGs) is regulated by at least 15 telomeric VSG expression sites where activation of any one site is changed periodically [7]. In addition to modulating VSG expression sites, it has a repertoire of several hundred VSG genes that can be activated by recombination [8]. These adaptations make the development of an effective vaccine targeting *T. brucei* highly improbable and very difficult. To treat early

stage gHAT, the CDC recommends several intravenous infusions or intramuscular injections of pentamadine. Late stage gHAT is treated with 56 intravenous infusions of eflornithine over 14 days. In the 2009, the introduction of nifurtimox-eflornithine combination therapy (NECT) reduced the number of eflornithine infusions to 14, in combination with oral nifurtimox 3 times per day for 10 days[9]. For early stage rHAT, suramin is administered as a single weekly intramuscular injection for 6 weeks, while Melarsoprol is administered by infusion over several days to treat the later stages. Melarsoprol is an organoarsenic based compound that results in potentially deadly encephalopathy in 5%-10% of patients[10]. All the drugs available to treat HAT require complex treatment regimens that are difficult to administer in rural regions of Africa where the majority of infections occur. The development of a single dose oral drug to treat both stages of infection would transform HAT treatment and contribute to its eradication.

Pyrimidine Pathway

Pyrimidine and purine biosynthesis or aquisition is essential to all life to generate precursors needed for the biosynthesis of DNA, RNA and sugar nucleotides [11, 12]. In Trypanosomatids, purines are obtained entirely by salvage routes through an array of interconnected and seemingly redundant pathways [13]. However, despite this redundancy, enzymes from the purine pathway including GMP synthase have been shown to be essential for pathogenicity *in vivo* [14]. In contrast, trypanosomatids are able to synthesize pyrimidines either through the *de novo* biosynthetic pathway or through salvage of preformed nucleosides and bases [12, 15, 16]. Genes have been identified for the complete *de novo* pyrimidine

biosynthetic pathway, for several key salvage enzymes and for a number of interconversion enzymes [17](Fig. 1.1). Genetic knockout studies have shown that loss of various *de novo* pyrimidine biosynthetic enzymes leads to pyrimidine auxotrophy that can be rescued by exogenous uracil [18-20]. These findings are consistent with reports that uracil transport is the primary route for pyrimidine salvage [15]. However knockout of UMP synthase lead to avirulence in mice suggesting that *in vivo* pyrimidine salvage may be insufficient to completely overcome loss of the *de novo* pathway [20]. These studies have shown that despite apparent redundancy, enzymes in both the pyrimidine and purine biosynthetic pathways can be essential, especially for *in vivo* virulence of *T. brucei*, which as an extracellular parasite lacks access to high intracellular concentrations of metabolites.

T. brucei lack several transporters and enzymes found in higher eukaryotes that may make them more vulnerable to disruption of the pyrimidine biosynthetic pathway. The primary pyrimidine transporter in *T. brucei* preferentially takes up uracil, whereas transport of uridine, 2'deoxyuridine, thymidine and cytidine is either non-existent or inefficient requiring high nucleoside concentrations [15]. Trypanosomatids lack dCMP deaminase (DCTD), an important contributor to dTTP biosynthesis through deamination of dCMP to dUMP in many higher eukaryotes [21, 22]. Instead trypanosomatids were thought to rely on dUTPase to convert uracil nucleotides synthesized by the *de novo* pathway into the thymine nucleotide pools [23].

T. brucei encodes three pyrimidine salvage enzymes: uracil phosphoribosyltransferase (UPRT), thymidine kinase (TK), and uridine phosphorylase (UPP), and additionally a cytidine deaminase (CDA) that can convert deoxycytidine to deoxyuridine (Fig. 1.1). *T. brucei* UPP was shown to prefer uridine and deoxyuridine as substrates, and the enzyme was reported not to be

essential based on RNAi knockdown studies [24]. In contrast to mammalian cells, which encode both cytosolic TK1 and mitochondrial TK2 [25-27], trypanosomatids possess only TK1. *Tb*TK is however a unique fusion of two TK domains that function as a pseudodimer. The N-terminal domain is catalytically inactive, while the C-terminal domain exhibits canonical TK activity [28]. Recent RNAi studies have suggested that TK is essential but a mechanistic understanding for why TK would be required has not emerged [29, 30].

Purine Pathway

Trypanosomatids, including *T. brucei*, are unable to synthesize the purine ring *de novo* [12, 13, 31, 32], while human cells are capable of both *de novo* purine synthesis and purine salvage [33] As a consequence, the parasite is auxotrophic for purines and expresses a myriad of purine transporters and salvage enzymes, including 3 phosphoribosyltransferases with overlapping specificities, an adenosine kinase and 6 enzymes that mediate nucleotide interconversion (Fig. 1.2). *T. brucei* encodes 12 equilibrative nucleoside transporters that facilitate uptake of purine nucleosides and nucleobases including hypoxanthine, guanine, inosine, and adenine [16, 34-36]. Many of the transporters have overlapping activities and stage-specific expression profiles. Salvage pathways are interconvertible and any single purine was shown to be sufficient to support growth *in vitro* [12]. These data suggested most enzymes in the purine salvage pathway were redundant.

In *Leishmania donovani*, a related parasitic protozoan, genetic knockout studies showed that none of the individual enzymes that convert bases or nucleosides to nucleotides are essential [32]. However, there is a preference for salvage of purines via hypoxanthine-

guanine phosphoribosyl transferase (HGPRT) and xanthine phosphoribosyl transferase (XPRT) as concurrent knockout of both in promastigote parasites was lethal *in vitro* [37, 38]. Salvage of adenine or adenosine was not sufficient to maintain purine nucleoside pools. These results were ascribed to the presence of adenine aminohydrolase activity, which depleted available adenine by converting it to hypoxanthine. These data also suggested the possibility that some of the interconversion enzymes in the purine salvage pathway could be essential for parasite growth. In support, knockout of adenylosuccinate lyase (ADSL) and adenylosuccinate synthetase (ADSS) in *Leishmania* could only be achieved in the presence of an adenine aminohydrolase inhibitor, and the ADSL knockout cells were severely reduced in their ability to infect mice [39].

Unlike *Leishmania* species, *T. brucei* is an extracellular parasite that does not have access to intracellular purine pools. The dominant nucleoside or base precursors in human serum and cerebrospinal fluid (CSF) are hypoxanthine, xanthine and inosine (serum and CSF concentrations are reported to range from 1 - 15 μM) while other purine bases and nucleosides are much less abundant or undetectable [12](Table 3.1). These data suggest the possibility that despite the apparent redundancy in the salvage pathway, purine salvage in *T. brucei* will funnel through XMP and IMP and that some of the interconversion enzymes required to generate GMP and AMP may be essential *in vivo*. Recently it has been shown that RNAi-mediated gene knockdown of ADSS and ADSL in *T. brucei* blood-stage parasites led to reduced growth *in vitro* and attenuated virulence in mice [40]. Several enzymes in the purine salvage pathway, including guanine monophosphate synthase (GMPS), are highly "druggable targets" (Fig. 3.1A), as defined by the availability of drug-like inhibitors of

homologs from other species [41], making them attractive targets for therapeutic intervention if determined to be essential.

GMPS is an aminotransferase that catalyzes amination of XMP to form GMP, which serves as the precursor for all guanylate nucleotides (Fig. 3.1B). GMPS links salvaged xanthine, hypoxanthine, adenine, and adenosine via XMP/IMP to GMP formation. GMP and AMP pools are connected via IMP in two steps via inosine monophosphate dehydrogenase (IMPDH) and GMPS, and in the opposite direction by GMP reductase (GMPR), which catalyzes the conversion of GMP to IMP. In the absence of GMPS, the parasite would be entirely dependent on salvage of guanine/guanosine to maintain GMP pools. It is likely that in these circumstances, physiological concentrations of guanine/guanosine may not support GMP pools.

The formation of AMP supported by two metabolic routes, formation via adenylosuccinate synthase (AdSS) and adenylsuccinate lyase (AdSL) or by direct salvage of adenine or adenosine. The conversion of IMP to adenylosuccinate by ADSS and subsequent formation of AMP by ADSS serves as a metabolic bridge to the salvage of xanthine, hypoxanthine, and guanine into AMP pools. Inhibition of either ADSS or ADSL effectively restricts the parasite to the salvage of adenine/adenosine to maintain AMP pools. Based on published RNAi data, physiological concentrations of adenine/adenosine are not sufficient to support adenine nucleotide synthesis when either ADSS or ASL activity is not present [38].

Research Goals

The sequencing of the *T. brucei* genome has provided the framework for our understanding of the pyrimidine pathway [42]. However, our current understanding of the *T. brucei* pyrimidine pathway is incomplete. A significant portion of research efforts have been directed towards elucidating the roles of the pyrimidine *de novo* pathway and some of the interconversion routes. The apparent redundancy of the pyrimidine salvage pathway is undoubtedly the reason for its neglect. A major research goal was to provide a more complete understanding of pyrimidine salvage and potentially identify novel drug targets. Specifically, I set out to determine if any of the salvage enzymes are essential to the parasite despite the presence of a *de novo* route. We anticipated that the outcome of this research may likely extent towards other trypanosomatids like *Leishmania* and *Trypanosoma cruzi*, as they share very similar features of nucleotide metabolism.

The highly redundant arrangement of the purine pathway has made work to identify drug targets a daunting task. My goal was to evaluate the possibility strategically depleting a subset of key metabolic enzymes to show that it is possible to bypass this redundancy and that a single enzyme could be essential. The identification of these targets could help spur the development of future drugs that inhibit the purine pathway. Using genetic techniques, I hoped to characterize a number of potential drug targets in Trypanosomes and provide insight into metabolic flux within the purine pathway.

Figure 1.1. *T. brucei* pyrimidine pathway. Green lines salvage routes, blue lines *de novo* pathway, black lines interconversion routes, and the red dotted line indicates a reaction that is not present in trypanosomatids. The numbers above each arrow represent the enzyme catalyzing the reaction (EC number): **1-6**: carbamoyl phosphate synthase (6.3.5.5), aspartate carbamoyl transferase (2.1.3.2), dihydroorotase (3.5.2.3), dihydroorotate dehydrogenase (1.3.3.1), orotate phosphoribosyltransferase (2.4.2.10), orotidine 5-phosphate decarboxylase (4.1.1.23); **7** UMP-CMP kinase (2.7.4.14); **8**: nucleoside diphosphatase (3.6.1.6); **9**: nucleoside diphosphate kinase (2.7.4.6); **10**: cytidine triphosphate synthase (6.3.4.2); **11**: ribonucleoside diphosphate reductase (1.17.4.1); **12**: thymidylate kinase (2.7.4.9); **13**: deoxyuridine triphosphate nucleotidohydrolase (dUTPase) (3.6.1.23); **14**:thymidylate synthase (2.1.1.45); **15**:cytidine deaminase (CDA) (3.5.4.5); **16**: thymidine kinase (TK)(2.7.1.21); **17**: uridine phosphorylase (2.4.2.3); **18**:uracil phosphoribosyltransferase (2.4.2.9); 19: HD-domain 5'-nucleotidase (3.1.3.89); **20**: UDP-glucose pyrophosphorylase (2.7.7.9); **21**: UTP N-acetyl-α-D-glucosamine-1-phosphate uridylyltransferase (2.7.7.23); **22**: UDP-glucose epimerase (5.1.3.2). The pathway was constructed based on the annotation described in [15], but modified to incorporate results from our TK and CDA genetic and metabolomics analysis. Additionally the scheme was modified to list enzyme **7** as able to function on both UMP and CMP based on the published report that one of seven encoded adenylate kinases (ADKG) was biochemically characterized and shown to be a UMP-CMP kinase [43].

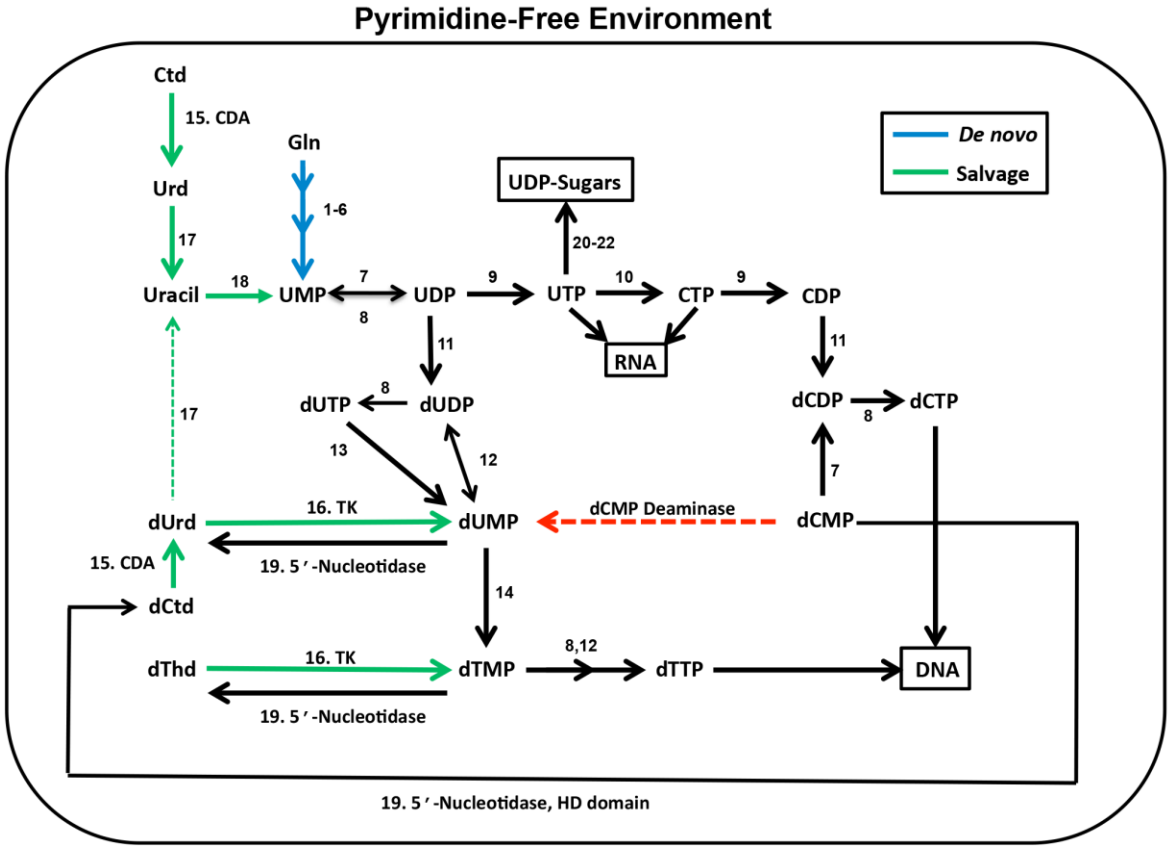

Figure 1.2. *T. brucei* purine pathway. Green lines represent salvage routes and black are interconversion routes. The abbreviations are as follows: GMPS (guanosine 5'-monophosphate synthase), GMPR (Guanosine 5'-monophosphate reductase), IMPDH (inosine 5'-monophosphate dehydrogenase), HGPRT (hypoxanthine-guanine phosphoribosyltransferase), XPRT (xanthine phosphoribosyltransferase), AdSS (adenylosuccinate synthase), AdSL (adenylosuccinate lyase). APRT (adenine

phosphoribosyltransferase).

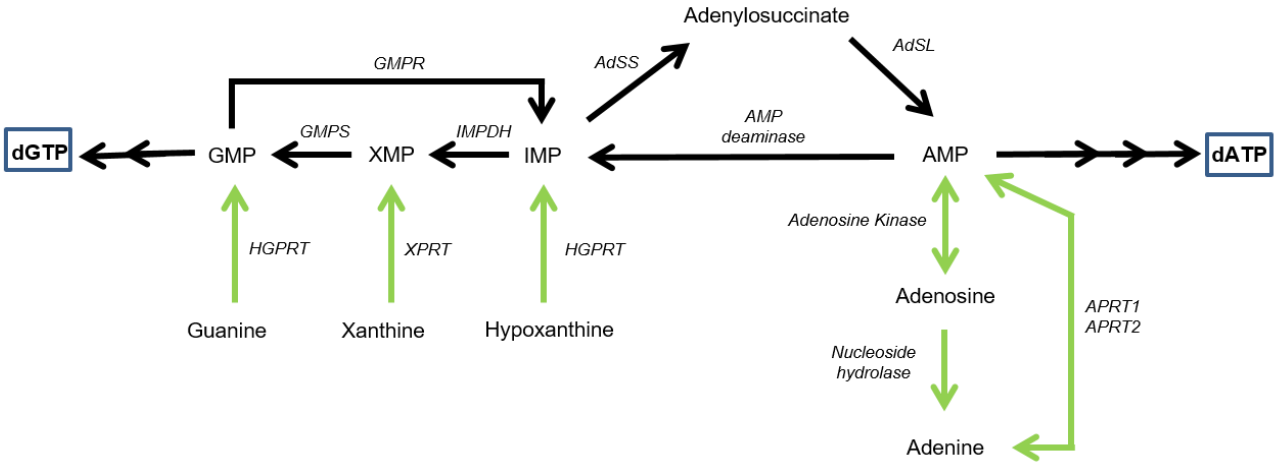

CHAPTER TWO

PYRIMIDINE SALVAGE ENZYMES ARE ESSENTIAL FOR THE DE NOVO BIOSYNTHESIS OF DEOXYNUCLEOTIDES IN *TRYPANOSOMA BRUCEI*

Introduction

The human pathogenic parasite *Trypanosoma brucei* possess both *de novo* and salvage routes for the biosynthesis of pyrimidine nucleotides. Consequently, they do not require salvageable pyrimidines for growth. Thymidine kinase (TK) catalyzes the formation of dTMP and dUMP and is one of several salvage enzymes that appear redundant to the *de novo* pathway. Surprisingly, we show through analysis of *TK* conditional null and RNAi cells that TK is essential for growth and for infectivity in a mouse model, and that a catalytically active enzyme is required for its function. Unlike humans, *T. brucei* and all other kinetoplastids lack dCMP deaminase (DCTD), which provides an alternative route to dUMP formation. Ectopic expression of human DCTD resulted in full rescue of the RNAi growth phenotype and allowed for selection of viable *TK* null cells. Metabolite profiling by LC-MS/MS revealed a build-up of deoxypyrimidine nucleosides in TK depleted cells. Knockout of cytidine deaminase (CDA), which converts deoxycytidine to deoxyuridine led to thymidine/deoxyuridine auxotrophy. These unexpected results suggested that *T. brucei* encodes an unidentified 5'-nucleotidase that converts deoxypyrimidine nucleotides to their corresponding nucleosides, leading to their dead-end build up in TK depleted cells at the expense of dTTP pools. Bioinformatics analysis identified several potential candidate genes that could encode 5'-nucleotidase activity including an HD-domain protein that we show catalyzes dephosphorylation of deoxyribonucleotide 5'-monophosphates. We conclude that TK is essential for synthesis of thymine nucleotides regardless of whether the nucleoside precursors originate from the *de novo* pathway or through salvage. Reliance on TK in the absence of DCTD may be a shared vulnerability among trypanosomatids and may provide a

unique opportunity to selectively target a diverse group of pathogenic single-celled eukaryotes with a single drug.

MATERIALS AND METHODS

Gene accession numbers

T. brucei gene sequences were obtained from TriTrypDB and the gene accession numbers are as follows: TK (Tb927.10.880), CDA (Tb927.9.3000), HD-domain 5'-nucleotidase (Tb927.9.10830), TERT (Tb927.11.10190). The *Hs*TK1 (P04183) and *Hs*DCTD (P32321) amino acid sequences were obtained from UniProt, and *Hsv*TK was derived from Addgene plasmid #48356.

T. brucei *in vitro growth*

Experiments were performed using *T. brucei* BSF SM cells genetically manipulated to express T7 RNA polymerase and the Tet repressor (TetR) [44]. Cells were grown in HMI-19 medium supplemented with 10% fetal bovine serum (FBS) at 37^{o}C in 5% CO_2. HMI-19 is a modified medium that we previously reported [14]. It was designed to contain more physiologically relevant purine and pyrimidine levels and it is supplemented with only 10 μM hypoxanthine and no added thymidine, except that present in FBS. To obtain completely pyrimidine-free conditions, normal FBS was replaced with dialyzed FBS in media where indicated. All cells were maintained in exponential growth (10^5-10^6 cells/mL). SM cells were maintained in G418 (2.5 μg/mL) to retain the T7 polymerase and TetR. *TK* and *CDA* RNAi and knockout lines were cultured in the appropriate antibiotic depending on the transfected plasmid

at the following concentrations unless otherwise stated: 2.5 μg/mL G418 (Life Technologies), 2.5 μg/mL blasticidin (InvivoGen), 2.5 μg/mL phleomycin (InvivoGen), 1-2 μg/mL hygromycin (Sigma), 0.1 μg/mL puromycin (Sigma), and 1 μg/mL Tet (RPI). For all nucleoside supplementation experiments 100 mM stocks of sterile filtered deoxyuridine (Sigma), thymidine (Sigma), uridine (Sigma), and uracil (Sigma) were added to cultures at concentrations indicated. All c-null lines were supplemented with 1 μg/mL Tet daily to maintain steady expression of Tet-regulated proteins. For pyrimidine and Tet free conditions, cells were washed (3 x 20 mL) with the appropriate media prior to beginning the growth experiments. For evaluation of growth rates, cells were washed and replated in media containing no antibiotics at a density of 20,000 cells/mL and diluted over the course of the study to maintain exponential growth. Cell density was determined using a hemocytometer (Bright-Line) with a lower limit of detection of 10^4cells/ml. Two technical replicates were averaged for each counted sample. Total cell numbers were calculated by multiplying cell density by the dilution factor and volume [45].

***Transfection of* T. brucei**

For each transfection, parasites (10^7) were suspended in Human T Cell Nucleofector Buffer (Lonzo)(100 μL) containing NotI linearized vector (5 μg) or purified PCR product (1 μg) as described [46]. All transfected DNA was confirmed by sequencing prior to transfection. Negative controls cells transfected with buffer only were prepared alongside samples to optimize selection conditions. Cells were transfected using protocol X-001 on the Amaxa Nucleofector (Lonza) and then transferred to media (25 ml) and allowed to recover 8 h prior to addition of selection antibiotics. Two dilutions (1:20 and 1:40) of culture, containing selection antibiotics,

were plated in 24-well plates at 2 ml/well. Negative control plates were monitored throughout the experiment to ensure selection was achieved. After several days, wells containing a cell density of about 10^6 cells/ml were selected for generation of clonal lines by limiting dilutions.

Generation of *T. brucei TK* conditional null cell lines

The *T. brucei* TK and human (*Hs*) DCTD expressing *TK* c-null cell lines were generated utilizing the fusion PCR method [46, 47]. Cloning primers are shown in Table 2.1. The first *TK* allele was replaced by the *HYG* resistance gene by PCR fusion of *TK* 5' and 3' UTRs to *HYG*. The *HYG* resistance gene was derived from the pLew90 vector [44] (a gift from George A.M. Cross). UTRs were amplified from genomic DNA isolated from SM cells. To generate the *TK* single allele knockout (SKO) line the purified PCR product was transfected into SM cells and hygromycin resistant cells were selected in medium containing G418 and hygromycin. The *TK* SKO line was then used to generate the remaining cell lines. A Tet-regulated vector containing either FLAG-tagged *Tb*TK or FLAG-tagged *Hs*DCTD was cloned as follows. The *T. brucei TK* or the human *DCTD* genes were PCR amplified from *T. brucei* SM genomic DNA or from human cDNA synthesized from RNA extracted from a human breast adenocarcinoma cell line (MDA-MB-231), respectively. For both constructs, the forward direction PCR primer contained a flanking 5' HindIII restriction site and an N-terminal FLAG tag; the reverse direction primer contained a flanking 3' BamHI restriction site. The restriction digested PCR products were ligated into the pLew100v5-phleo vector (a gift from George A.M. Cross). The pLew100v5-phleo vector was linearized by the NotI restriction enzyme to facilitate integration into the rRNA spacer region. Linearized vector (5 μg) was transfected into the *TK* SKO cell line and selected

for resistance to phleomycin. The resulting clones were screened to identify those with the tightest level of Tet regulation of the ectopically expressed protein. Finally, the remaining *TK* allele was replaced by a *PAC* resistance gene synthesized by GenScript. The *PAC TK* UTR fusion product was generated as described above and transfected into *TK* SKO cells expressing either *T. brucei* TK or *Hs*DCTD grown in Tet containing medium for 2 days prior to transfection. *TK* c-null cells were selected and maintained in G418, phleomycin, hygromycin, puromycin, and Tet (added daily). PCR primers flanking the 5' and 3'UTRs were used to confirm that the *TK* gene had been replaced by the selectable markers.

Generation of the TK RNAi T. brucei BSF cell line.

RNAit (http://trypanofan.bioc.cam.ac.uk/software/RNAit.html) was used to identify a suitable 566 bp region located in the *TK* 3'UTR. The 3'UTR was targeted to allow compatibility with *Tb*TK rescue plasmids (described below), that utilize instead the *ALD* 3'UTR. Genomic DNA isolated from SM cells was used as template for PCR amplification of the target region and TA cloned into the Gateway vector pCR8/GW/TOPO (Life Technologies). The Tet inducible stem loop was created by addition of Gateway LR Clonase to a reaction containing both the Gateway vector (100 ng) and pTrypRNAiGate vector (100 ng) [48]. *TK* SKO (*hyg*) cells were transfected with the vector and integration into the rRNA spacer region was selected using phleomycin. For studies of the effects of *TK* knockdown, Tet was added daily to induce formation of the hairpin leading to knockdown of *TK* mRNA. Cells were grown in the absence of other antibiotics for these studies.

Cloning of RNAi rescue constructs and TK mutants

The *Tb*TK rescue construct under control of the Tet promoter was generated using the same approach described above for the c-null cell line except that an N-terminal AU1-tag was included instead of a FLAG-tag to allow detection of the expressed protein. The gene encoding the *Hs*TK open reading frame was synthesized by GenScript and cloned into the pUC57 vector, which was used for subsequent PCR amplification to generate the FLAG-tagged *Hs*TK rescue construct. *Hsv*TK was amplified from the pHJ17 Hyg-TK-loxP vector (Addgene). To generate the *Tb*TK E286A and *Hs*TK K32I mutants, both wild-type genes were subcloned into the pCR2.1-TOPO TA vector (Invitrogen). Complimentary PCR primers containing the desired point mutation were synthesized. Phusion polymerase (NEB) was used to amplify the entire vector according the to the following parameters: initial denaturation at 95ºC for 30 s followed by 18 cycles of denaturation at 95ºC for 30 s, annealing at 68ºC for 1 min, and amplification at 72ºC for 5 min. Each reaction (50 µL) was treated with DpnI (NEB)(1 µL) overnight at 37 ºC followed by transformation into T10 cells and selection with ampicillin (100 µg/ml). Clones were sequenced using M13 primers. All constructs contained flanking 5' HindIII and 3' BamHI restriction sites that permitted ligation into the pLew100v5-bsd vector[46]. The vectors were linearized with NotI and transfected into *TK* RNAi cells as described above.

Generation of the* T. brucei cda *null cell line

SM cells were transfected with the *HYG* resistance gene flanked by the *CDA* 5' and 3' UTRs, generated by fusion PCR as described above, to generate the SKO in medium containing

G418 and hygromycin. For the remaining allele, a fusion PCR product containing the *PAC* resistance gene was transfected into the SKO cells. Null cells were selected in growth medium containing G418, hygromycin, puromycin, and Thd (500 μM). PCR primers flanking the *CDA* 5' and 3' UTRs were used to confirm replacement of the *CDA* alleles.

Liquid chromatography-tandem mass spectrometry (LC-MS/MS) metabolomics analysis

T. brucei TK expressing *TK* c-null cells were grown with or without Tet for 24 h and CDA null cells were grown with or without thymidine (0.5 mM) for 12 h. Cells (10^8) were harvested by centrifugation (3500 RPM, 5 min) and then washed in cold PBS (50 mL). Washed pellet was resuspended in 1 mL pre-chilled (-80ºC) 80% methanol and incubated on ice for 10 min. The cell extract was centrifuged (16,000 x g, 4^{o}C, 20 min) to remove insoluble debris and 0.9 mL of supernatant was dried using a vacuum centrifuge. Samples were stored at -80ºC prior to analysis. For pyrimidine-free studies, a starter culture was washed, as described above, and grown in pyrimidine-free medium for 48 h prior to the start of the experiment. Targeted metabolite profiling by LC-MS/MS was performed as previously described allowing for detection of ~ 130 standard metabolites [49]. While this method allowed for quantitation of many key nucleosides and bases, the deoxynucleotides were not profiled as they are not part of the trained set of the facility. In order to attempt to identify these metabolites we isolated a larger cell number (5×10^8cells) and again used targeted LC-MS/MS for detection as described [50]. Levels of deoxynucleotides in wild-type control SM cells were barely detectable so null lines were not analyzed.

Thymidine triphosphate (TTP) quantitation by enzymatic assay

Because we were unable to quantitate dTTP by LC-MS/MS approaches we employed a previously reported enzymatic assay that monitors Klenow DNA polymerase catalyzed incorporation of H^3-dATP into synthetic oligonucleotides in a reaction that is proportional to the amount of dNTP [51, 52]. Through use of a standard curve the targeted dNTP concentration in the sample can then be determined. The oligo template that was used for the assay was as reported [51]. To prepare cell extracts, *TK* c-null cells were grown with or without Tet for 24 or 48 h in standard HMI-19 media supplemented with normal FBS and were harvested by centrifugation (3500 RPM, 5 min) and washed once with PBS. The pellets were resuspended in 60% methanol (250 μL) and incubated at -20°C overnight. Cell extracts were placed in a boiling water bath for 5 min, centrifuged (16,000xg, 20 min, 4°C), and then the soluble fraction was dried by vacuum centrifugation. Dried extracts were dissolved in 100 μL sample buffer (40 mM Tris-HCl pH 7.4, 10 mM $MgCl_2$). Each reaction (100 μL) contained 40 mM Tris-HCl (pH 7.4), 10 mM $MgCl_2$, 5 mM DTT, 0.25 μM oligonucleotide template, 1.5 μg RNase A, 0.25 μM ^{3}H-dATP (ARC- 17.2 Ci/mmol), 0.3 units Klenow Fragment (NEB), and cell extract (10 μL) or dTTP standard. Reactions were incubated at 37°C for 1 hr before spotting (85 μL of reaction) onto DE81 paper disks (23 mm-GE Healthcare), which were then air dried. Disks were washed (3 x 10 min) with 25 mL 5% Na2HPO4, rinsed once with water (25 mL) and absolute ethanol (15 mL). Dried disks were placed in scintillation liquid and radioactivity was measured by

scintillation counting. A standard curve was generated with 0-4 pmol dTTP (New England BioLabs).

Nucleotide sugar analysis.

T. brucei cells ($2x10^7$) were pelleted by centrifugation (3500 RPM, 5 min), washed in cold PBS once and then resuspended in 1 mL pre-chilled methanol. Samples were freeze-thawed in liquid nitrogen, placed on ice for 10 min, and centrifuged (16,000 x g for 10 min at 4ºC) to remove insoluble debris. A portion of the supernatant (0.8 mL) was vacuum dried and the residue resuspended in 40 mM sodium phosphate, pH 7.4. Samples were syringe filtered (Millex GV 0.22 μM –Millipore) to remove fine particles. High-Performance Anion Exchange Chromatography (HPAEC) analysis was performed as published [53] but with a modified elution gradient that was optimized for the separation of UDP-GalNAc, UDP-GlcNAc, UDP-Gal and UDP-Glc. Briefly, chromatography was performed on a Dionex ICS3000 HPAEC system with a CarboPac PA1 analytical column (4 mm Å~ 250 mm) and guard column (4 mm Å~ 50 mm). The method was performed with eluents 1 mM NaOH (E1) and 1 M NaOAc, 1 mM NaOH (E2) as follows: 0 min - 20% E2, 10 min - 45% E2, 25 min - 45% E2, 35 min - 45% E2, 40 min - 100% E2, 50 min - 100% E2, 55 min - 20% E2, 65 min - 20% E2. Equal amounts of sample (approximately 50 Mio cells) were analyzed within each experiment and the signal divided by cell count. Synthetic standards were acquired from Promega.

RNA and DNA purification

DNAzol (Molecular Research Center) was used to isolate genomic DNA from *T. brucei* cells. Typically, $5x10^7$ cells were collected for DNA extraction using guidelines recommended by the manufacturer. Total RNA was extracted from samples ($3x10^7$cells) using TRIzol (Invitrogen), following the manufacturer's protocol.

Quantitation of mRNA by qPCR

As described above, total RNA was isolated from samples and treated with DNaseI (Invitrogen) to eliminate gDNA contamination. A cDNA reverse transcription kit (Applied Biosystems) was used to synthesize cDNA for downstream analysis. Relative mRNA abundance was quantified using iTaq SYBR Green Supermix with ROX (Bio-Rad) utilizing a standard curve for each set of primers per experiment. For all experiments, *TERT* was used as a reference gene [54]. Data was collected on the CFX96 (Bio-Rad) and analysis was performed using the Pfaffl method [55].

Virulence studies in mice

Mice (C57BL/6J) were purchased from Wakeland Laboratory (UT Southwestern) and were group-housed in filter-top cages. The animal facility has standard laboratory conditions: 21 to 22°C ambient temperature and a 12 h light/12 h dark cycle. Chow and water were available *ad libitum*. Both doxycycline (Dox) water and water only (controls), were supplemented with 0.1% saccharin to ensure animals drank the Dox supplemented water. Mice from each group were introduced to the study drinking water 2 days prior to infection. Water bottles were protected from light and replaced every 2-3 days. Mice drank approximately 12.5 mL of water daily. Mice

(8 weeks old, n = 6) (12 in total, 3 per study arm) were infected intraperitoneally with 10^3 SM or *TK* c-null parasites ± Dox. Prior to the infection *TK* c-null parasites were propogated in +Tet conditions to ensure parasite viability at the start of the study. Mice were monitored for parasitemia starting three days post-infection by collecting 1 μL of blood from the tail in a 1:150 dilution of medium and counted using a hemocytometer as described [56]. Mice were monitored for 30 days post infection.

Western blot analysis

Cells ($5x10^7$) were harvested by centrifugation (3500 RPM, 5 min), washed twice in cold PBS (10 mM Na_2HPO_4, 1.8 mM KH_2PO_4, 137 mM NaCl, 2.7 mM KCl, pH 7.4), and resuspended (50 uL) in trypanosome lysis buffer (50 mM Hepes, pH 8.0, 100 mM NaCl, 5 mM, β-mercaptoethanol, 2 mM PMSF, 1 mg/mL leupeptin, 2 mg/mL antipain, 10 mg/mL benzamidine, 1mg/mL pepstatin, 1 mg/mL chymostatin). Cells were lysed by 3 freeze/thaw cycles. Insoluble debris was pelleted by centrifugation (16,000 x g, 20 min, 4°C) and the soluble fraction was collected. The Bio-Rad Protein Assay reagent was used to determine protein concentration with bovine serum albumin (BSA) used to generate a standard curve. Total protein (20 μg) was resolved by 12% SDS-PAGE and transferred to a PVDF membrane using the Mini Trans-Blot Cell (BioRad). Membranes were blocked by 5% non-fat dry milk in Tris-buffered saline (TBS) (20 mM Tris (pH 7.6), 150 mM NaCl) for 1 h then incubated with a primary antibody in 5% milk and TBS-T (TBS + 0.1% Tween-20) overnight at 4ºC. The following dilutions were used for each primary antibody: αFLAG 1:1000 (Rabbit polyclonal-Thermo Fisher), αAU1 1:1000 (Mouse monoclonal – Covance), α*Hs*TK 1:500 (Mouse monoclonal -

Thermo Fisher), α*Tb*BiP 1:100,000 (Covance). For detection of the primary antibody, the membrane was incubated in a 1:10,000 dilution of a Protein A-HRP conjugate (Abcam) in TBS-T (5% milk) for 1 hour at room temperature. The membrane was washed 5 x 5min with TBS-T and incubated in SuperSignal West Pico Chemiluminescent Substrate (Thermo Scientific) for 5 minutes. The membrane was visualized by the ImageQuant LAS 4000 (GE).

Data Analysis

Graphs were generated in GraphPad Prism version 7.0a for Mac, GraphPad Software, San Diego California USA (www.graphpad.com), and statistical analysis was performed as indicated in the figure legends.

Genomic analysis to identify possible nucleotidyltransferase enzymes

The KEGG (Kyoto Encyclopedia of Genes and Genomes[57, 58]) pyrimidine metabolic pathway highlights two enzymatic reactions (EC 3.1.3.5 and EC 3.1.3.89) that perform the 5'-(deoxy)nucleotidase activity required to produce pyrimidine deoxynucleosides in other organisms. We searched all reviewed UniProtKB [59] entries with these two described enzyme activities, identifying 561 genes with EC 3.1.3.5 activity and 70 genes with EC 3.1.3.89 activity. We sorted the identified genes according to their assigned PFAM domains [60], keeping nine representative sequences from each unique PFAM, which correspond to five different fold groups (Table 2.2). For stringent identification of *T. brucei* protein sequences with potential 5' nucleotidase activity, the representative sequences were used as queries to search the NCBI NR database using PSI-BLAST [61] (5 iterations, E-value cutoff 0.001), storing the resulting

position-specific scoring matrix as a checkpoint file for re-initiating BLAST against a database of protein sequences from the *T. brucei* genome (E-value cutoff 1). Identified *T. brucei* protein sequences were assigned PFAM domains using batch CD search [62], keeping those sequences with PFAM domains described as possessing 5'-nucleotidase activity. To identify all potential *T. brucei* protein sequences with domains related to those described as having 5'-nucleotidase activity, we queried the *T. brucei* genome using RPS-BLAST (E-value cutoff 0.006) with a library of sequence profiles downloaded from the conserved domain database (CDD ID in Table 2.3) corresponding to each described 5'-nucleotidase PFAM in Table 2.1. Identified sequences were crosschecked for the presence of the query domain using batch CD search [62] or HHPRED [63, 64], reporting the positive hits using the initial RPS-BLAST E-values in Table 2.3.

Cloning, expression and enzymatic assay of T. brucei 5'-nucleotidase (HD-fold, YfbR-like).

The DNA sequence for the *T. brucei 5'-nucleotidase* **(**HD-fold, YfbR-like) was obtained from TriTryDB (Tb927.9.10830). The *E. coli* codon optimized gene was synthesized by GenScript. PCR was used to generate flanking BsaI and XbaI restriction sites that allowed for cloning into the pE-SUMO(KAN) vector (LifeSensors, Malvern, PA) and expression as a N-terminal His_6-SUMO fusion protein. The nucleotidase pE-SUMO vector was transformed into BL21 cells. Cells were cultured in 2L LB-KAN (50 µg/mL) media at 37°C until OD_{600} 0.7, then cooled to 16°C and induced by 500 µM IPTG (Isopropyl β-D-1-thiogalactopyranoside) for 16 h. Cells were collected by centrifugation and suspended in buffer A (500 mM NaCl, 50 mM HEPES pH 7.5, 5 mM imidazole, 5% glycerol, 5 mM 2-

mercaptoethanol) supplemented with 2 mM PMSF (phenylmethane sulfonyl fluoride) and a protease inhibitor cocktail (1 mg/mL leupeptin, 2 mg/mL antipain, 10 mg/mL benzamidine, 1 mg/mL pepstatin, 1 mg/mL chymostatin). Cells were lysed by cell disruptor and the cell debris removed by centrifugation. Supernatant was applied to a HisTrap HP column (GE Healthcare) and washed with buffer A. The His_6-SUMO nucleotidase fusion was eluted using a gradient of 5-45% buffer B (500 mM NaCl, 50 mM HEPES pH 7.5, 5% glycerol, 5 mM 2-mercaptoethanol, 500 mM imidazole). Fractions were analyzed by SDS-PAGE and those containing the *T. brucei* YfbR-like 5'-nucelotidase were pooled, concentrated (10 kDa MWCO Millipore) and dialyzed against buffer A. . The His_6-Sumo tag was removed by overnight incubation at 4^oC with His_6-tagged Ubiquitin-like-specific protease 1 (ULP1) as described [65]. After incubation the mixture was applied to a second HisTrap HP column and cleaved 5'-nucelotidase was collected in the flow-through, while His_6-tagged ULP-1 and impurities were retained on the resin. The flow through was concentrated and protein purity was assessed to be >98% by SDS-PAGE analysis. To provide an alternative purification method, His_6-Sumo tagged 5'-nucleotidase eluted from the first Ni^{+2} column was further purified by Gel Filtration chromatography on a SuperDex 200 Prep Grade column (GE Healthcare) using buffer A. Protein concentration was determined by Bradford Assay (Bio-Rad).

T. brucei 5'-nucleotidase activity was assessed using an endpoint assay for released inorganic phosphate (P_i) using Malachite Green as the detection reagent as described [66, 67]. Briefly, each reaction (160 µL) contained 50 mM HEPES pH 7.5, 0.5 mM $CoCl_2$, 1 mM substrate, and enzyme. The reactions were incubated for 10 - 30 min (to confirm linearity) at

37°C and then 50 uL was treated with 100 mM EDTA. Malachite green reagent (150 µL) was added to each quenched reaction and incubated at room temperature for 5 min prior to measurement at 650 nm. A range of substrate (0.1 – 1.0 mM), metal (0.5 – 10 mM) and enzyme (25 – 100 nM) concentrations were tested to confirm linear dependence on enzyme concentration and to confirm that the reaction rate versus substrate curve was a saturable process. The production of P_i was measured at 650 nm. Absorbance was converted to µmoles of Pi using a standard curve generated using phosphate standard (Cayman Chemical) ranging from 0-100 µM. For the substrate and metal ion specificity studies shown in Fig. 2.20, assays were run with 100 nM enzyme for 20 min using a substrate concentration of 1 mM. Metal ion concentrations are indicated on the graph. All data were collected in triplicate.

Results

Thymidine kinase (TK) is essential for growth of bloodstream form (BSF) T. brucei

To evaluate the essentiality of TK, we attempted to generate a *TK* null cell line in *T. brucei* BSF single marker (SM) cells. *T. brucei* is diploid, therefore minimally two alleles are present for each gene. Allelic replacement via homologous recombination was achieved by transfecting parasites with a PCR product containing a resistance marker flanked by the *TK* 5' and 3' UTRs. Removal of the first allele was successful; however we were unable to replace the last allele after repeated attempts, suggesting essentiality. To further evaluate this hypothesis, a *TK* conditional null (*TK* c-null) cell line was generated. The single allele knockout cells (SKO) were transfected with a vector conferring tetracycline (Tet) regulated expression of N-terminally

FLAG tagged *T. brucei* TK (Flag-*Tb*TK). Expression of FLAG-*Tb*TK was induced by addition of Tet and the remaining *TK* allele was successfully removed generating the *TK* c-null cell line. PCR amplification of the TK locus confirmed replacement by the two selectable markers (Fig. 2.1). To determine the effects caused by the loss of TK expression on cell growth, Tet was removed from the medium, which led to rapid growth arrest and near total cell death by day 3 (Fig. 2.2A). Coincident with this growth arrest, *TK* transcript (by qPCR) and the TK protein (western blot) were depleted within 24 h after Tet removal, confirming good regulatory control of the ectopic *TK* copy (Figs. 2.2A,B). Parasites reemerged several days later, likely due to the loss of Tet regulation. This has been reported to be a common phenomenon in *T. brucei*, likely due to mutations resulting in the loss of Tet regulation, e.g. [14, 44, 68, 69]. The *TK* c-null cells grew normally in pyrimidine-free medium (containing dialyzed fetal bovine serum) in the presence of Tet confirming that *T. brucei* is not auxotrophic for pyrimidines (Fig. 2.2A). Upon subsequent removal of Tet, TK depletion led to cell death with a similar time course to medium containing non-dialyzed (normal) serum.

TK depleted cells are unable to establish an infection in mice

In vivo studies were performed to determine if TK was essential to support *T. brucei* infection in mice. In parallel to *T. brucei* SM infected mice, two groups (n=3) of *TK* c-null infected mice were given either doxycycline (Dox) treated water or water only. As expected mice infected with SM cells in either condition (+/- Dox) had detectable levels of parasitemia by 72 h post infection, with fatalities occurring in all mice in both groups by day 6 (Figs. 2.2C and 2.3). Similarly, all *TK* c-null infected mice treated with Dox to maintain expression of the Tet-

regulated TK copy eventually died within the timeframe of the study. One mouse in this group showed a delayed time before succumbing to parasitemia suggesting some variability in TK expression levels in the *TK* c-null cells. Mice infected with the *TK* c-null strain treated only with water remained healthy and had no detectable levels of parasitemia past 30 days. Thus we conclude that TK is essential for *T. brucei* virulence and infectivity *in vivo*.

TK RNAi-induced growth arrest is reversed by expression of TK from multiple species

The finding that TK is essential in *T. brucei* is puzzling as no clear mechanistic role for TK in parasite fitness is apparent. *T. brucei* requires TK, which is a pyrimidine salvage enzyme; yet there is no requirement for salvageable pyrimidines for growth. To gain further mechanistic insight into this conundrum, we sought to address three possible explanations for the essentiality of TK: 1) parasites require an active TK enzyme, but it makes a novel product; 2) the TK protein, but not its catalytic activity is needed in some regulatory capacity; 3) parasites require formation of dUMP/dTMP by TK to balance pathway flux even under conditions where all pyrimidine precursors originate from the *de novo* pathway.

To provide additional mechanistic insight, an inducible RNAi cell line targeting *TK* mRNA was created so that we could easily introduce various rescue plasmids to address our mechanistic hypotheses. A Tet-regulated vector capable of producing a hairpin transcript targeting the 3'UTR of *TK* was generated and transfected into the *TK* SKO cell line. Induction of *TK* RNAi by addition of Tet led to a significant growth defect, although the growth defect was not as severe as observed for *TK* c-null cells (Fig. 2.4A, B). *TK* mRNA expression was reduced to 20-25% of control levels by RNAi targeting the *TK* transcript (Fig. 2.4C). However, the

reduction in *TK* transcript levels was less in comparison to that observed in the *TK* c-null cells, explaining why the effect on cell growth was less pronounced.

To shed light on whether a novel TK product was being formed we transfected parasites with plasmids encoding rescue proteins from three different sources: AU1-tagged *T. brucei* TK, FLAG-tagged human *Hs*TK, and *Herpes simplex* TK (*Hsv*TK). *Hs*TK has been shown to have more stringent substrate specificity than the *T. brucei* enzyme [28], whereas the viral *Hsv*TK possesses broader substrate specificity than the human enzyme [70]. Rescue protein expression was also under control of Tet promoter. Thus, addition of Tet to these cells induces simultaneous knockdown of endogenous *TK* and expression of the tagged rescue protein. We found that the growth phenotype was reversed by expression of TK from all three species: *T. brucei* (*Tb*TK)(Fig. 2.4A), human (*Hs*TK) (Fig. 2.4B) and viral TK (*Hsv*TK) (Fig. 2.5A). Expression of *Tb*TK and *Hs*TK was confirmed by western blot (Figs. 2.4A,B) and knockdown of endogenous *TK* was monitored by qPCR (Fig. 2.4. C). Viral TK expression was confirmed by the observance of ganciclovir sensitivity that was less apparent in cells expressing *T. brucei* TK (Fig. 2.5C). Ganciclovir is a subversive substrate of *Hsv*TK leading to premature chain termination of newly synthesized DNA [71]. The ability of both *Hs*TK and *Hsv*TK to rescue the *TK* RNAi growth phenotype shows that *T. brucei* TK is unlikely to catalyze a novel reaction, as the required activity is present in enzymes from other species that are known to have a range of substrate specificities.

Catalytically active TK is required for rescue of TbTK RNAi cells

To confirm that *Tb*TK's essential function is dependent on catalytic activity, mutations in the active site of both *Tb*TK and *Hs*TK were created. We targeted two conserved residues (Fig. 2.6) with described roles in the TK catalytic mechanism: *T. brucei* E286, which is reported to function as a proton acceptor [72] and human K32 which is an essential ATP binding residue [73]. Rescue plasmids were constructed as described above with the mutant TKs under the control of the Tet promoter and transfected into the *TK* RNAi line. In contrast to the wild type enzymes, neither the *Tb*TK E286A nor *Hs*TK K32I active site mutants were able to reverse the RNAi induced growth phenotype (Fig. 2.4D,E). These data demonstrate that TK catalytic activity is required for its role in *T. brucei* cell survival.

Deoxyuridine supplementation partially rescues the RNAi-induced growth phenotype

While our data clearly show that *T. brucei* is not a pyrimidine auxotroph, we exploited the fact that the *TK* RNAi line retains partial TK activity (the knockdown is only 75-80% effective by RNAi (Fig. 2.4C)) to assess whether we could use pyrimidine rescue to determine which TK product was needed for *T. brucei* growth. We found that high concentrations (significantly above physiological levels) of deoxyuridine (dUrd) resulted in the partial rescue of the RNAi growth phenotype (Figs. 2.7 and 2.8) (5 mM rescued but 1 mM did not). However, similar levels of uridine (Urd) (Figs. 2.7. B and 2.8. B) or thymidine (dThd)(Figs. 2.7C and 2.8C) did not restore growth and dThd (0.15 – 1.0 mM) was in fact growth inhibitory to the *TK* RNAi +Tet induced cells but not to cells that expressed TK (-Tet), suggesting some type of feedback regulation. In contrast, the addition of dUrd or uracil to *TK* c-null cells, which are >99% depleted

of *Tb*TK, were unable to circumvent lethality of the *TK* knockout showing that TK activity is required for dUrd rescue (Figs 2.7D and 2.9). These data confirm that TK plays an essential role in maintaining dUMP pools.

Human dCMP deaminase rescues TK-deficient cells

The ability of dUrd to partially reverse the RNAi growth phenotype highlights an interesting feature in *T. brucei* pyrimidine metabolism. In most mammals, it has been suggested that a significant portion of dTTP is derived from dUMP produced by dCMP deaminase (DCTD)[21, 22]. Trypanosomatids lack this enzyme, restricting the number of metabolic routes dedicated to dUMP formation. We hypothesized that due to the lack of DCTD, trypanosomatids require TK to supplement dUMP pools. To test this hypothesis a Tet-regulated vector encoding human DCTD (*Hs*DCTD) was transfected into the *TK* RNAi cell line to drive simultaneous expression of *Hs*DCTD and knockdown of endogenous *Tb*TK. The expression of FLAG-tagged *Hs*DCTD completely rescued the *TK* RNAi-induced growth phenotype (Fig. 2.10A). Expression of FLAG-tagged *Hs*DCTD was confirmed by western blot and qPCR analysis confirmed that *TK* mRNA expression was simultaneously reduced (Fig. 2.10B). To further demonstrate that *Hs*DCTD can functionally replace TK, a *TK* null cell line was created in the background of FLAG-tagged *Hs*DCTD Tet-regulated expression plasmid. Both *TK* alleles were replaced by selectable markers through homologous recombination in the presence of Tet to maintain expression of *Hs*DCTD. PCR amplification of the region flanking the *TK* 5' and 3' UTRs confirmed replacement of *TK* with the selectable markers (Fig. 2.1B). PCR analysis also confirmed that the *TK* gene was no longer detectable in genomic DNA from the *TK* null cells.

Removal of Tet from this cell line led to depletion of FLAG-tagged *Hs*DCTD and resulted in a severe growth phenotype by day 2 after Tet removal (Fig. 2.10C). Cell growth of the *Hs*DCTD *TK* null line was less severely impacted than the *TK* c-null line expressing Tet-regulated *Tb*TK from the rescue plasmid, perhaps reflecting a higher residual expression level of *Hs*DCTD (Fig. 2.10C). By day 5 after Tet withdrawal cells began growing again coincident with re-expression of *Hs*DCTD, again suggestive of emergence of cells that have mutations leading to loss of Tet regulation (Fig. 2.10C). Thus, the data support the hypothesis that TK is essential in *T. brucei* and that its role is to contribute to the formation of dUMP in the absence of DCTD.

Metabolomic analysis reveals an accumulation of nucleoside substrates upon TK depletion

Analysis of ~130 soluble metabolites from *TK* c-null cells was performed by liquid chromatography-tandem mass spectrometry (LC-MS/MS) to determine the impact of TK depletion on metabolite pools (Figs. 2.11-2.14). Extracts were collected from *TK* c-null cells grown in medium containing normal non-dialyzed serum at 24 h ± Tet. An early time point was selected so that metabolite pools would be less affected by non-specific changes resulting from cell death later in the time course. Significant changes in the measured metabolite levels were mostly confined to pyrimidine nucleosides: there was a 15-30-fold accumulation of the TK substrates dUrd and dThd, a 3-fold accumulation of dCtd, and a 70-fold increase in thymine levels (Fig. 2.11). In contrast, the pyrimidine nucleotides CMP and UMP were not significantly changed by TK depletion, suggesting that the *de novo* pathway was able to maintain the uridine nucleotide pools. In further support, HPLC analysis of UDP-sugars was performed (Fig. 2.11B). Nucleotide sugars are formed from UTP, thus their measurement provides a read-out of effects

on intracellular UTP concentrations. The relative abundance of UDP-GlcNAc, UDP-Galactose, and UDP-Glucose were not significantly changed by TK depletion, confirming that UTP pools are not linked to TK activity. Thymidine nucleotide pools were not detected by the LC-MS/MS analysis so instead we quantitated dTTP levels using an enzymatic assay and found that dTTP levels were reduced to 30% of control levels 48 h after Tet removal, confirming TK is essential for synthesis of dTTP (Fig. 2.11C).

To better understand the consequences of TK depletion in a pyrimidine-free medium the LC-MS/MS analysis was repeated for *TK* c-null cells grown in medium supplemented with dialyzed serum (Figs. 2.11D, 2.12-2.14). Similar to the results for cells grown in normal serum based medium, we observed a statistically significant build up of TK substrates dUrd and dThd, and of the dUrd precursor dCyd, though the increases (3-6-fold) were less than observed for cells grown in normal serum based medium. We also observed changes in the levels of TCA intermediates including decreases in citrate and aconitate and an increase in α-ketoglutarate, and perturbations in other metabolites related to pyrimidine biosynthesis including decreased carbamoylphoshate (CP) and acetyl-ornithine (30 and 80%, respectively) and a 2-fold increase in homocysteine (Fig. 2.11C,D). Not all of these latter changes reached statistical significance. Some modest effects were also observed on several purines: an increase in xanthine and/or hypoxanthine was observed in both medium conditions, which may suggest some type of cross-regulation between pyrimidine and purine biosynthetic pathways. Thymine was only observed in cells grown in medium supplemented with non-dialyzed serum, which could supply a source for thymine, confirming genomic analysis that suggests *T. brucei* does not encode thymine biosynthetic enzymes.

Deletion of cytidine deaminase induces pyrimidine auxotrophy

The finding that the deoxypyrimidine nucleoside pools build up upon TK depletion for cells grown in pyrimidine-free (dialyzed serum based) medium suggests that an undiscovered biosynthetic route for formation of deoxypyrimidine nucleosides must be present in *T. brucei*. To investigate if deoxycytidine could be involved in formation of dUMP and dTMP we decided to characterize the effects of depleting cytidine deaminase (CDA) on parasite growth. Based on the current annotation of the pyrimidine biosynthetic pathway, CDA like TK should catalyze a redundant reaction, since the deoxynucleotide pools can be supplied from the *de novo* pathway. However, attempts to generate a *CDA* null were unsuccessful, and indeed the *CDA* null could only be obtained in the presence of 500 μM dThd (Figs. 2.15 and 2.16). Upon removal of dThd, *CDA* null cells exhibited a severe growth defect (Fig. 2.15A). Cells cultured for longer eventually died around day 7-10 after dThd removal. Additional pyrimidine rescue studies revealed that both dThd and dUrd were capable of rescuing growth (EC_{50} of 6-20 μM), whereas uracil (up to 250 μM) was not (Figs. 2.15C-E). The concentrations of dThd and dUrd required for rescue are significantly above reported human blood levels (range of 0.2 – 0.6 μM; http://www.hmdb.ca).

CDA null cells were grown ± dThd for 12 h in media supplemented with dialyzed FBS and the metabolite pools were analyzed by LC-MS/MS as described above. Overall the effects of CDA depletion on cellular metabolism were very similar to the effects observed after depletion of TK, confirming a link between the roles of the two enzymes. We observed a significant build up (~7-fold) in the CDA substrate, dCtd, for the *CDA* null cells grown in the absence of Thd that

was accompanied by changes in TCA intermediates and other metabolites that serve as precursors for *de novo* pyrimidine biosynthesis (Fig. 2.17 and 2.18). These changes include increases in α-ketoglutarate (11-fold), glutamate (7-fold) and homocysteine (2-fold), and decreases in carbamoyl phosphate (2-fold). We also observed decreased levels of several amino acids, of polyamines, particularly N-acetyl putrescine and decreased levels of several purine mono-phosphate nucleotides. Neither dUrd nor dThd were detected in CDA null cells in the presence or absence of added dThd, suggesting they were either not formed (dUrd) or rapidly metabolized (dThd). In the absence of CDA, the buildup of dCtd suggests that the pyrimidine deoxynucleotides have been sequestered into a dead-end product that would be expected to lead to depletion of key nucleotides and to cell death as was observed for the TK null cells. These data support a role for CDA in the interconversion of deoxycytidine, deoxyuridine and thymidine pools, which is needed to balance these pools in a cell like *T. brucei* that expresses TK but not DCTD.

T. brucei proteins with domains that can perform 5'-nucleotidase activity.

In order to identify the potential enzyme(s) responsible for converting deoxypyrimidine nucleotides into their corresponding nucleosides we undertook a bioinformatics analysis of the *T. brucei* genome. 5'-nucleotidase activities that catalyze formation of deoxyuridine, deoxycytidine, or thymidine from their respective mono-phosphate nucleotides are ascribed to two EC numbers (EC3.1.3.5 and EC3.1.3.89). Inspection of domain types performing these activities revealed nine protein families defined by PFAM, with all having homologous structure representatives in the PDB (Table 2.2.). The families further merge into five different homologous fold types;

including three different α/β sandwich folds (phosphoglycerate mutase-like, SurE-like, and HAD domain-related), one α+β four-layer sandwich fold (metallo-dependent phosphatases), and one all-α fold (HD-domain). The phosphoglycerate mutase-like representatives are limited to mammalian acid phosphatases, prostate (ACPP) enzymes that convert extracellular AMP to adenosine (i.e. ecto 5' nucleotidase activity) [74]. An additional identified enzyme (NT5E) from the metallo-dependent phosphatase fold group exhibits a similar ecto 5'-nucleotidase activity [75]. Examples of this fold group in both eukaryotes and bacteria contain signal peptides and are extracellular. In contrast, the remaining SurE, HAD domain-related, and HD-domain representatives appear cytosolic.

We found evidence for all of the 5'-nucleotidase homologous fold types in the *T. brucei* genome with the exception of the SurE fold class (Table 2.3.). We identified nine phosphoglycerate mutase-like sequences, 33 metallo-dependent phosphatase sequences, 16 HAD domain-related sequences, and one HD-domain sequence (Table 2.3.). The presence of numerous examples of potential 5'-nucleotidase domains, many of which are annotated as hypothetical proteins, suggests multiple possible proteins that *T. brucei* could use to form deoxyuridine, deoxycytidine, or thymidine *de novo*. However, three of the identified genes possess specific PFAM domains described as having 5'-nucleotidase activity (EC 3.1.3.5 or EC 3.1.3.89) and thus are the highest ranked candidates. One encodes a HD domain protein: hypothetical protein (Tb927.9.10830) and two encode HAD-like domains: a putative *p*-nitrophenylphosphatase (Tb927.8.7510) and a hypothetical protein (Tb09.211.1880). The *T. brucei* HD domain protein is a homolog of *E. coli* 5'-nucleotidase YfbR (Table 2.2) while the *T. brucei* HAD-domain proteins are related to enzymes shown to have 5'-nucleotidase activity in both yeast and *E. coli*. [66, 76,

77]. These enzymes have been reported to have broad substrate specificity functioning on all three pyrimidine deoxy-mononucleotides

***T. brucei* HD domain protein encodes a metal dependent 5'-nucleotidase.**

To provide support for our hypothesis that *T. brucei* encodes a 5'-nucleotidase we cloned, expressed and purified the HD domain homolog (Tb927.9.10830) of the bacterial 5'-nucleotidase YfbR (Fig. 2.19). We found that the *T. brucei* YfbR-like HD protein showed a metal dependent 5'-nucleotidase activity (Fig. 2.20A). Similar to the bacterial enzyme it was most active in the presence of Co^{+2} (0.5 mM), but activities within 2-4-fold of levels observed for Co^{+2} were also obtained using Mn^{+2} (0.5 mM) and physiological levels of Mg^{+2} (10 mM). No activity was observed in the presence of Zn^{+2} or EDTA. The specific activity of the *T. brucei* HD domain 5'-nucleotidase was very similar to the reported activity of *E. coli* YfbR [66]. The *T. brucei* enzyme showed a broad substrate range functioning on both pyrimidine and purine deoxyribonucleoside and ribonucleoside 5'-monophosphates, though it was most active on the deoxypyrimidine nucleotides (dCMP, dUMP and dTMP) (Fig. 2.20B). It showed no activity towards diphosphate nucleotides. The *T. brucei* enzyme was somewhat more promiscuous then *E. coli* YfbR, which was unable to catalyze hydrolysis of ribonucleoside 5-monophosphates [66]. Both *T. cruzi* and *Leishmania* encode homologs of the *T. brucei* HD-domain 5'-nucleotidase (Table 2.2. and 2.3.) suggesting they both also will be able to convert 5'-deoxyribonucleotide monophosphates to their respective nucleosides.

Single-celled eukaryotic pathogens that encode TK but lack DCTD

To assess if TK essentiality was likely to extend to other pathogenic protozoa we utilized the KEGG pathway database to determine the distribution of TK and DCTD throughout eukaryotes (Fig. 2.21). A striking disparity was observed within protists when compared to higher eukaryotes. The vast majority of higher eukaryotes possess both TK and DCTD, which may explain TK's non-essential role in these organisms. In contrast, the kinetoplastids and a number of other protozoan human pathogens such as *Giardia* encode only TK, suggesting that TK may be essential in these organisms as well. We also note that several of the protists such as *Entamoeba histolytica,* which lack DCTD, instead encode dCTP deaminase, an enzyme found almost exclusively in bacteria. Similar to DCTD, the ability to deaminate dCTP to dUTP offers an alternative path from cytosine to thymine nucleotide pools and thus we would predict that TK would not be essential in these species. Interestingly, these organisms represent the only eukaryotic KEGG organisms that have dCTP deaminase.

Conclusions

T. brucei encodes a complete *de novo* pyrimidine biosynthetic pathway, as well as a number of pyrimidine salvage enzymes that were thought to be redundant based on the presence of the *de novo* pathway. Herein we describe the first comprehensive analysis of the role of the pyrimidine salvage enzymes in *T. brucei* and we show that while *T. brucei* is not auxotrophic for pyrimidines, both TK and CDA are essential for *in vitro* growth and TK is essential for infectivity *in vivo* as well. The finding that these enzymes are essential could not be explained by the current annotation of the pyrimidine pathway in *T. brucei*. Our mechanistic analysis of the *TK* and *CDA* null cell lines uncovered the existence of an interconversion network between the

deoxypyrimidine nucleoside and nucleotide pools, including the presence of a previously unknown 5'-nucleotidase that converts deoxycytidine, deoxyuridine and thymidine nucleotides to their respective nucleosides. In the absence of TK or CDA to balance this 5'-nucleotidase activity, the metabolic cycle breaks down leading to dead-end buildup of deoxypyrimidine nucleosides and to cell death. The existence of this recycling pathway provides a mechanism for the parasite to interconvert and balance the relative levels of the deoxyuridine, deoxycytidine and thymidine pools whether they originate from the *de novo* pathway or through salvage. Our conclusions are supported by the following arguments.

Firstly, TK is essential for both *in vitro* growth and infectivity in a mouse model of *T. brucei* infection and for formation of dTTP despite the fact that *T. brucei* is not a pyrimidine auxotroph. Thus the essential role of TK is not to salvage externally acquired pyrimidine precursors. Our data clearly show that TK activity is required for its function and that it plays a key role in the synthesis of dUMP, even for cells grown in a pyrimidine-free environment. We found that the function of TK can be replaced by expression of human DCTD, which provides an alternative route to dUMP formation from dCMP in many higher eukaryotes [21, 22]. DCTD has been shown to be essential for cell cycle progression and formation of dTTP pools in eukaryotes that lack TK (e.g. *Schizosaccharomyces pombe*) [78]. These data suggest that DCTD and TK can have functionally redundant roles in contributing to dTTP pools, supporting our observation that TK is essential for formation of thymine nucleotides in *T. brucei*.

The next significant key to the puzzle came from analysis of metabolomic data from the *TK* c-null cell line. These data showed that even in the absence of external pyrimidines the TK substrates dUrd and dThd, as well as the dUrd precursor dCtd build up, leading to a dead-end

accumulation of these precursors away from the essential deoxynucleotide pools resulting in depletion of dTTP. In the absence of an exogenous supply of these nucleosides the current annotation of the *T. brucei* genome does not provide a mechanism for these nucleosides to be synthesized, suggesting the presence of a missing enzyme that catalyzes conversion of deoxynucleotides into deoxynucleosides. The findings that *CDA* null cells are auxotrophic for dThd or dUrd further support this hypothesis since based on redundancy in the pathway, CDA should not be essential under any conditions. Furthermore the *CDA* null data support the presence of an enzymatic link between the deoxycytidine-containing nucleotide pools and dCtd/dUrd, since either dUrd or Thd are required for growth of *CDA* null cells. These data are consistent with previous published untargeted metabolomics data showing that isotope-labeled glucose was incorporated into both dUrd and dThd, and thus that *T. brucei* was capable of synthesizing these nucleosides *de novo* [79]. Lastly, the inability of uracil to rescue the growth deficit of the *CDA* null cells shows that uridine phosphorylase is not able to efficiently convert uracil to dUrd, eliminating the only known potential source for dUrd biosynthesis in *T. brucei*. Uridine phosphyorylase was previously suggested to be the source of dUrd, based on the isotope-labeled glucose study[79], but our result is consistent with previous reports that 5-fluorouracil and 5-fluoro-Urd are not substrates for this enzyme [15].

Thus taken together, our data lead to the conclusion that *T. brucei* encodes an unidentified 5'-nucleotidase that converts dCMP and dTMP to dCtd and dThd, respectively. We identified a number of potential candidate genes in *T. brucei* that could encode this activity, including a homolog of the *E. coli* HD protein YfbR and two strong candidates from the HAD-domain related family. Notably we showed that the *T. brucei* YfbR homolog encodes a metal

dependent 5'-nucleotidases with broad substrate specificity functioning on all three pyrimidine deoxy-mononucleotides. Whether or not the *T. brucei* YfbR homolog is the only 5'-nucleotidase in *T. brucei*, or whether it is even the dominant enzyme with this capability remain open questions. Mammalian cells encode at least seven 5'-nucleotidases with overlapping specificities [80-82] and *E. coli* encodes minimally three, one each from the HD, HAD and SurE superfamilies [66]. Thus it is likely that other candidate *T. brucei* genes identified in our bioinformatics analysis will also display activity. In mammalian cells the 5'-nucleotidases have been shown to be required for regulation of cellular dNTP levels and to provide a mechanism to maintain balanced ratios between the pools, which is essential for high fidelity DNA synthesis [82]. Like the *T. brucei* HD-domain 5'-nucleotidase, all described nucleotidases from the various families exhibit broad substrate specificity. The broad specificity allows these enzymes to function in a ubiquitous capacity for intercoversion of the nucleotide pools.

The finding of 5'-nucleotidase activity in *T. brucei* leads directly to the essentiality of both TK and CDA, as in their absence the dead-end buildup of pyrimidine nucleosides leads to depletion of pyrimidine deoxynucleotides and to cell death. Within this context, the ability of DCTD to rescue the *TK* null cell line suggests that DCTD is able to effectively compete with the 5'-nucleotidase for the dCMP pools, converting sufficient amounts to dUMP where it can be efficiently shunted to dTMP even in the absence of TK. The existence of the metabolic cycle involving TK, CDA and 5'-nucleotidase provides the cell with a mechanism to interconvert between the deoxyuridine, deoxycytidine and deoxythymidine pools allowing presumably for better regulation and balance of their relative levels. While dUMP can also be formed from UDP, this pathway is apparently not sufficient to keep up with dUMP needs in the face of the

dead-end accumulation of the TK substrates in the absence of TK. However this pathway remains an important additional source of dUMP as null mutants of dUTPase have been reported to be thymidine auxotrophs [23].

Our metabolomic analysis also uncovered some additional insights into *T. brucei* metabolism and regulation. In the presence of an outside source of pyrimidines (non-dialyzed serum), the pyrimidine nucleosides dUrd, dCyd, dThd and thymine accumulated in the *TK* c-null cells to higher levels than for cells grown in pyrimidine-free medium (dialyzed serum). These data confirm that in the absence of TK there is dead-end accumulation of these nucleosides but they also suggest that uridine phosphorylase is not a significant drainage point for these pools. Thus *T. brucei* uridine phosphorylase primarily catalyzes conversion of Urd to uracil, while it is not capable of synthesizing dUrd (as described above), or using it efficiently as a substrate. This hypothesis is consistent with previous reports that the recombinant *T. brucei* enzyme is 10-fold more active on Urd than dUrd [24]. Our metabolomic data also suggest that one response of *T. brucei* to TK depletion is increased nucleoside transport despite the fact that the upregulated transport was unable to relieve the growth block. A similar accumulation in dUrd in the presence of normal serum was previously reported for *T. brucei* BSF treated with thymidylate synthase inhibitors [15] suggesting this is a common response to starvation of thymine nucleotides.

Finally, we noted that the levels of TCA intermediates were significantly perturbed in both the *TK* c-null and *CDA* null cells, including significant increases in α-ketoglutarate and homocysteine upon loss of TK expression or removal of thymidine from the *CDA* null cells. α-ketoglutarate is formed in the transamination reaction that generates L-Asp, which in turn is required for the first step in *de novo* pyrimidine biosynthesis, while homocysteine leads to

formation of methionine then 5,10-methylene tetrahydrofolate, needed to convert dUMP to dTMP. Taken together with an observed decrease in carbamoyl phosphate, another precursor of the *de novo* pathway, the data suggest the cells may attempt to compensate for the loss of TK by increasing flux through the *de novo* pathway. Finally we also observed a significant decrease in acetyl-ornithine/acetyl-putrescine. It is not immediately apparent how these metabolites are synthesized, but their presence in *T. brucei* has been previously noted [79]. It is also not immediately clear what role they may play in pyrimidine biosynthesis, but both the synthesis and degradation of acetyl-ornithine can be catalyzed by aminotransferases, and in the case of its degradation this pathway links back to glutamate pools, and thus potentially to pyrimidine biosynthesis. The specific aminotransferases that catalyze these reactions are not annotated in the *T. brucei* genome, but aminotransferases have been reported to have broad and redundant substrate specificities in *E. coli* [83].

While a key aspect of our work was to elucidate the role of TK and CDA in linking the *de novo* pathway to synthesis of the deoxynucleotide pools, we have also validated TK as a drug target in *T. brucei* by showing that it is essential both *in vitro* and *in vivo*. The finding that the *TK* c-null cells cannot be rescued by exogenous pyrimidines shows it would not be possible for even an intracellular parasite to get around the block.. Our work additionally showed that CDA is essential for *in vitro* growth of blood form *T. brucei*. While we did not determine if CDA is required for virulence *in vivo*, it remains a possibility provided that blood thymidine levels are below those required for rescue. Pyrimidine deoxynucleosides levels in human blood are reported to be ~10-fold below the EC_{50} that we measured for efficient rescue of *CDA* null growth. Furthermore, *T. brucei* has low affinity and/or poor efficiency transporters for

deoxynucleosides [15], suggesting that *CDA* may be essential for infection in humans. However, additional studies will be needed to address this question conclusively.

The presence of multiple pathways to synthesize dUMP appears to be an important shared characteristic amongst many eukaryotic cells, with the data suggesting that some organisms require either TK or DCTD to link *de novo* biosynthesis to the thymine deoxynucleotides. Interestingly, our bioinformatics analysis shows that other single-celled eukaryotic pathogens, including all three disease-causing trypanosomatids, encode TK but lack DCTD. These data suggest that TK may be essential in these other pathogens and may potentially provide a path forward to develop drugs that have pan-activity against a range of human pathogens. However, the essentiality in other organisms would be dependent on the presence of the 5'-nucleotidase activity and likely also on limited catabolism of dUrd back to uracil by uridine phosphorylase. In support, the *Leishmania major* TK null cell line showed severely reduced growth rates [84]. In contrast, deletion of TK from *Cryptosporidium parvum* was not lethal, which is predicted by the presence of both TK and DCTD [85]. The finding that human cells contain both TK and DCTD, and that TK is not essential in human cells [86] supports the potential for selectively targeting TK from the eukaryotic pathogens that lack DCTD. Thus in conclusion, the unexpected finding that TK is essential in *T. brucei* and its mechanistic role in supporting *de novo* pyrimidine biosynthesis has uncovered a unique opportunity for the potential development of a pan-trypanosomatid therapy.

Figure 2.1. PCR analysis confirms replacement of *tk* alleles with selectable markers. Amplification of the *TK* locus using primers flanking the *TK* 5' and 3' UTRs (A,B),

selectable markers(A,B), and *TK* ORF (B). The *TK* locus was amplified from genomic DNA extracted from *TK* c-null and WT SM cells and the selectable markers were amplified from *TK* c-null genomic DNA. The *TK* gene was amplified from both the WT SM and human DCTD expressing *TK* null genomic DNA.

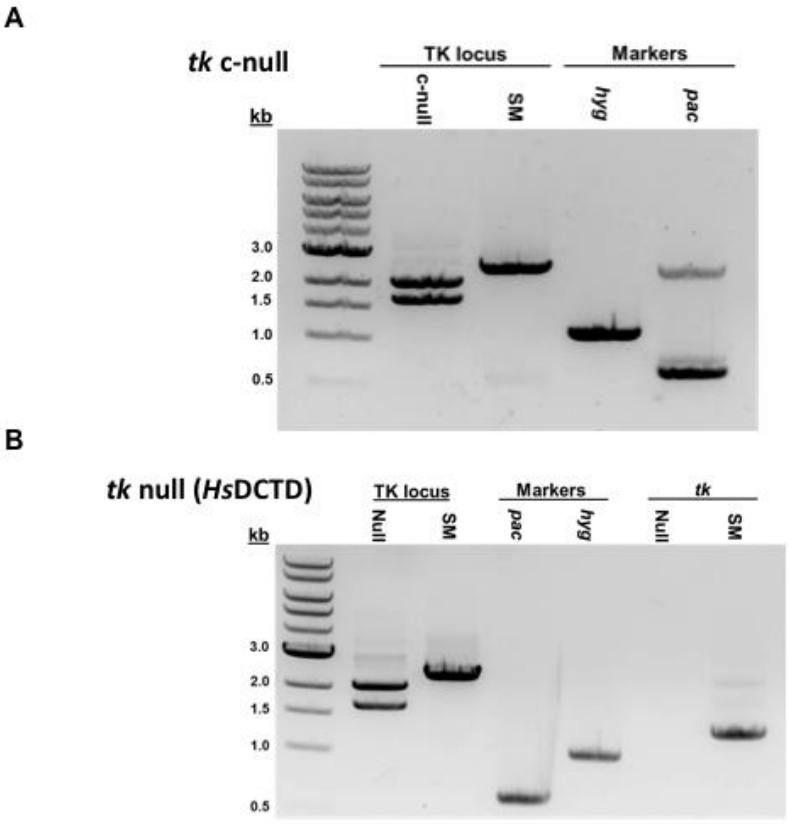

Figure 2.2. TK is essential for *in vitro* growth and infectivity in mice. A. Growth analysis of *TK* c-null cells and wild-type SM cells ±Tet. Expression of ectopic FLAG-tagged *Tb*TK is under Tet control, thus removal of Tet leads to loss of *Tb*TK expression. Cells were grown in HMI-19 medium supplemented with either normal serum (NS) or dialyzed serum (DS). Cell growth was monitored for the indicated days. Error bars represent standard deviation (SD) for triplicate biological replicates. Inset shows western blot analysis of FLAG-tagged *Tb*TK expression ±Tet for 24h. *Tb*BiP was detected as a loading control. B. qPCR analysis comparing mRNA expression levels of *Tb*TK to the TERT control ±Tet for 24 h. Error bars represent standard error of the mean (SEM) for triplicate data. C. Survival analysis of wild-type SM and TK c-null infected mice (±Dox) 1 - 30 days post infection for three mice per group. Filipa Ferreira helped perform the *in vivo* mice studies.

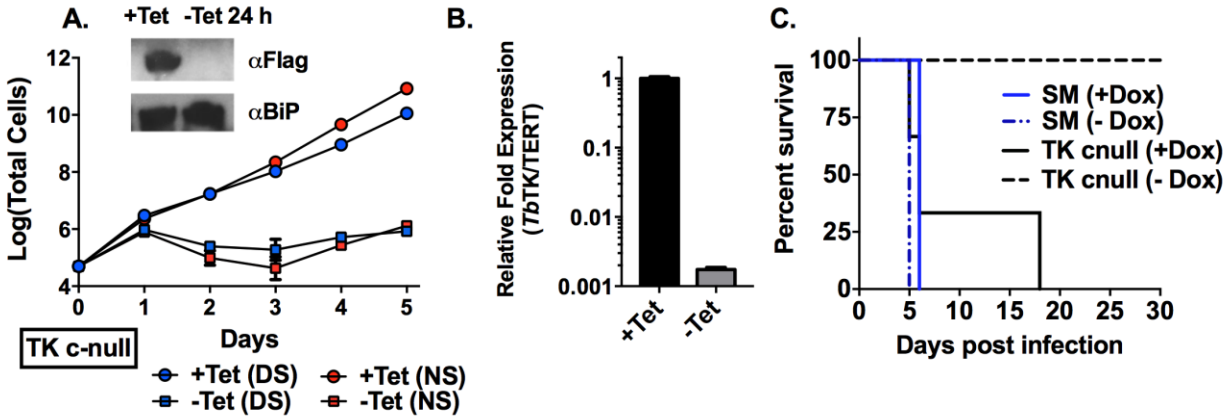

Figure 2.3 Infection of mice with *TK* c-null cells and wild-type SM cells. Graphs show parasitemia levels (cells/ml) in blood collected the first 6 days post infection for the three mice per each group. A. SM cells ±Dox. B. *TK* c-null cells ±Dox. Mouse #2 in the TK c-null

+Dox arm was delayed in the course of infection and did not succumb to parasitemia until day 18. Parasites were not observed at any time over the 30 days in the TK c-null -Dox treated animals.

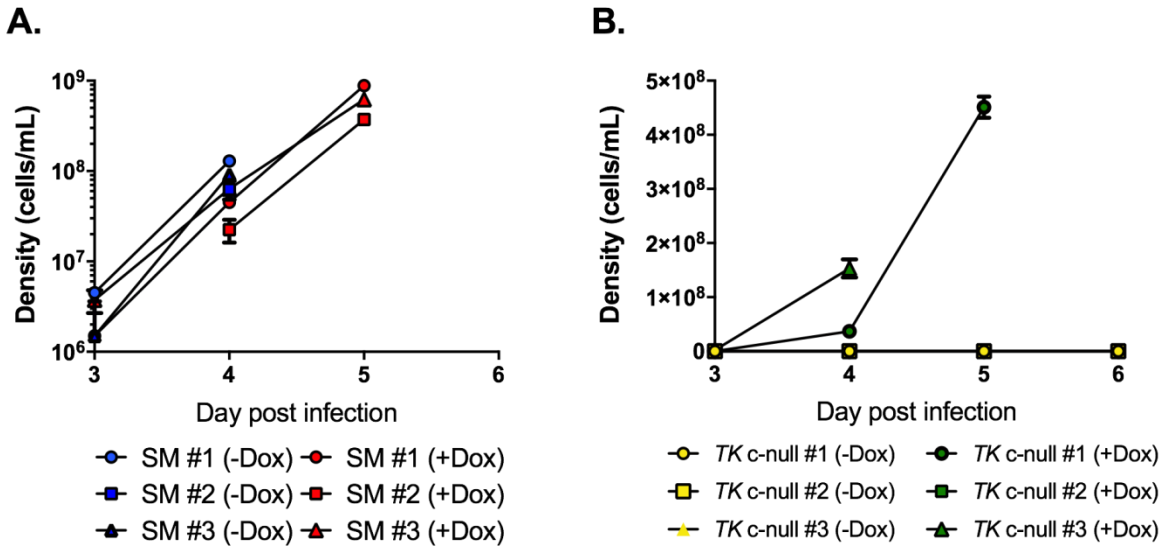

Figure 2.4. Catalytically active TK is required to rescue the *TK* RNAi growth phenotype. A-B. Growth analysis of TK RNAi cells (±Tet) expressing *Tb*TK or *Hs*TK under Tet control. Cell growth was monitored for the indicated days. Error bars represent SD for triplicate biological replicates. C. qPCR analysis of *Tb*TK mRNA levels in *TK* RNAi knockdown cells in the absence and presence of the *Hs*TK rescue plasmid 48 h after Tet addition. Error bars represent SEM for triplicate data. Data were normalized to TK levels in wild-type SM cells. D-E. Growth analysis of *TK* RNAi cells (±Tet) expressing active-site mutant TK enzymes, *Tb*TK E286A or *Hs*TK K32I under Tet control. Error bars represent SD for triplicate biological

replicates. Insets show western blots of the AU1-*Tb*TK (A), FLAG-*Tb*TK (D) or FLAG-*Hs*TK (B,E) rescued RNAi lines comparing ±Tet for 48 h, though in panel E, *Hs*TK K32I was detected with a *Hs*TK antibody. *Tb*BiP was detected as a loading control.

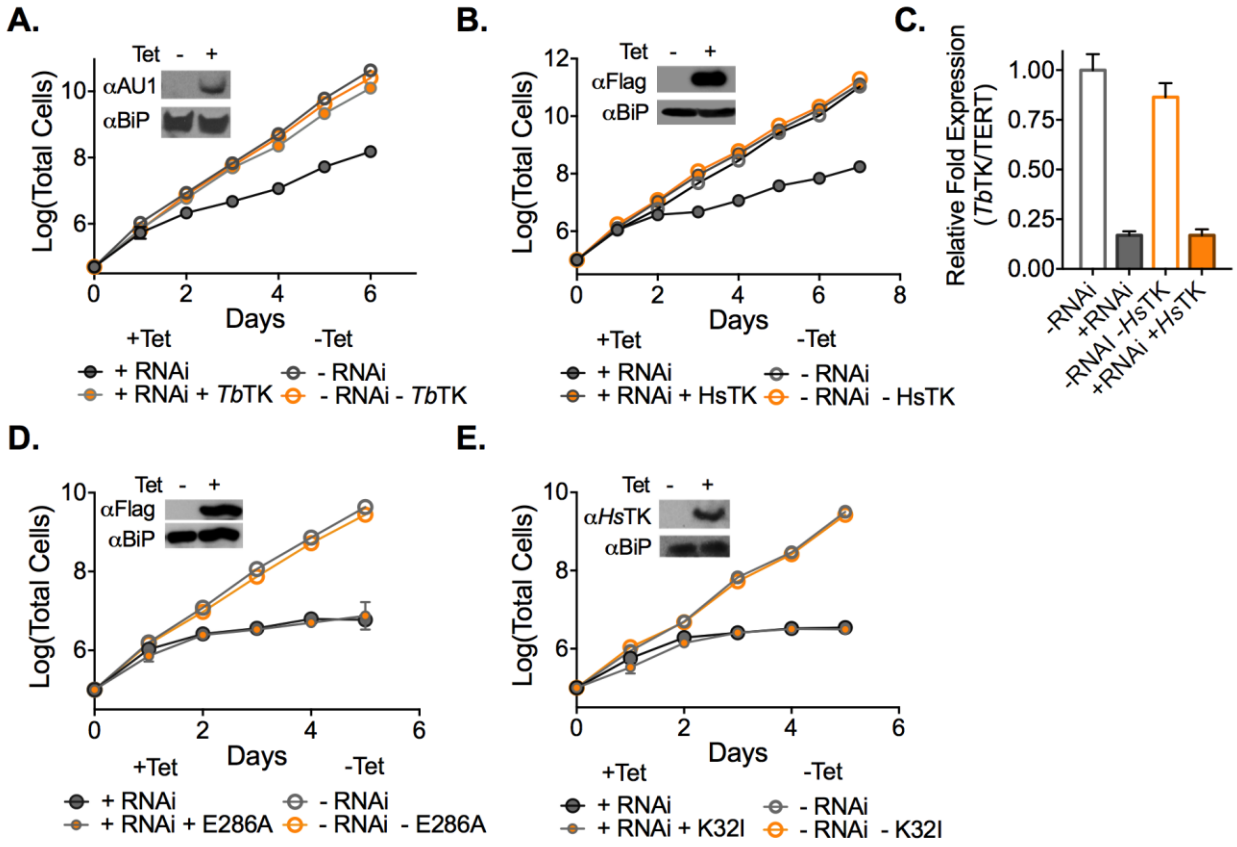

Figure 2.5. Growth analysis of TK RNAi cells (±Tet) expressing Tet regulated HsvTK grown in parallel with the TK RNAi control (±Tet). A. Growth analysis of TK RNAi cells (±Tet) expressing Tet regulated *Tb*TK or HsvTK grown in the presence or absence of ganciclovir (GCV-50 µg/ml). B. qPCR analysis of relative TK expression in *Hsv*TK rescue cells 48 h after Tet supplementation compared to SM (WT) cells. *Tb*TK expression is normalized with TERT expression and error bars represent standard error of the mean (SEM)

calculated from triplicate data. C. All growth experiments were performed in HMI-19 media and the error bars represent the standard deviation (SD) for biological triplicates.

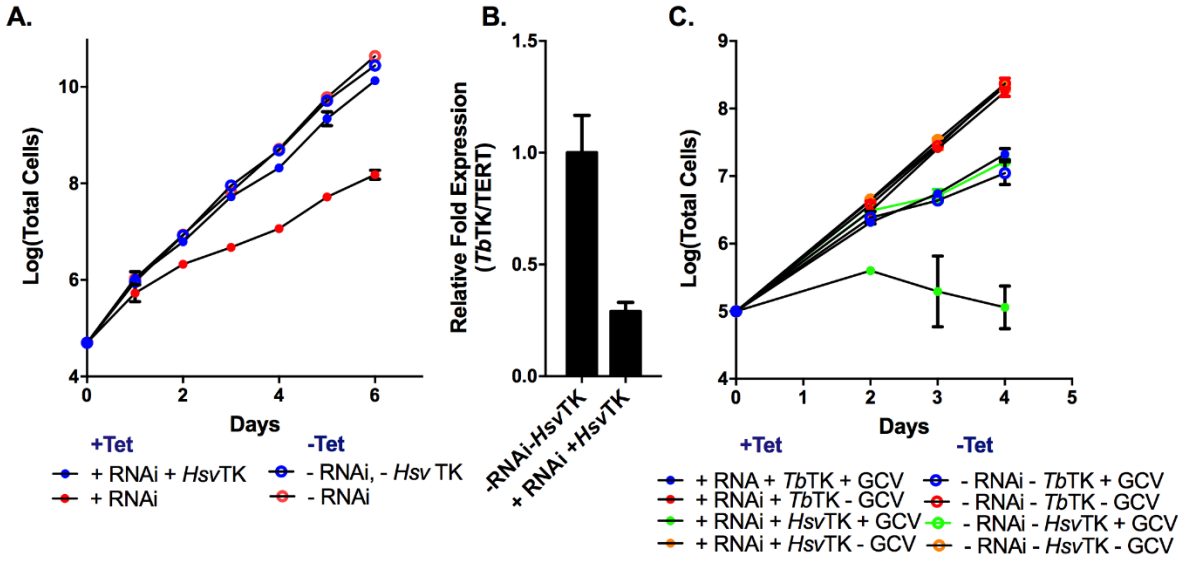

Figure 2.6. Amino acid sequence alignment (Clustal Omega version 1.2.2) of TKs from select species. E. coli (*Ec*-P23331), Humans (*Hs* – P04183), Mus muscaris (*Mm* – P04184), *Leishmania donovani* (*Ld* – Q4QC75), inactive N-terminal *Tb*TK domain, and active C-terminal *Tb*TK domain. Residues highlighted in green represent highly conserved residues in active TKs selected for the mutagenesis studies (*Tb*TK E286A and *Hs*TK K32I).

```
EcTK          -----------------MAQLYFYYSAMNAGKSTALLQSSYNYQERGMRTVVYTAEIDDR   43
HsTK          MSCINLPTVLPGSPSKTRGQIQVILGPMFSGKSTELMRRVRRFQIAQYKCLVIKYAKDTR   60
MmTK          MSYINLPTVLPSSPSKTRGQIQVILGPMFSGKSTELMRRVRRFQIAQYKCLVIKYAKDTR   60
LdTK          ---------------MFRGRIELIIGPMFAGKTTELMRRVKREIHARRSCFVIKYSKDTR   45
NT-TbTK       -------------MHDGDGNIELIIGPMFAGKTTELMRRVQRHKHAQRSCYIINYSRN-S   46
CT-TbTK       ------------VPNGAHGRIELIIGPMFAGKTTELMRRVQRHKHAQRSCYIIKYTGDTR   48
                                ..: .  . * :**:* *::   .         : .   :

EcTK          FGAGKVSSRIGLSSPAKLFNQNSSLFDEIRAEHEQQAIHCVLVDECQFLTRQQVYELSEV   103
HsTK          YSSSF-CTHDRNTMEA-L---PACLLRDVA--QEALGVAVIGIDEGQFFPDIV--EFCEA   111
MmTK          YSNSF-STHDRNTMDA-L---PACMLRDVT--QESLGVAVIGIDEGQFFPDIV--DFCEM   111
LdTK          YDEHNVASHDQLMLRAQA---AVSQLTEVR--DTWKRFDVLAIDEGQFFSDLV--NFCNT   98
NT-TbTK       YQNQRLSTHDQLSLTANV---SIAKLSEVC--DEWRDYDVIAVDNGQFFPDVV--GFCAR   99
CT-TbTK       YSEGAITSHDQRALTANV---SVSNLHDVG--DEWRKYDVIAVDEGQFFPGVA--AFCSK   101
              :      ::      *       . : ::   .       : :*: **:       :.

EcTK          VDQLDIPVLCYGLRTDFRGELFIGSQYLLAWSDKLVELKTICFCGRKASMVLRLDQAGRP   163
HsTK          MANAGKTVIVAALDGTFQRKPFGAILNLVPLAESVVKLTAVCMECFREAA-----YTKRL   166
MmTK          MANEGKTVIVAALDGTFQRKAFGSILNLVPLAESVVKLTAVCMECFREAA-----YTKRL   166
LdTK          AADAGKVVMVSALDGDYRRKPFGQICELVPYCEAVDKLTAVCMMCHEQPAC----FTRRT   154
NT-TbTK       AANEGKTVIVSALDVDCRETPFDEVCRLVPRAESVLKLSAVCMECHEHDAF----LTYRT   155
CT-TbTK       AADSGKVVIVSALDADYLQEPFEEICLLVSRADSVVKLSAVCMECHNRKAS----FTYRT   157
                :    *:  .*        *     *:  .: : :*.::*:   .         : *

EcTK          YNEGEQVVIGGNERYVSVCRKHYKEALQVDSLTAIQ------ERHRHD------------   205
HsTK          GTEKEVEVIGGADKYHSVCRLCYFKKASGQPAGPDN--------KENCPVPGK-------   211
MmTK          GLEKEVEVIGGADKYHSVCRLCYFKKSSAQTAGSDN---------KNCLVLGQ-------   210
LdTK          VNVEQQELIGGADMYIATCRECYSKQQLPSIEEMRTQQMAIKEVEKRYLGMSDKR---AT   211
NT-TbTK       IESNERELYGGADMYLAVCRWCYKQLTMSHVDAQ-----------------KTSASTAA   197
CT-TbTK       VKSDERKLVGGSDMYMSVCRSCYETKRNMVQTEKYIY---------SCVGINEGSYSECS   208
                  :  : ** : * :.**  *

EcTK          ------------------------------------------------------------   205
HsTK          PGEA--VAARKLFAPQQILQCSPAN-----------------------------------   234
MmTK          PGEA--LVVRKLFASQQVLQYNSAN-----------------------------------   233
LdTK          AGPQTPEKPAGGWGTKTGVATLPTMATEGAASSGASAGMKSGRDLCEVQTFTTEAPKYQR   271
NT-TbTK       ------VVPNGAHG-----------------------------------------------   205
CT-TbTK       PGPS-ERSSAGTSGVQTSVKVDEQNCTEPNT-EAKKMPLKRKRNQMAVDTT---------   257


EcTK          -------------   205
HsTK          -------------   234
MmTK          -------------   233
LdTK          VEPACTASAASSE   284
NT-TbTK       -------------   205
CT-TbTK       -------------   257
```

Figure 2.7. Effects of nucleoside supplementation on growth in TK RNAi or c-null cells. Growth analysis of TK RNAi cells supplemented with: A. dUrd (1 or 5 mM). B. Urd and dUrd (5 mM). C. dThd (0.5 or 1 mM) D. dUrd supplementation of TK c-null cells (±Tet). TK c-null cells express an ectopic copy of *Tb*TK under Tet control. Error bars represent SD for triplicate biological replicates.

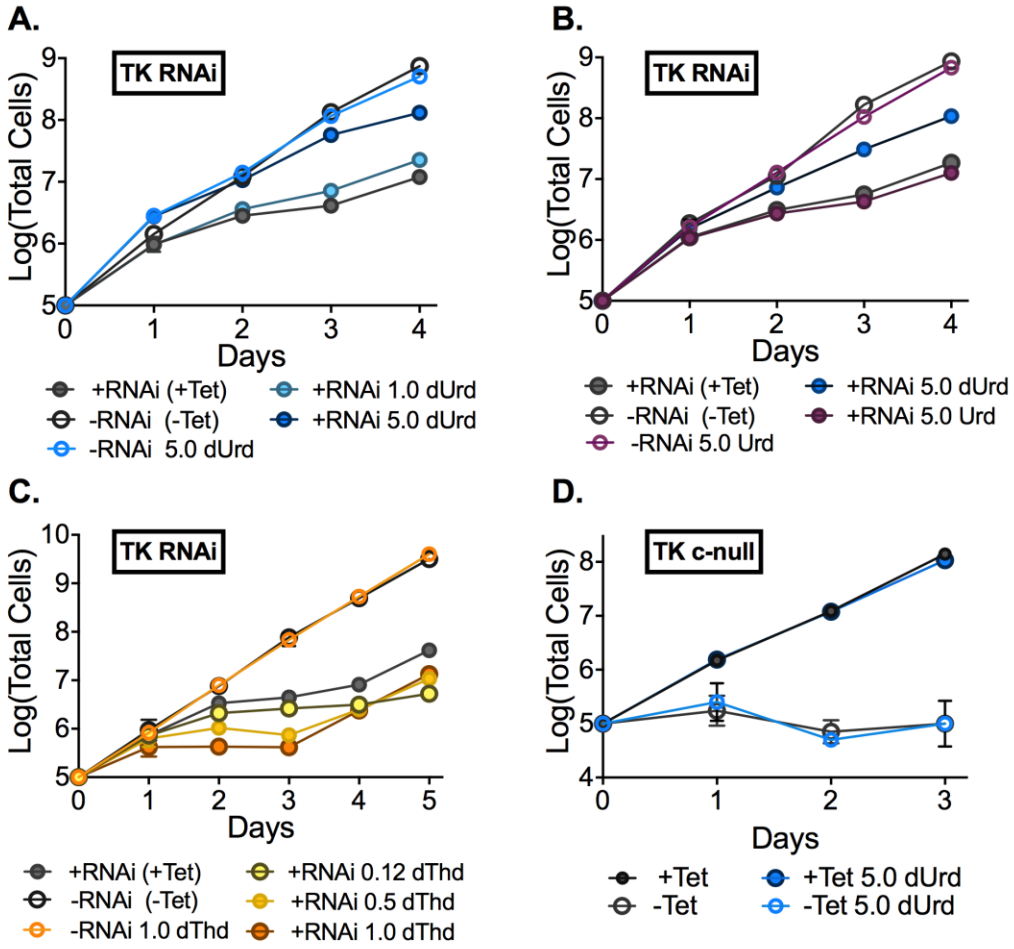

Figure 2.8. Treatment of *TK* RNAi cells grown minus Tet plus various nucleoside supplements. These are control studies for data reported in Fig. 2.7 to demonstrate that exogenous nucleosides don't effect growth of cells that are expressing TK. A. Cells were grown in normal serum based media plus 0, 1 or 5 mM dUrd in the absence of Tet. B. Cells were grown plus or minus 5 mM dUrd or Urd. C. Cells were grown plus 0, 0.12, 0.5 or 1.0 mM dThd. Error bars represent the standard deviation (SD) for biological triplicates.

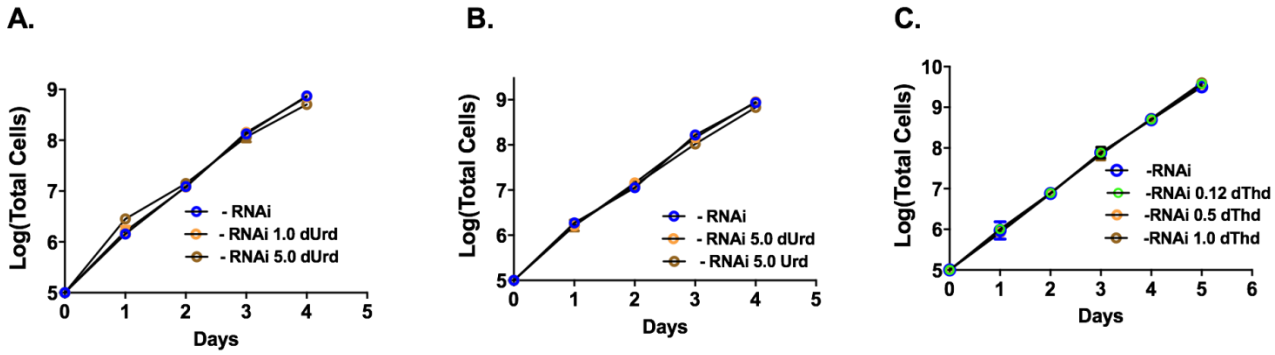

Figure 2.9. Uracil supplementation is unable to rescue loss of TK in TK c-null cells. A. Growth analysis of TK c-null cells (±Tet) in HMI-19 media supplemented with uracil (μM). Error bars represent the standard deviation (SD) for biological triplicates.

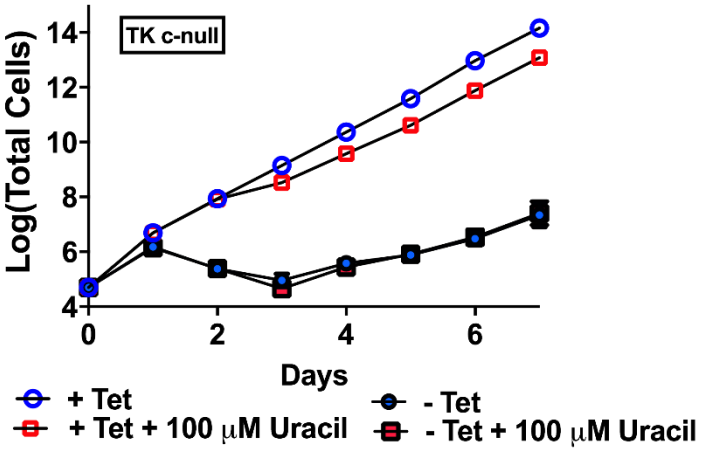

Figure 2.10. *Hs*DCTD rescues the growth defect in *Tb*TK RNAi and *Tb*TK null cell lines. A. Growth curves for *TK* RNAi cells or *TK* RNAi cells containing a Tet-regulated expression plasmid for *Hs*DCTD. Cell growth was monitored ±Tet for the indicated days. Error bars represent SD for triplicate biological replicates. Inset shows a Western blot of *Hs*DCTD expression ± Tet at 48 h. B. qPCR analysis of *Tb*TK mRNA expression in both the

TK RNAi cell line and the TK RNAi *Hs*DCTD rescue line (±Tet 48 h). Error bars represent SEM for triplicate data. Data were normalized to the -Tet control, which is in the background of a single allele TK knockout. C. Growth analysis of TK null cells expressing either FLAG-tagged *Tb*TK (c-null) or FLAG-tagged *Hs*DCTD under the control of the Tet promoter. Error bars represent SD for triplicate biological replicates. Inset shows western blot analysis of the *Hs*DCTD *TK* null cells 2 days and 5 days after Tet withdraw.

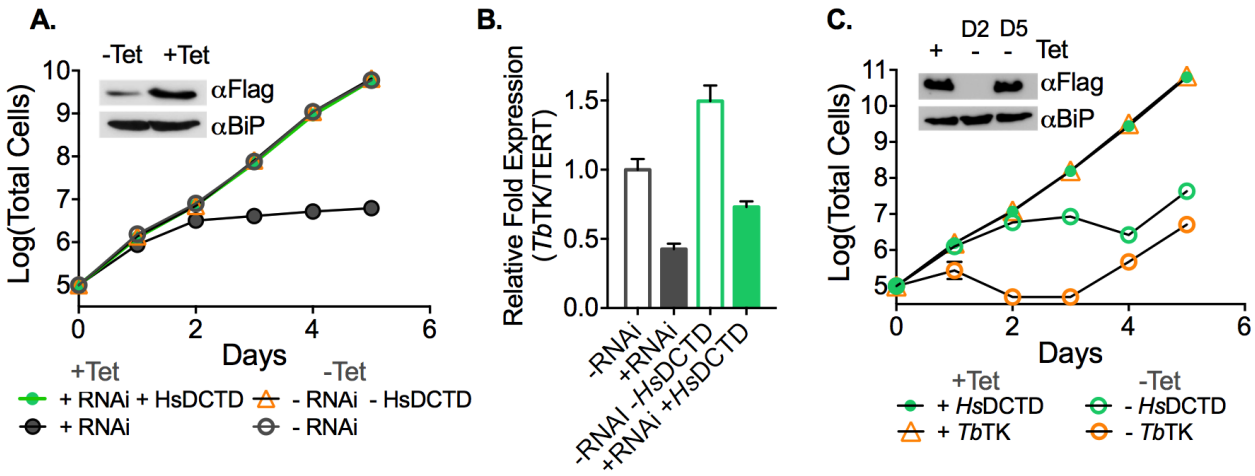

Figure 2.11. Metabolomic analysis of *TK* c-null cells. A. Detected pyrimidine and purine bases, nucleosides and nucleotides for cells grown in HMI-19 medium supplemented with normal serum (NS). The ratios (fold change) of metabolite levels in the absence of Tet for 24h compared to cells grown with Tet are plotted. B. HPAEC analysis of nucleotide sugars ±Tet at 24 h. C. Quantitation of dTTP by enzymatic assay ± Tet at 24 and 48 h for cell grown in HMI-19 supplemented with NS. D. Fold change of detected pyrimidine and purine bases, nucleosides and nucleotides ± Tet at 24 h for cells grown in HMI-19 medium supplemented with dialyzed serum (DS). E. Fold change of TCA intermediates ±Tet at 24 h for cells grown in HMI-19 medium supplemented with DS. Metabolites shown for C and D are from the

same experiment. All data were collected in biological triplicate and error bars represent the SEM calculated for the ±Tet ratio by Graph Pad Prism using the baseline-correction algorithm. For A, D and E, multiple T test analysis was performed in GraphPad Prism comparing the +Tet and -Tet conditions for each study. Statistical significance was determined without correction for multiple comparisons and without assuming a consistent standard deviation. For C, data were analyzed using one way ANOVA with Dunnett's multiple comparison test. Metabolites that showed a significant difference between the conditions are marked * $P<0.05$, ** $P<0.01$, *** $P<0.001$. Abbreviations are common nomenclature or have been previously defined except for CP, carbamoyl phosphate, R5P, ribose 5'-phosphate, 7m-guanosine, 7-methyl guanosine, succinate/m-malonic acid, succinate/methyl-malonic acid. Nicole Nishchan helped perform the HPAEC analysis of nucleotide sugars and Zeping Hu collected the metabolomics data.

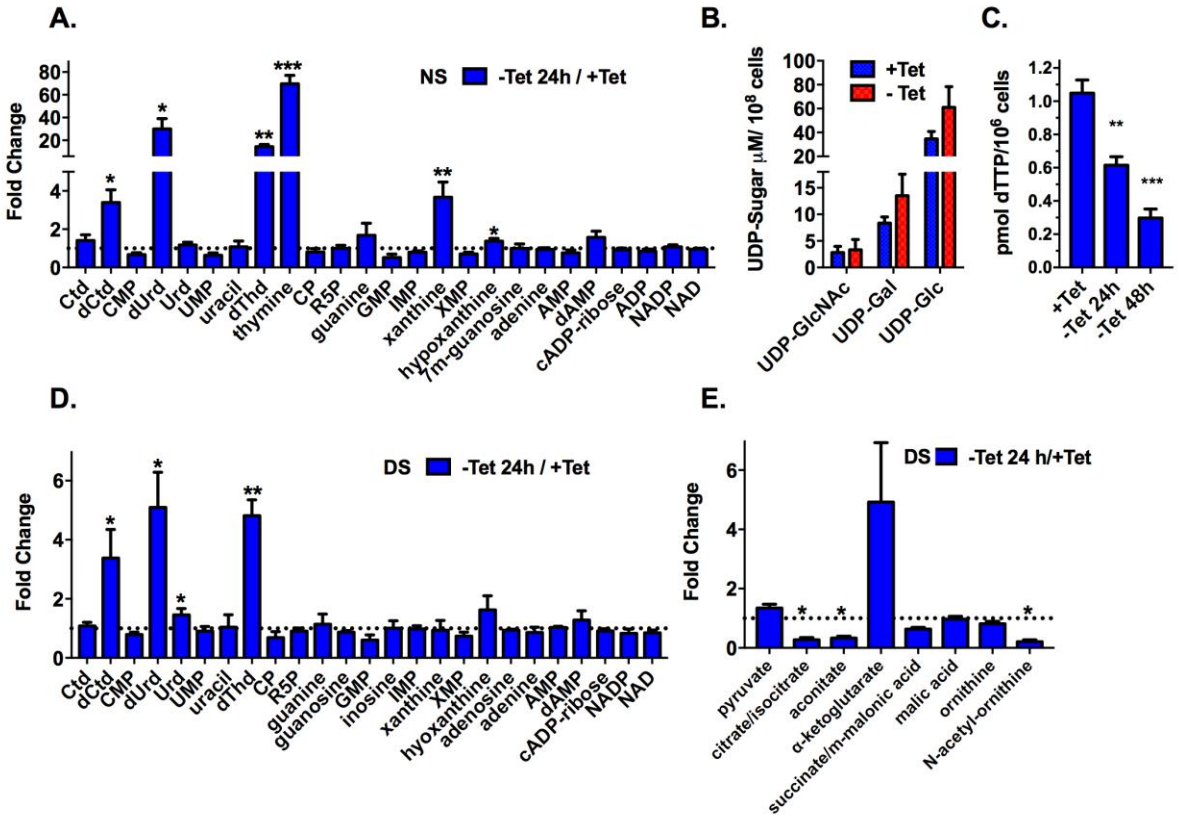

Figure 2.12. Metabolomic profiling of *TK* c-null cells. A-B. Heat maps represent average fold changes (-Tet 24hr/+Tet) in relative metabolite abundance. A) normal serum (NS); B) dialyzed serum (DS). For NS, pink indicates fold changes exceeding the scale (fold change > 10).

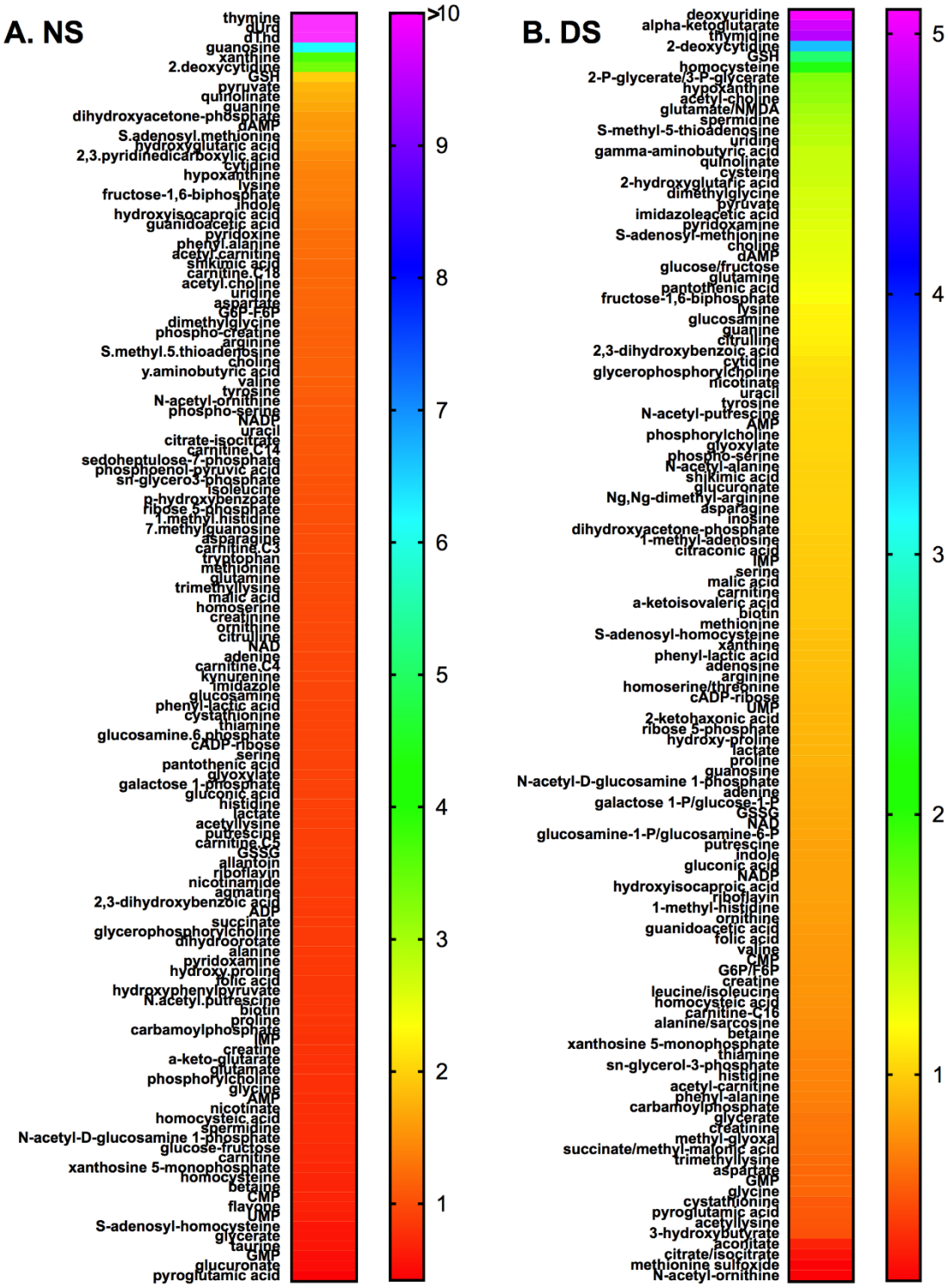
A. NS
thymine
dUrd
dThd
guanosine
xanthine
2.deoxycytidine
GSH
pyruvate
quinolinate
guanine
dihydroxyacetone-phosphate
dAMP
S.adenosyl.methionine
hydroxyglutaric acid
2,3.pyridinedicarboxylic acid
cytidine
hypoxanthine
lysine
fructose-1,6-biphosphate
indole
hydroxyisocaproic acid
guanidoacetic acid
pyridoxine
phenyl.alanine
acetyl.carnitine
shikimic acid
carnitine.C18
acetyl.choline
uridine
aspartate
G6P-F6P
dimethylglycine
phospho-creatine
arginine
S.methyl.5.thioadenosine
choline
y.aminobutyric acid
valine
tyrosine
N-acetyl-ornithine
phospho-serine
NADP
uracil
citrate-isocitrate
carnitine.C14
sedoheptulose-7-phosphate
phosphoenol-pyruvic acid
sn-glycero3-phosphate
isoleucine
p-hydroxybenzoate
ribose 5-phosphate
1.methyl.histidine
7.methylguanosine
asparagine
carnitine.C3
tryptophan
methionine
glutamine
trimethyllysine
malic acid
homoserine
creatinine
ornithine
citrulline
NAD
adenine
carnitine.C4
kynurenine
imidazole
glucosamine
phenyl-lactic acid
cystathionine
thiamine
glucosamine.6.phosphate
cADP-ribose
serine
pantothenic acid
glyoxylate
galactose 1-phosphate
gluconic acid
histidine
lactate
acetyllysine
putrescine
carnitine.C5
GSSG
allantoin
riboflavin
nicotinamide
agmatine
2,3-dihydroxybenzoic acid
ADP
succinate
glycerophosphorylcholine
dihydroorotate
alanine
pyridoxamine
hydroxy.proline
folic acid
hydroxyphenylpyruvate
N.acetyl.putrescine
biotin
proline
carbamoylphosphate
IMP
creatine
a-keto-glutarate
glutamate
phosphorylcholine
glycine
AMP
nicotinate
homocysteic.acid
spermidine
N-acetyl-D-glucosamine 1-phosphate
glucose-fructose
carnitine
xanthosine 5-monophosphate
homocysteine
betaine
CMP
flavone
UMP
S-adenosyl-homocysteine
glycerate
taurine
GMP
glucuronate
pyroglutamic acid
>10
9
8
7
6
5
4
3
2
1
B. DS
deoxyuridine
alpha-ketoglutarate
thymidine
2-deoxycytidine
GSH
homocysteine
2-P-glycerate/3-P-glycerate
hypoxanthine
acetyl-choline
glutamate/NMDA
spermidine
S-methyl-5-thioadenosine
uridine
gamma-aminobutyric acid
quinolinate
cysteine
2-hydroxyglutaric acid
dimethylglycine
pyruvate
imidazoleacetic acid
pyridoxamine
S-adenosyl-methionine
choline
dAMP
glucose/fructose
glutamine
pantothenic acid
fructose-1,6-biphosphate
lysine
glucosamine
guanine
citrulline
2,3-dihydroxybenzoic acid
cytidine
glycerophosphorylcholine
nicotinate
uracil
tyrosine
N-acetyl-putrescine
AMP
phosphorylcholine
glyoxylate
phospho-serine
N-acetyl-alanine
shikimic acid
glucuronate
Ng,Ng-dimethyl-arginine
asparagine
inosine
dihydroxyacetone-phosphate
1-methyl-adenosine
citraconic acid
IMP
serine
malic acid
carnitine
a-ketoisovaleric acid
biotin
methionine
S-adenosyl-homocysteine
xanthine
phenyl-lactic acid
adenosine
arginine
homoserine/threonine
cADP-ribose
UMP
2-ketohaxonic acid
ribose 5-phosphate
hydroxy-proline
lactate
proline
guanosine
N-acetyl-D-glucosamine 1-phosphate
adenine
galactose 1-P/glucose-1-P
GSSG
NAD
glucosamine-1-P/glucosamine-6-P
putrescine
indole
gluconic acid
NADP
hydroxyisocaproic acid
riboflavin
1-methyl-histidine
ornithine
guanidoacetic acid
folic acid
valine
CMP
G6P/F6P
creatine
leucine/isoleucine
homocysteic acid
carnitine-C16
alanine/sarcosine
betaine
xanthosine 5-monophosphate
thiamine
sn-glycerol-3-phosphate
histidine
acetyl-carnitine
phenyl-alanine
carbamoylphosphate
glycerate
creatinine
methyl-glyoxal
succinate/methyl-malonic acid
trimethyllysine
aspartate
GMP
glycine
cystathionine
pyroglutamic acid
acetyllysine
3-hydroxybutyrate
aconitate
citrate/isocitrate
methionine sulfoxide
N-acetyl-ornithine
5
4
3
2
1

Figure 2.13. Metabolomic profiling of *TK* c-null cells. Fold change (-Tet 24h/+Tet) as described in Fig. 2.11 for A, B) TCA cycle metabolites NS vs DS or for C, D) polyamines NS vs DS. Error bars represent SEM calculated from biological triplicate data. Metabolites that showed a significant difference between the conditions are marked * P<0.05, ** P<0.01. Statistical significance was calculated as described in Fig. 2.11.

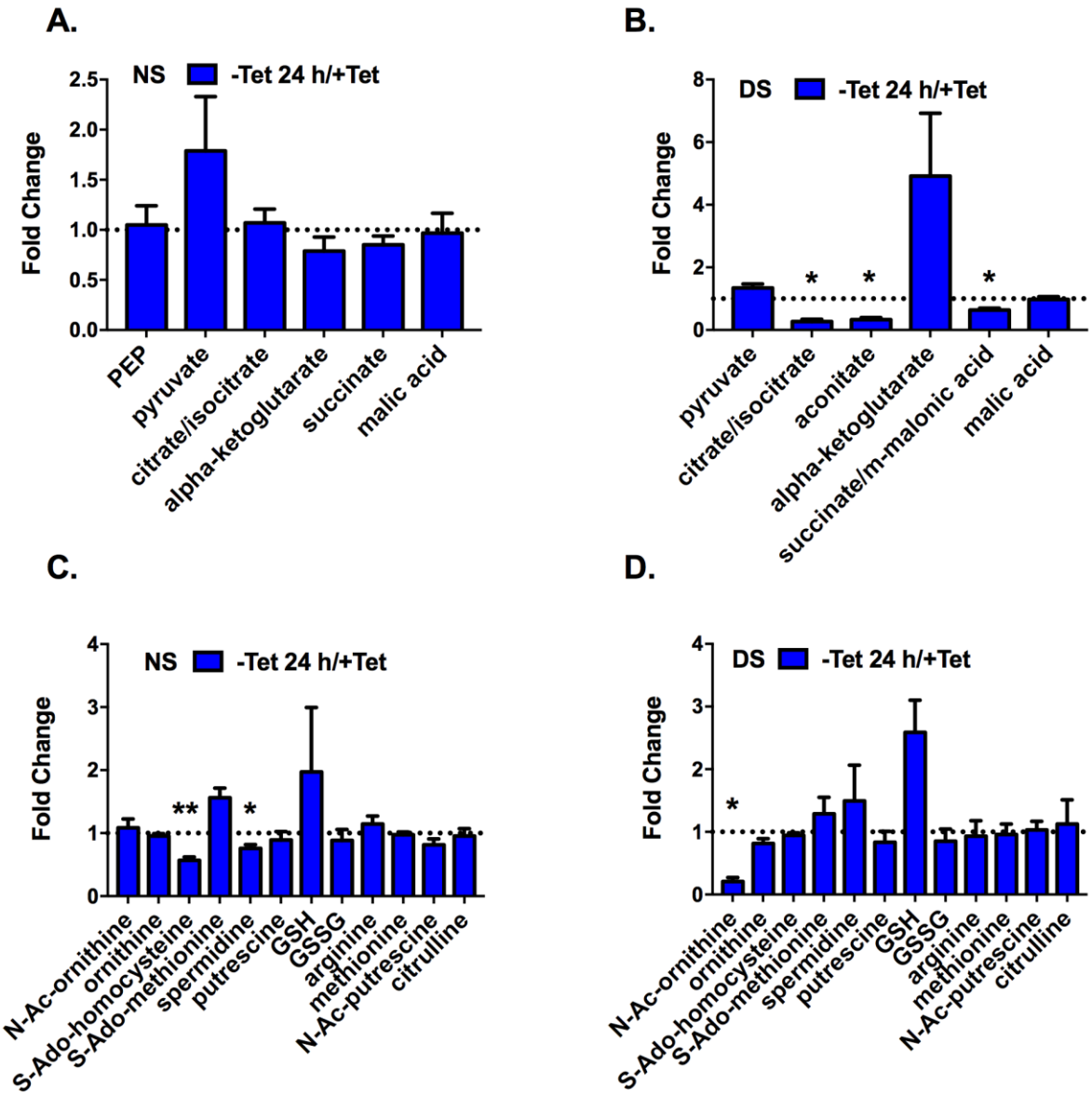

Figure 2.14. TK depletion in pyrimidine-free conditions resulted in perturbations of amino acid metabolism. A-B. Fold change (-Tet 24h/+Tet) in relative abundance of amino acids and related metabolites grown in NS and DS. Error bars represent SEM calculated from biological triplicate data and statistical analysis is as described in Fig. 2.11. and 2.12.

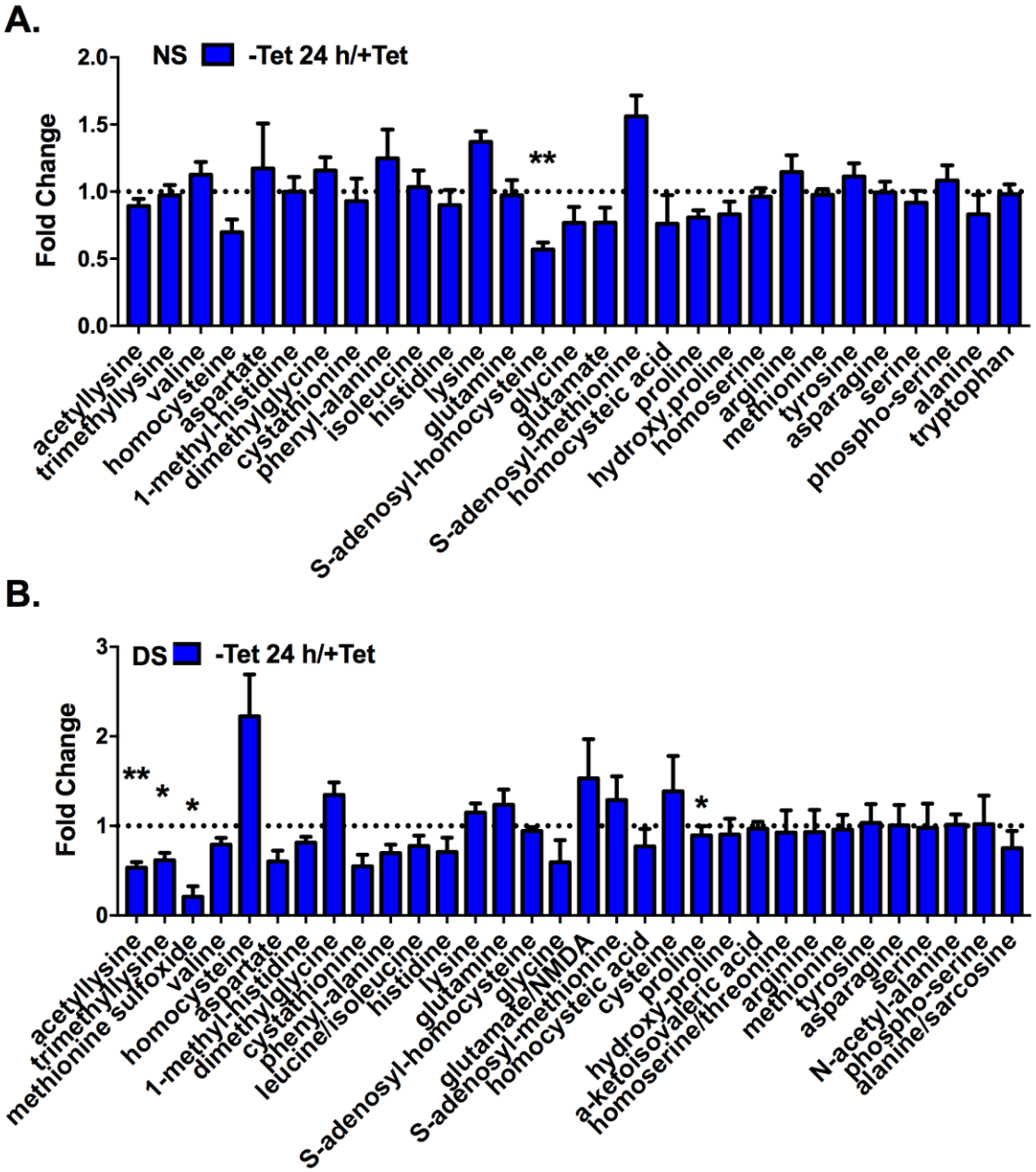

Figure 2.15. Deletion of the *T. brucei CDA* gene induces pyrimidine auxotrophy. A. Growth curves for *CDA* null cells grown in HMI-19 or HMI-19 media supplemented with 500 µM dThd. Cell growth was monitored for the indicated days. Error bars represent SD for triplicate biological replicates. B. qPCR analysis of CDA expression in wild-type SM and *CDA* null cells. Error bars represent SEM for triplicate data. C-E. Growth analysis of *CDA* null cells supplemented with dThd (C), dUrd (D) or uracil (E) over a range of concentrations at 48 h. Error bars represent the range for duplicate biological replicates. dThd and dUrd dose response curves were fitted to the Agonist vs response (three parameters) equation in GraphPad Prism (line represents the fit), to obtain ED_{50} for growth stimulation. ED_{50} = 20 µM (2.9 – 61) for dThd and 6.8 µM (3.8 – 13) for dUrd, where values in parenthesis represent the 95% confidence interval.

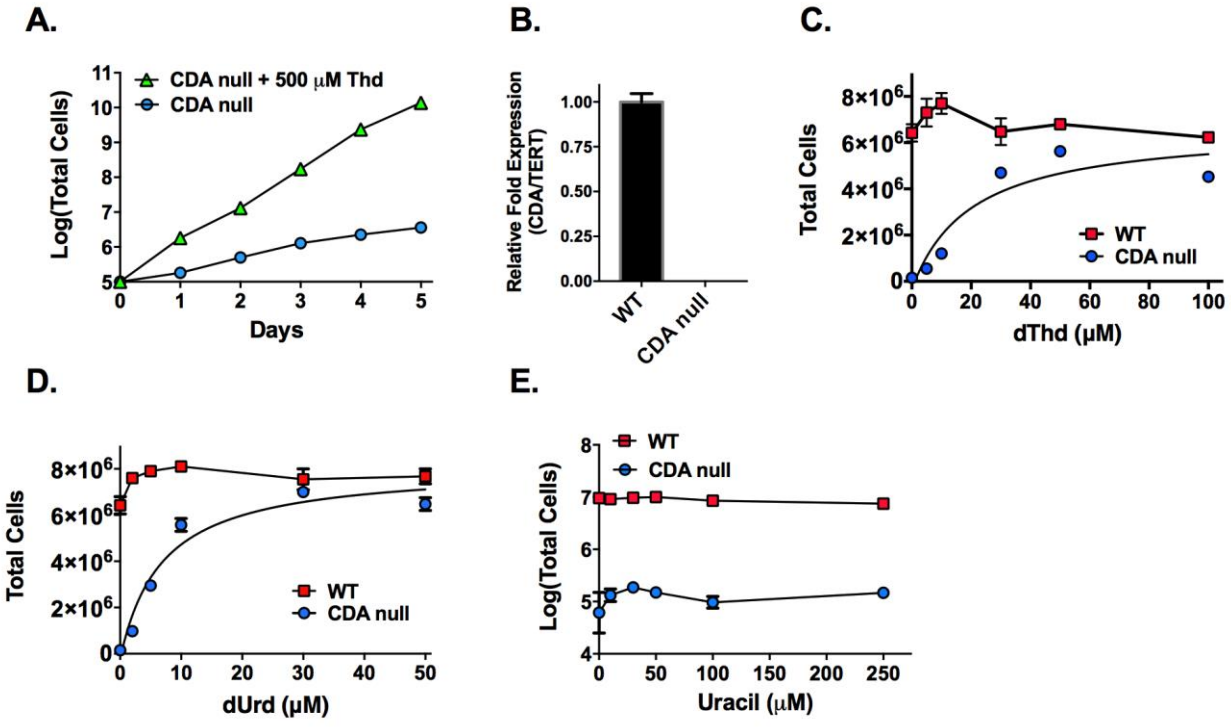

Figure 2.16. PCR analysis confirms replacement of *CDA* alleles with selectable markers. A. Amplification of the *CDA* locus using primers flanking the *CDA* 5' and 3' UTRs,

selectable markers, and *CDA* ORF. The *CDA* locus was amplified from genomic DNA extracted from *CDA* null and SM cells. The selectable markers were amplified from *CDA* null genomic DNA. The *CDA* gene was amplified from both SM and *CDA* null genomic DNA. B. The puromycin selection marker and *CDA* gene possessed similar sized PCR products. The PCR product corresponding to the amplified puromycin resistance gene contained a unique EcoRV restriction site, allowing for discrimination between the two PCR products.

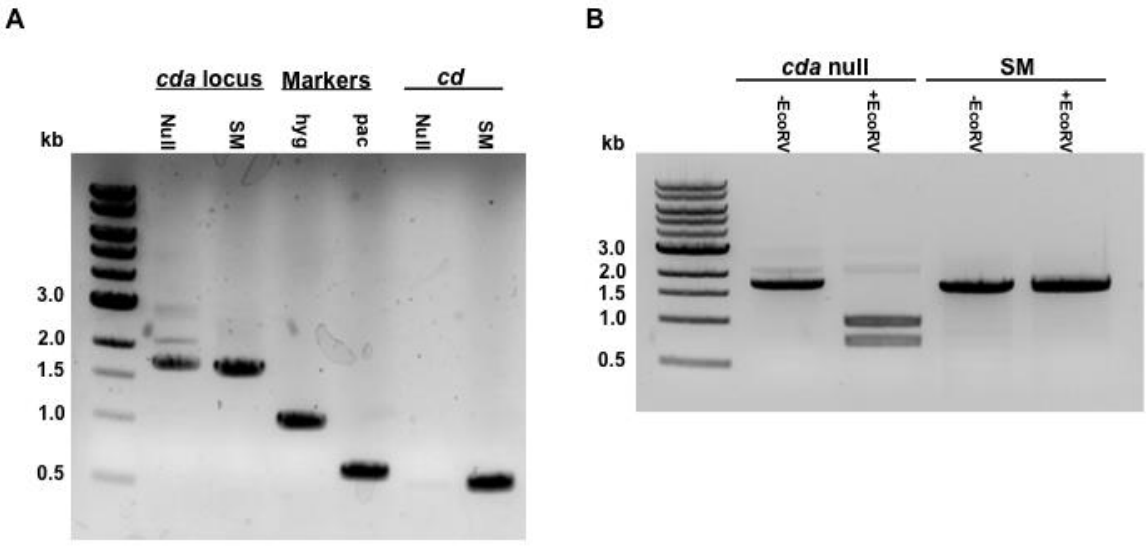

Figure 2.17. Metabolomic profiling of *CDA* null cells. Fold change in relative metabolite abundance comparing CDA null cells (-Thd 12h/+Thd) grown in serum-based media in the absence of Thd for 12 h versus cells grown in media supplemented with 0.5 mM Thd. Panels represent A) nucleotides B) polyamines C) amino acids and D) TCA cycle intermediates. Error bars represent SEM calculated from biological triplicate data. Metabolites that showed a significant difference between the conditions are marked * $P<0.05$, ** $P<0.01$. Statistical significance was calculated as described in Fig. 2.11.

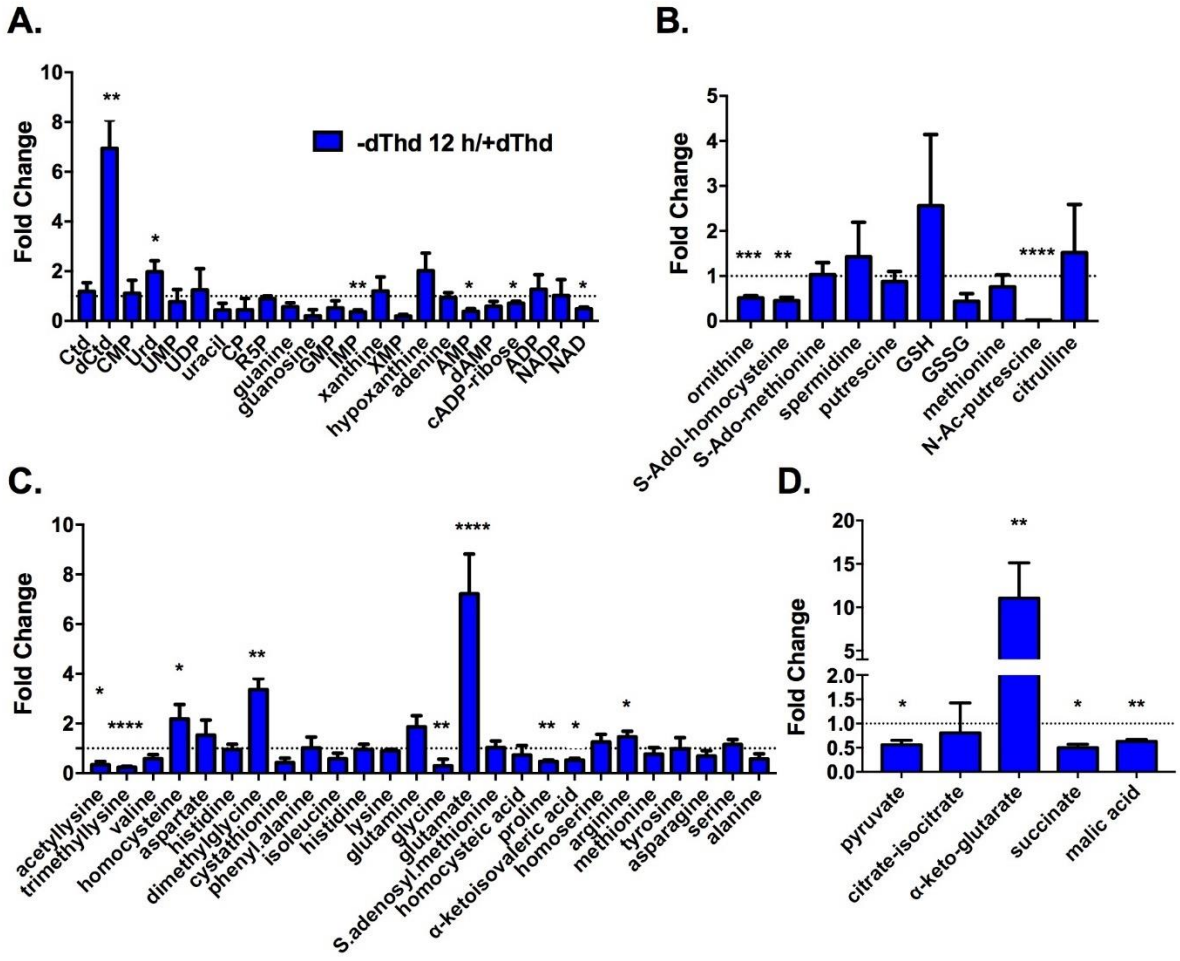

Figure 2.18. Metabolomic profiling of *CDA* null cells. Heat map represent average fold changes (-Thd 12hr/+Thd) in relative metabolite abundance. The presence of thymine in the +Thd treated cells is likely caused by contamination of the commercial Thd source with thymine. Cells colored gray represent a fold decrease greater than 10. Zeping Hu collected the metabolomic data.

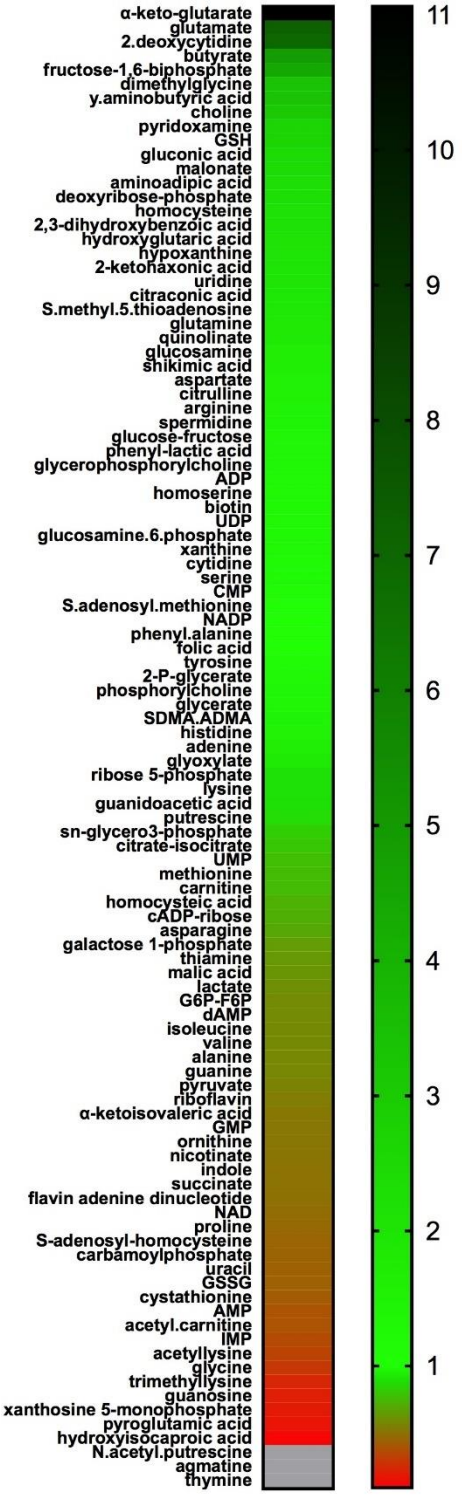
α-keto-glutarate
glutamate
2.deoxycytidine
butyrate
fructose-1,6-biphosphate
dimethylglycine
y.aminobutyric acid
choline
pyridoxamine
GSH
gluconic acid
malonate
aminoadipic acid
deoxyribose-phosphate
homocysteine
2,3-dihydroxybenzoic acid
hydroxyglutaric acid
hypoxanthine
2-ketohaxonic acid
uridine
citraconic acid
S.methyl.5.thioadenosine
glutamine
quinolinate
glucosamine
shikimic acid
aspartate
citrulline
arginine
spermidine
glucose-fructose
phenyl-lactic acid
glycerophosphorylcholine
ADP
homoserine
biotin
UDP
glucosamine.6.phosphate
xanthine
cytidine
serine
CMP
S.adenosyl.methionine
NADP
phenyl.alanine
folic acid
tyrosine
2-P-glycerate
phosphorylcholine
glycerate
SDMA.ADMA
histidine
adenine
glyoxylate
ribose 5-phosphate
lysine
guanidoacetic acid
putrescine
sn-glycero3-phosphate
citrate-isocitrate
UMP
methionine
carnitine
homocysteic acid
cADP-ribose
asparagine
galactose 1-phosphate
thiamine
malic acid
lactate
G6P-F6P
dAMP
isoleucine
valine
alanine
guanine
pyruvate
riboflavin
α-ketoisovaleric acid
GMP
ornithine
nicotinate
indole
succinate
flavin adenine dinucleotide
NAD
proline
S-adenosyl-homocysteine
carbamoylphosphate
uracil
GSSG
cystathionine
AMP
acetyl.carnitine
IMP
acetyllysine
glycine
trimethyllysine
guanosine
xanthosine 5-monophosphate
pyroglutamic acid
hydroxyisocaproic acid
N.acetyl.putrescine
agmatine
thymine
11
10
9
8
7
6
5
4
3
2
1

Figure 2.19. Sequence alignment of *T. brucei* YfbR-like 5'nucleotidase with representative eukaryotic and bacterial homologs. Sequences closest to the protein encoded by *T. brucei* Tb09.211.2190 were collected by BLAST against the RefSeq database, with HDDC2 being the closest representative in human. We generated a multiple sequence alignment with PROMALS-3D using the structures of human HDDC2 (4dmb), *E.coli* YfbR (2pau), *M.magnetotacticum* (3kh1), *P.furiosus* (1xx7), and *A.fulgidus* (1ynb); together with select HDDC2 homologs defined by HomoloGene and representative protists close to *T.brucei*. The HDDC2/YfbR sequences are ubiquitous, with representatives all three domains of life. Representatives are labeled to the left by PDB ID or NCBI accession, followed by species, and colored according to taxonomy: bacteria (blue labels), archaea (red labels), and eukaryota (animals black, fungi orange, plants green, and protists magenta). Secondary structures are indicated above the alignment, with H representing helix. Active site residues defined in YfbR (2pau) are invariant and are labeled above the alignment, including metal coordinating residues (H), nucleotide phosphate binding (P), nucleotide ribose binding, (R), and catalytic (C). Residue positions are highlighted according to conservation: including mainly hydrophobic (yellow) and small (gray) positions that dictate structure, and mainly polar (black) positions that dictate function. The YfbR structure (2pau) was of the E72A mutant enzyme so the alignment shows the residue as an Ala (red) even though the wild-type enzyme contains a Glu at this position. The alignment was performed by Lisa Kinch.

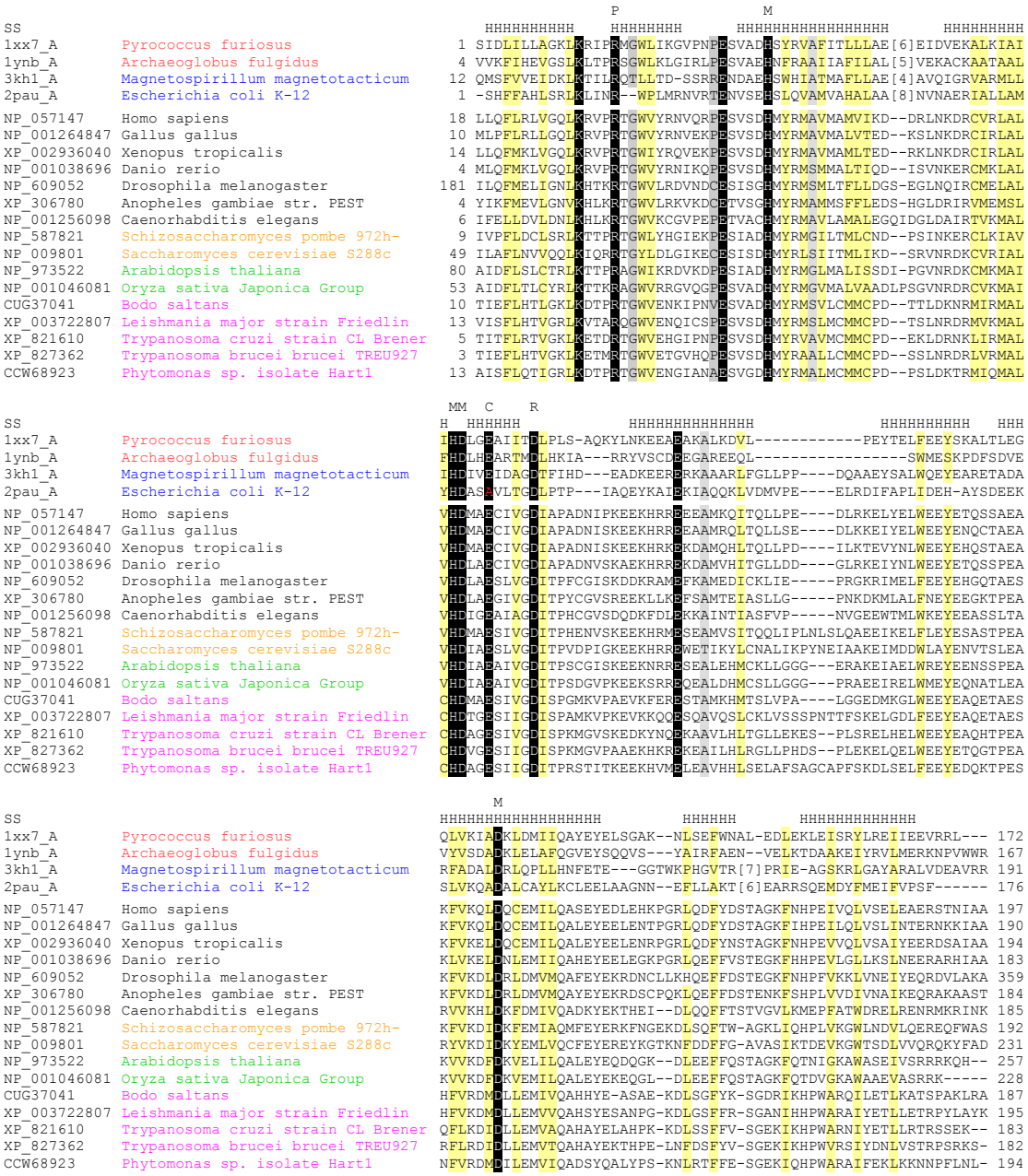
SS HHHHHHHHHH HHHHHHHH HHHHHHHHHHHHHHHHH HHHHHHHHH
1xx7_A Pyrococcus furiosus 1 SIDLILLAGKLKRIPRMGWLIKGVPNPPSVADHSYRVAFITLLLAE[6]EIDVEKALKIAI
1ynb_A Archaeoglobus fulgidus 4 VVKFIHEVGSLKLTPRSGWLKLGIRLPPSVAEHNFRAAIIAFILAL[5]VEKACKAATAAL
3kh1_A Magnetospirillum magnetotacticum 12 QMSFVVEIDKLKTILRQTLLTD-SSRRPNDAEHSWHIATMAFLLAE[4]AVQIGRVARMLL
2pau_A Escherichia coli K-12 1 -SHFFAHLSRLKLLINR--WPLMRNVRTPNVSEHSLQVAMVAHALAA[8]NVNAERIALLAM
NP_057147 Homo sapiens 18 LLQFLRLVGQLKRVPRTGWVYRNVQRPPSVSDHMYRMAVMAMVIKD--DRLNKDRCVRLAL
NP_001264847 Gallus gallus 10 MLPFLRLLGQLKRVPRTGWVYRNVEKPPSVSDHMYRMAVMALVTED--KSLNKDRCIRLAL
XP_002936040 Xenopus tropicalis 14 LLQFMKLVGQLKRVPRTGWIYRQVEKPPSVSDHMYRMAVMAMLTED--RKLNKDRCIRLAL
NP_001038696 Danio rerio 4 MLQFMKLVGQLKRVPRTGWVYRNIKQPPSVSDHMYRMSMMALTIQD--ISVNKERCMKLAL
NP_609052 Drosophila melanogaster 181 ILQFMELIGNLKHTKRTGWVLRDVNDCPSISGHMYRMSMLTFLLDGS-EGLNQIRCMELAL
XP_306780 Anopheles gambiae str. PEST 4 YIKFMEVLGNVKHLKRTGWVLRKVKDCPTVSGHMYRMAMMSFFLEDS-HGLDRIRVMEMSL
NP_001256098 Caenorhabditis elegans 6 IFELLDVLDNLKHLKRTGWVKCGVPEPPTVACHMYRMAVLAMALEGQIDGLDAIRTVKMAL
NP_587821 Schizosaccharomyces pombe 972h- 9 IVPFLDCLSRLKTTPRTGWLYHGIEKPPSIADHMYRMGILTMLCND--PSINKERCLKIAV
NP_009801 Saccharomyces cerevisiae S288c 49 ILAFLNVVQQLKIQRRTGYLDLGIKECPSISDHMYRLSIITMLIKD--SRVNRDKCVRIAL
NP_973522 Arabidopsis thaliana 80 AIDFLSLCTRLKTTPRAGWIKRDVKDPPSIADHMYRMGLMALISSDI-PGVNRDKCMKMAI
NP_001046081 Oryza sativa Japonica Group 53 AIDFLTLCYRLKTTKRAGWVRRGVQGPPSVADHMYRMGVMALVAADLPSGVNRDRCVKMAI
CUG37041 Bodo saltans 10 TIEFLHTLGKLKDTPRTGWVENKIPNVPSVADHMYRMSVLCMMCPD--TTLDKNRMIRMAL
XP_003722807 Leishmania major strain Friedlin 13 VISFLHTVGRLKVTARQGWVENQICSPPSVSDHMYRMSLMCMMCPD--TSLNRDRMVKMAL
XP_821610 Trypanosoma cruzi strain CL Brener 5 TITFLRTVGKLKETDRTGWVEHGIPNPPSVSDHMYRVAVMCMMCPD--EKLDRNKLIRMAL
XP_827362 Trypanosoma brucei brucei TREU927 3 TIEFLHTVGKLKETMRTGWVETGVHQPPSVSDHMYRAALLCMMCPD--SSLNRDRLVRMAL
CCW68923 Phytomonas sp. isolate Hart1 13 AISFLQTIGRLKDTPRTGWVENGIANAPSVGDHMYRMALMCMMCPD--PSLDKTRMIQMAL
SS H HHHHHH HHHHHHHHHHHHHH HHHHHHHHHH HHH
1xx7_A Pyrococcus furiosus IHDLGEAIITDLPLS-AQKYLNKEEAEAKALKDVL----------PEYTELFEEYSKALTLEG
1ynb_A Archaeoglobus fulgidus FHDLHEARTMDLHKIA---RRYVSCDEEGAREEQL----------SWMESKPDFSDVE
3kh1_A Magnetospirillum magnetotacticum IHDIVEIDAGDTFIHD---EADKEERERKAAARLFGLLPP----DQAAEYSALWQEYEARETADA
2pau_A Escherichia coli K-12 YHDASEVLTGDLPTP---IAQEYKAIEKIAQQKLVDMVPE----ELRDIFAPLIDEH-AYSDEEK
NP_057147 Homo sapiens VHDMAECIVGDIAPADNIPKEEKHRREEEAMKQITQLLPE----DLRKELYELWEEYETQSSAEA
NP_001264847 Gallus gallus VHDMAECIVGDIAPADNISKEEKHRREEAAMRQLTQLLSE----DLKKEIYELWEEYENQCTAEA
XP_002936040 Xenopus tropicalis VHDMAECIVGDIAPADNISKEEKHRKEKDAMQHLTQLLPD----ILKTEVYNLWEEYEHQSTAEA
NP_001038696 Danio rerio VHDLAECIVGDIAPADNVSKAEKHRREKDAMVHITGLLDD----GLRKEIYNLWEEYETQSSPEA
NP_609052 Drosophila melanogaster VHDLAESLVGDITPFCGISKDDKRAMEFKAMEDICKLIE-----PRGKRIMELFEEYEHGQTAES
XP_306780 Anopheles gambiae str. PEST VHDLAEGIVGDITPYCGVSREEKLLKEFSAMTEIASLLG-----PNKDKMLALFNEYEEGKTPEA
NP_001256098 Caenorhabditis elegans VHDIGEAIAGDITPHCGVSDQDKFDLEKKAINTIASFVP-----NVGEEWTMLWKEYEEASSLTA
NP_587821 Schizosaccharomyces pombe 972h- VHDMAESIVGDITPHENVSKEEKHRMESEAMVSITQQLIPLNLSLQAEEIKELFLEYESASTPEA
NP_009801 Saccharomyces cerevisiae S288c VHDIAESLVGDITPVDPIGKEEKHRREWETIKYLCNALIKPYNEIAAKEIMDDWLAYENVTSLEA
NP_973522 Arabidopsis thaliana VHDIAEAIVGDITPSCGISKEEKNRRESEALEHMCKLLGGG---ERAKEIAELWREYEENSSPEA
NP_001046081 Oryza sativa Japonica Group VHDIAEAIVGDITPSDGVPKEEKSRREQEALDHMCSLLGGG---PRAEEIRELWMEYEQNATLEA
CUG37041 Bodo saltans CHDMAESIVGDISPGMKVPAEVKFEREETAMKHMTSLVPA----LGGEDMKGLWEEYEAQETAES
XP_003722807 Leishmania major strain Friedlin CHDTGESIIGDISPAMKVPKEVKKQQESQAVQSLCKLVSSSPNTTFSKELGDLFEEYEAQETAES
XP_821610 Trypanosoma cruzi strain CL Brener CHDAGESIVGDISPKMGVSKEDKYNQEKAAVLHLTGLLEKES--PLSRELHELWEEYEAQHTPEA
XP_827362 Trypanosoma brucei brucei TREU927 CHDVGESIIGDISPKMGVPAAEKHKREKEAILHLRGLLPHDS--PLEKELQELWEEYETQGTPEA
CCW68923 Phytomonas sp. isolate Hart1 CHDAGESIIGDITPRSTITKEEKHVMELEAVHHLSELAFSAGCAPFSKDLSELFEEYEDQKTPES
SS HHHHHHHHHHHHHHHHHH HHHHHH HHHHHHHHHHHHH
1xx7_A Pyrococcus furiosus QLVKIADKLDMIIQAYEYELSGAK--NLSEFWNAL-EDLEKLEISRYLREIIEEVRRL--- 172
1ynb_A Archaeoglobus fulgidus VYVSDADKLELAFQGVEYSQQVS---YAIRFAEN--VELKTDAAKEIYRVLMERKNPVWWR 167
3kh1_A Magnetospirillum magnetotacticum RFADAIDRLQPLLHNFETE---GGTWKPHGVTR[7]PRIE-AGSKRLGAYARALVDEAVRR 191
2pau_A Escherichia coli K-12 SLVKQADALCAYLKCLEELAAGNN--EFLLAKT[6]EARRSQEMDYFMEIFVPSF------ 176
NP_057147 Homo sapiens KFVKQIDQCEMILQASEYEDLEHKPGRLQDFYDSTAGKFNHPEIVQLVSELEAERSTNIAA 197
NP_001264847 Gallus gallus KFVKQIDQCEMILQALEYEELENTPGRLQDFYDSTAGKFIHPEILQLVSLINTERNKKIAA 190
XP_002936040 Xenopus tropicalis KFVKELDQCEMILQALEYEELENRPGRLQDFYNSTAGKFNHPEVVQLVSAIYEERDSAIAA 194
NP_001038696 Danio rerio KLVKEIDNLEMIIQAHEYEELEGKPGRLQEFFVSTEGKFHHPEVLGLLKSLNEERARHIAA 183
NP_609052 Drosophila melanogaster KFVKDIDRLDMVMQAFEYEKRDNCLLKHQEFFDSTEGKFNHPFVKKLVNEIYEQRDVLAKA 359
XP_306780 Anopheles gambiae str. PEST KFVKDIDRLDMVMQAYEYEKRDSCPQKLQEFFDSTENKFSHPLVVDIVNAIKEQRAKAAST 184
NP_001256098 Caenorhabditis elegans RVVKHIDKFDMIVQADKYEKTHEI--DLQQFFTSTVGVLKMEPFATWDRELRENRMKRINK 185
NP_587821 Schizosaccharomyces pombe 972h- KFVKDIDKFEMIAQMFEYERKFNGEKDLSQFTW-AGKLIQHPLVKGWLNDVLQEREQFWAS 192
NP_009801 Saccharomyces cerevisiae S288c RYVKDIDKYEMLVQCFEYEREYKGTKNFDDFFG-AVASIKTDEVKGWTSDLVVQRQKYFAD 231
NP_973522 Arabidopsis thaliana KVVKDFDKVELILQALEYEQDQGK--DLEEFFQSTAGKFQTNIGKAWASEIVSRRRKQH-- 257
NP_001046081 Oryza sativa Japonica Group KVVKDFDKVEMILQALEYEKEQGL--DLEEFFQSTAGKFQTDVGKAWAAEVASRRK----- 228
CUG37041 Bodo saltans HFVRDMDLLEMIVQAHHYE-ASAE-KDLSGFYK-SGDRIKHPWARQILETLKATSPAKLRA 187
XP_003722807 Leishmania major strain Friedlin HFVKDMDLLEMVVQAHSYESANPG-KDLGSFFR-SGANIHHPWARAIYETLLETRPYLAYK 195
XP_821610 Trypanosoma cruzi strain CL Brener QFLKDIDLLEMVAQAHAYELAHPK-KDLSSFFV-SGEKIKHPWARNIYETLLRTRSSEK-- 183
XP_827362 Trypanosoma brucei brucei TREU927 RFLRDIDLLEMVTQAHAYEKTHPE-LNFDSFYV-SGEKIKHPWVRSIYDNLVSTRPSRKS- 182
CCW68923 Phytomonas sp. isolate Hart1 NFVRDMDILEMVIQADSYQALYPS-KNLRTFFE-SGEKIQHPWARAIFEKLKKNNPFLNL- 194

Figure 2.20. Steady-state kinetic analysis of *T. brucei* YfbR-like 5'-nucleotidase. A. Metal ion dependence. dCMP (1 mM) was used as the substrate and metal concentrations are noted on the figure. B. Substrate preference. Substrate concentrations were 1 mM and these assays were run in the presence of 0.5 mM Co^{+2}. The < symbol on the graph indicates that the activity was below the level of detection. Data were collected in triplicate and error bars represent the SD of the mean.

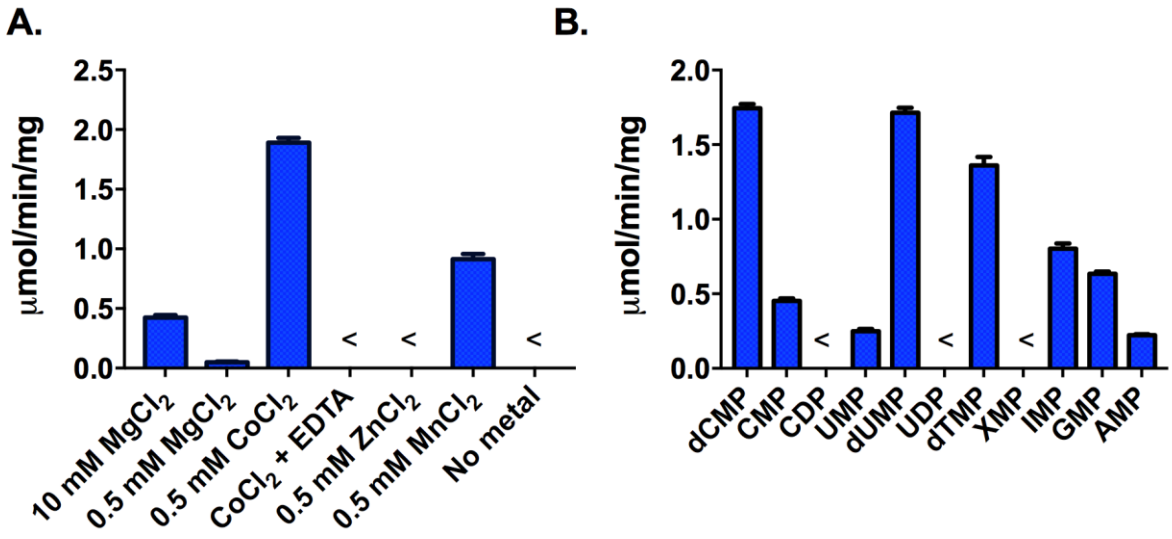

Figure 2.21. Venn diagram showing the distribution of TK, DCTD and dCTP deaminase in representative protists and higher eukaryotes. The overlapping regions represent organisms that possess both of the indicated genes.

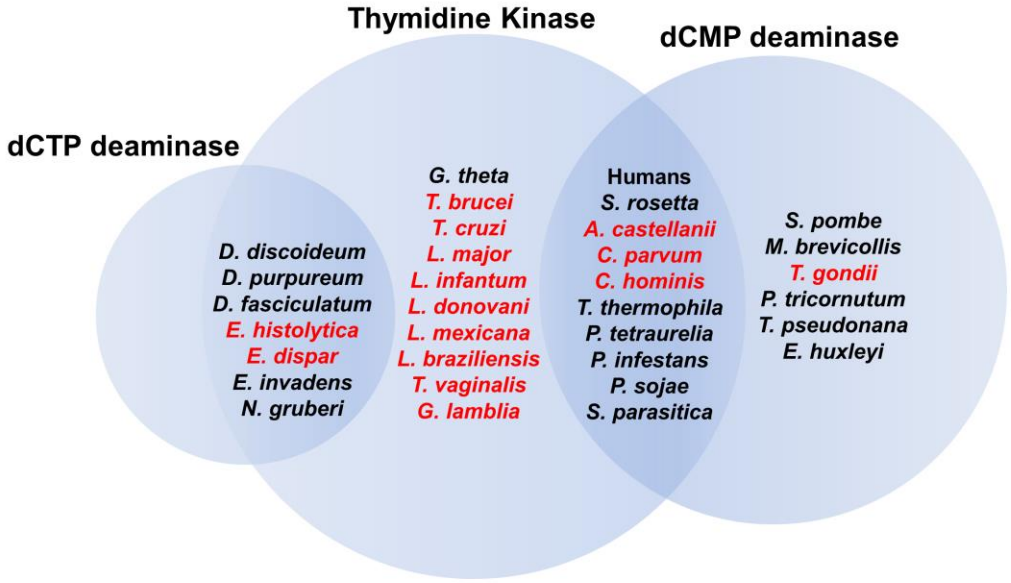

Table 2.1. PCR and cloning primers. List of cloning primers and corresponding sequences (5'-3') used throughout the study. The primer names contain information regarding their target, restriction sites, and functions.

#	Primer name	Sequence (5' to 3')
1	*Tb* TK 5' UTR forward	cggaagagttctttgtgctttgtag
2	*Tb* TK 3' UTR reverse	ccttcaggttcgtgtgaatgttcttc
3	*Tb* TK 5' UTR reverse (HYG)	ggtgagttcaggctttttcatttgcaatgttgagatgttggtgattcctgtcg
4	*Tb* TK 3' UTR forward (HYG)	gtccgagggcaaaggaatagtgccaggtgtactattgcgcaacg
5	*Tb* TK 5' UTR reverse (PAC)	gtgggcttgtactcggtcatttgcaatgttgagatgttgg
6	*Tb* TK 3' UTR forward (PAC)	gacccgcaagcccggtgcctgatgccaggtgtactattgc
7	*Tb* TK fusion forward	ctaactgagaagctcatcctttc
8	*Tb* TK fusion reverse	ccaaaggtgtacggctacgataagg
9	HYG forward	atgaaaaagcctgaactcacc
10	HYG reverse	ctattcctttgccctcggac
11	PAC forward	atgaccgagtacaagcccac
12	PAC reverse	tcaggcaccgggcttgcgggt c
13	*Tb* TK HindIII NT-FLAG forward	gctaaagcttatggactacaaagacgacgacgacaaacacgacggagatggcaat
14	*Tb* TK BamHI reverse	tagcggatccctaagtagtatcaacggccatttg
15	*Tb* TK 3' UTR RNAi forward	ttggttcgttacttttcccgagg
16	*Tb* TK 3' UTR RNAi reverse	accttgacaagcgtttcaccac
17	*Tb* TK ORF qPCR reverse	acatgtacttggctgtgtgc
18	*Tb* TK ORF qPCR reverse	atgtcttctgcgcatcaacg
19	*Tb* TK HindIII forward	gctaaagcttatgcacgacggagatggcaat
20	*Tb* TK BamHI AU1 reverse	tagcggatcctcatttgtcgtcgtcgtcttgtagtcagtagtatcaacggccatttg
21	*Hs* TK HindIII forward	gctaaagcttatgtcgtgtatcaatctcccaac
22	*Hs* TK BamHI FLAG reverse	tagcggatccctatttgtcgtcgtcgtcttgtagtcgtttgctgggctacactggag
23	*Tb* TK E286A forward	gtgatcgcggtggatgccggccaatttttcctgg
24	*Tb* TK E286A reverse	ccaggaaaaaattggccggcatccaccgcgatcac
25	*Hs* TK K32I forward	ccaatgttttccggcatctctaccgaacttatgcg
26	*Hs* TK K32 reverse	cgcataagttcggtagagatgccggaaaacattgg
27	*Hsv* TK forward	gctaaagcttatggcctcgtaccccggcca tc
28	*Hsv* TK reverse	tagcggatcctcagttagcctcccccatctcccgggcaaac
29	CDA 5' UTR forward	gaggcgcaaataggctggttgtgc
30	CDA 3' UTR reverse	cggtataataagcagcagcaaaag
31	CDA 5' UTR reverse (HYG)	ggtgagttcaggctttttcattgtgacgcgatgcttctccc
32	CDA 3' UTR forward (HYG)	gtccgagggcaaaggaataggtaaacggtttctgaggggggcg
33	CDA 5' UTR reverse (PAC)	gtgggtttatactcggtcattgtgacgcgatgcttctccc
34	CDA 3' UTR forward (PAC)	gactcgaaagccaggtgcctaagtaaacggtttctgaggggggcg
35	PAC (optimized) forward	atgaccgagtataaacccacag
36	PAC (optimized) reverse	ttaggcacctggctttcgagtc
37	CDA fusion forward	gcgaatacgcgaaaggttatggg
38	CDA fusion reverse	gaatcgcgggaaagttgctgcgg
39	CDA ORF qPCR forward	tgaagaccggttgcttgaag
40	CDA ORF qPCR reverse	tggacagtaacttcgctggtg
41	*Hs* DCTD HindIII FLAG forward	gctaaagcttatggactacaaagacgacgacgacaaaagtgaagtttcctgcaagaaacg
42	*Hs* DCTD BamHI reverse	tagcggatccctactgcaacttttgactcggtctg
43	dTTP assay oligo 1	ttattattattattaggcggtggaggcgg
44	dTTP assay oligo 2	ccgcctccaccgcc
45	Nucleotidase BsaI forward	gcggtctcaaggtatggacaccatcgaattcctgc
46	Nucleotidase XbaI reverse	gctctagattagctcttacggctcggacggg

Table 2.2. 5'-nucleotidase PFAM domain representatives. Representative [1]PFAM family structure or [2]representative homologous structure identified by HHPRED. This analysis was performed by Lisa Kinch and Nick Grishin.

Entry	Gene	EC	Pfam ID	PFAM Family	PDB ID	ECOD H
P15309	ACPP	3.1.3.5	PF00328	His_Phos_2	1rpa[1]	Phosphoglycerate mutase-like
P0A840	surE	3.1.3.5	PF01975	SurE	1l5x[1]	SurE-like/CoA-transfer-ase family (CaiB/BaiF)
P21589	NT5E	3.1.3.5	PF00149; (PF02872)	Metallophos; (5_nucleotid_C)	1ush[1]	Metallo-dependent phosphatases
P49902	NT5C2	3.1.3.5	PF05761	5_nucleotid	2bde[1]	HAD domain-related
Q9H0P0	NT5C3A	3.1.3.5	PF05822	UMPH-1	2bdu[1]	HAD domain-related
Q9BXI3	NT5C1A	3.1.3.5	PF06189	5-nucleotidase	2b82[2]	HAD domain-related
P0AF24	nagD	3.1.3.5	PF13344	Hydrolase_6	5aes[1]	HAD domain-related
P0A8Y1	yjjG	3.1.3.5	PF13419	Hydrolase_2	4eek[1]	HAD domain-related
P76491	yfbR	3.1.3.89	PF13023	HD_3	3kh1[1]	HD-domain/PDEase-like

Table 2.3. *T. brucei* sequences with identified 5'nucleotidase signatures

Accession	Annotation	Tb gene locus	CDD ID	E-value	Fold group
XP_844652.1	serine/threonine protein phosphatase PP1	Tb927.4.5030	249630	3.0E-31	metallophosphatase
XP_847568.1	serine/threonine protein phosphatase PP1	Tb927.8.7390	249630	4.0E-31	metallophosphatase
XP_828883.1	serine/threonine protein phosphatase catalytic subunit	Tb11.01.0450	249630	4.0E-29	metallophosphatase
XP_843718.1	serine/threonine-protein phosphatase	Tb927.3.1240	249630	5.0E-28	metallophosphatase

XP_829256.1	protein phosphatase 4 catalytic subunit	Tb11.01.3770	249630	6.0E-27	metallophosphatase
XP_844512.1	serine/threonine-protein phosphatase PP1	Tb927.4.3620	249630	2.0E-25	metallophosphatase
XP_844513.1	serine/threonine-protein phosphatase PP1	Tb927.4.3630	249630	2.0E-25	metallophosphatase
XP_844514.1	serine/threonine-protein phosphatase PP1	Tb927.4.3640	249630	2.0E-25	metallophosphatase
XP_829753.1	protein phosphatase 2A catalytic subunit	Tb11.01.8740	249630	3.0E-25	metallophosphatase
XP_844506.1	serine/threonine protein phosphatase PP1	Tb927.4.3560	249630	1.0E-24	metallophosphatase
XP_845108.1	serine/threonine protein phosphatase	Tb927.5.4380	249630	2.0E-22	metallophosphatase
XP_827850.1	serine/threonine protein phosphatase type 5	Tb10.05.0110	249630	2.0E-22	metallophosphatase
XP_844511.1	serine/threonine-protein phosphatase PP1	Tb927.4.3610	249630	2.0E-22	metallophosphatase
XP_001219099.1	Ser/Thr protein phosphatase	Tb927.1.4050	249630	6.0E-22	metallophosphatase
XP_829310.1	serine/threonine protein phosphatase	Tb11.01.4320	249630	2.0E-21	metallophosphatase
XP_803443.1	serine/threonine protein phosphatase	Tb09.160.0480	249630	1.0E-20	metallophosphatase
XP_844337.1	serine/threonine protein phosphatase	Tb927.4.1870	249630	2.0E-20	metallophosphatase
XP_822896.1	serine/threonine protein phosphatase	Tb10.70.0250	249630	6.0E-18	metallophosphatase
XP_846950.1	hypothetical protein	Tb927.8.1130	249630	7.0E-18	metallophosphatase
XP_828574.1	protein phosphatase	Tb11.02.2630	249630	1.0E-17	metallophosphatase
XP_951632.1	DNA repair protein	Tb927.2.4390	249630	6.0E-16	metallophosphatase
XP_822888.1	serine/threonine protein phosphatase 2b catalytic subunit A2	Tb10.70.0350	249630	2.0E-15	metallophosphatase
XP_845187.1	serine/threonine protein phosphatase	Tb927.6.640	249630	3.0E-13	metallophosphatase
XP_844583.1	serine/threonine protein phosphatase	Tb927.4.4330	249630	6.0E-12	metallophosphatase
XP_847629.1	diadenosine tetraphosphatase	Tb927.8.8040	249630	5.0E-11	metallophosphatase

XP_845580.1	serine/threonine protein phosphatase	Tb927.6.4630	249630	3.0E-10	metallophosphatase
XP_844887.1	hypothetical protein	Tb927.5.2130	249630	5.0E-09	metallophosphatase
XP_845198.1	serine/threonine protein phosphatase	Tb927.6.750	249630	3.0E-08	metallophosphatase
XP_823252.1	hypothetical protein	Tb10.406.0620	249630	1.0E-04	metallophosphatase
XP_001218808.1	hypothetical protein	Tb927.1.1050	249630	2.0E-04	metallophosphatase
XP_844261.1	hypothetical protein	Tb927.4.1110	249630	1.0E-03	metallophosphatase
XP_845245.1	hypothetical protein	Tb927.6.1230	249630	2.0E-03	metallophosphatase
XP_829485.1	vacuolar sorting protein	Tb11.01.5900	249630	2.0E-03	metallophosphatase
XP_829370.1	membrane-bound acid phosphatase 1 precursor	Tb11.01.4701	249773	4.0E-38	Histidine Phosphatase
XP_822949.1	membrane-bound acid phosphatase 2	Tb10.6k15.3560	249773	3.0E-31	Histidine Phosphatase
XP_822937.1	acid phosphatase	Tb10.6k15.3720	249773	7.0E-24	Histidine Phosphatase
XP_829237.1	membrane-bound acid phosphatase	Tb11.01.3610	249773	1.0E-08	Histidine Phosphatase
XP_828374.1	glycerolphosphate mutase	Tb11.02.0440	249773	2.0E-06	Histidine Phosphatase
XP_829098.1	phosphoglycerate mutase-like protein	Tb11.01.2110	249773	3.0E-04	Histidine Phosphatase
XP_828373.1	hypothetical protein	Tb11.02.0430	249773	6.0E-04	Histidine Phosphatase
XP_822699.1	fructose-6-phosphate2-kinase	Tb10.70.2700	249773	4.0E-03	Histidine Phosphatase
XP_828515.1	hypothetical protein	Tb11.02.1940	249773	4.0E-03	Histidine Phosphatase
XP_829590.1	hypothetical protein	Tb11.v4.0008	147785	6.0E-03	HAD domain-related
XP_847580.1	p-nitrophenylphosphatase	Tb927.8.7510	257673	2.0E-23	HAD domain-related
XP_827334.1	hypothetical protein	Tb09.211.1880	257673	5.0E-23	HAD domain-related
XP_828918.1	haloacid dehalogenase-like hydrolase	Tb11.01.0120	257673	6.0E-05	HAD domain-related
XP_828367.1	hypothetical protein	Tb11.02.0360	257673	1.0E-03	HAD domain-related
XP_823441.1	hypothetical protein	Tb10.389.1370	257673	3.0E-03	HAD domain-related
XP_844391.1	hypothetical protein	Tb927.4.2410	257744	5.0E-08	HAD domain-related
XP_829616.1	hypothetical protein	Tb11.01.7230	257744	1.0E-07	HAD domain-related
XP_827907.1	hypothetical protein	Tb10.61.2520	257744	2.0E-05	HAD domain-related
XP_846144.1	hypothetical protein	Tb927.7.5210	257744	4.0E-04	HAD domain-related
XP_845010.1	calcium-translocating P-type ATPase	Tb927.5.3400	257744	5.0E-04	HAD domain-related
XP_823353.1	hypothetical protein	Tb10.26.0480	257744	8.0E-04	HAD domain-related
XP_822666.1	hypothetical protein	Tb10.70.3070	257744	2.0E-03	HAD domain-related

XP_822886.1	phosphomannomutase	Tb10.70.0370	257744	3.0E-03	HAD domain-related
XP_829314.1	hypothetical protein	Tb11.01.4360	257744	3.0E-03	HAD domain-related
XP_828217.1	copper-transporting ATPase-like protein	Tb11.47.0023	257744	6.0E-03	HAD domain-related
XP_827362.1	hypothetical protein	Tb927.9.10830	257465	3.0E-38	HD-domain*

**Note: the homologs of Tb927.9.10830 (HD-domain) are present in T. cruzi:*

(XP_821610.1) Tc00.1047053508461.150 and L. donovani: (XP_003864995.1) LDBPK_354170

CHAPTER THREE

GMP SYNTHASE IS ESSENTIAL FOR VIABILITY ANDINFECTIVITY OF *T. BRUCEI* DESPITE A REDUNDANT PURINE SALVAGE PATHWAY

Introduction

The causative agent of human African trypanosomiasis, *Trypanosoma brucei*, lacks *de novo* purine biosynthesis and depends on purine salvage from the host. The purine salvage pathway is redundant and contains two routes to guanosine-5'-monophosphate (GMP) formation: conversion from xanthosine-5'-monophosphate (XMP) by GMP synthase (GMPS) or direct salvage of guanine by hypoxanthine-guanine phosphoribosyltransferase (HGPRT). We show recombinant *T. brucei* GMPS efficiently catalyzes GMP formation. Genetic knockout of GMPS in bloodstream parasites led to depletion of guanine nucleotide pools and was lethal. Growth of *gmps* null cells was only rescued by supraphysiological guanine concentrations (100 μM) or by expression of an extrachromosomal copy of GMPS. Hypoxanthine was a competitive inhibitor of guanine rescue, consistent with a common uptake/metabolic conversion mechanism. In mice, *gmps* null parasites were unable to establish an infection demonstrating that GMPS is essential for virulence and that plasma guanine is insufficient to support parasite purine requirements. These data validate GMPS as a potential therapeutic target for treatment of HAT. The ability to strategically inhibit key metabolic enzymes in the purine pathway unexpectedly bypasses its functional redundancy by exploiting both the nature of pathway flux and the limited nutrient environment of the parasite's extracellular niche. This work was performed in collaboration with Qiong Li, whom performed the protein purification, steady-state kinetics, cell cycle analysis, and cloning of the vectors related to the Tet regulated GMPS.

Materials and Methods

TriTrypDB gene accession numbers

GMPS, Tb927.7.2100; IMPDH, Tb927.10.16120; GMPR, Tb927.5.2080; ADSS, Tb927.11.3650; ADSL, Tb927.9.7550; HGPRT, Tb927.10.1470, Tb927.10.1400; XPRT, Tb927.10.1390; APRT, Tb927.7.1780, Tb927.7.1790; AD, Tb927.9.7180, Tb927.9.9740, Tb927.11.3850, Tb927.11.15750; NH, Tb927.3.2960; GDA, Tb927.5.4560; dihydroorotate dehydrogenase (DHODH), Tb927.5.3830 and telomerase reverse transcriptase (TERT), Tb927.11.10190.

GMPS protein expression, purification and assay

GMPS expression and purification. The full-length, codon-optimized *gmps* gene was synthesized by Genscript® and cloned into the customized pET28 (TEV) vector [87] using *Bam*HI and *Hin*dIII (No spaces) restriction sites to generate an N-terminal His_6-tag fusion protein. The GMPS-pET28 (TEV) construct was transformed into phage-resistant *E. coli* (Novagen). Cultures (2 L) were grown at 37°C to OD_{600} 0.6 - 0.8 and *Tb*GMPS expression was induced by the addition of 200 μM IPTG (isopropylthio-β-galactoside). Cells were incubated overnight at 20°C, harvested by centrifugation and then resuspended in lysis buffer (150 mM NaCl, 50 mM HEPES pH 8.0, 10%(v/v) glycerol, and 10 mM imidazole) supplemented with protease inhibitors (PICI, 1 mg/mL leupeptin 2 mg/ml antipain and 1 mg/mL leupeptin 10 mg/ml benzamidine; PICII, 1 mg/ml pepstatin, 1 mg/ml chymostatin

(Sigma)). Cells were lysed by cell disruptor (pressure of 10000-15000 p.s.i.), cell debris was removed by centrifugation and supernatants were applied to a Ni^{+2} - column (GE Healthcare Life Science) equilibrated in buffer A (150 mM NaCl, 50 mM Hepes pH 8.0, 10 %(v/v) glycerol, and 10 mM imidazole). *Tb*GMPS was eluted using a gradient from 10 – 100 % buffer B (buffer A plus 100 mM imidazole) (This correct? 100 mM seems low). DTT (10 mM) was added to the fractions containing the eluted protein, which were pooled together and concentrated to 40 mg/mL (30 kDa MWCO Millipore). Protein concentration was determined by Bradford assay [88]. *Tb*GMPS purity was >95% based on SDS-PAGE analysis.

Steady-state kinetic analysis of GMPS activity

Activity of *Tb*GMPS was monitored using a coupled spectrophotometric assay based on PP_i-dependent phosphofructokinase [89]. Reaction rates were monitored by following oxidation of NADH at 340 nm ($\varepsilon = 6220 M^{-1} cm^{-1}$). The standard assay reaction consisted of buffer (90 mM Tris HCl pH 8.5, 10 nM GMPS, 20 mM $MgCl_2$, and 0.1 mM DTT), 2 mM ATP, 5 mM glutamine, 0.10 mM xanthosine monophosphate (XMP), 0.066 ml pyrophosphate reagent (Sigma P7275) and recombinant *T. brucei* GMPS (10 nM)(linearity confirmed from 4 - 64 nM) in a reaction volume of 0.2 ml. The reaction was performed in Greiner 96 area flat bottom plates (Phenix Research) at RT and monitored continuously over time (0 – 20 min) on a BioTek Synergy H1 hybrid reader spectrophotometer. To determine the steady state kinetic constants, the concentration of one substrate (XMP 3.8 - 180 μM, ATP 25 - 1200 μM, glutamine 50 - 2000 μM) was varied while keeping the other two at

saturating concentrations. Fixed substrate concentrations were: XMP, 0.15 mM; ATP, 2 mM; and glutamine, 5 mM. Data were collected in triplicate and fitted to the Michalis-Menten equation ($Y=V_{max}*X/(K_m+X)$) using GraphPad Prism (San Diego). For determination of Acivicin (Sigma) inhibition constants (IC_{50}), inhibitor concentrations were varied in a 3-fold dilution series (1 – 300 μM) using the standard reaction conditions (above). Assay time was 10 min. Data were collected in triplicate and were fitted by GraphPad Prism using the log(inhibitor) vs. response – variable slope (four parameters) equation.

T. brucei cultivation and generation of transgenic cell lines

All studies were done using *T. brucei* bloodstream form (BSF) single marker cells (SM) engineered to express T7 RNA polymerase and tetracycline (Tet) repressor [44]. Cell lines were maintained at exponential growth (10^5-10^6 cells/ml) in HMI-11 [90] or HMI-19 medium supplemented with 10% fetal bovine serum (FBS) (Tet minus certified) at 37°C under 5% CO_2. HMI-19 medium has the same composition as HMI-11 media except it was modified by the omission of hypoxanthine and thymidine. SM cells were grown in G418(2.5 μg ml^{-1}) to maintain the TetR and T7 polymerase inserts. Transfections were performed as described [91] using Not I-linearized DNA (5 μg) with an Amaxa Nucleofector II followed by selection with the appropriate antibiotic. Antibiotic concentrations were: 2.5 μg ml^{-1} G418 (Life Technology), 2.5 μg ml^{-1} phleomycin (InvivoGen), 2 μg ml^{-1} blasticidin S (Sigma), 1 μg ml^{-1} hygromycin B (Sigma), 0.1 μg ml^{-1} puromycin (Sigma) and 1 μg ml^{-1} Tet (RPI). Where indicated, nucleosides or bases, guanine (Sigma-Aldrich), guanosine (Sigma-Aldrich), hypoxanthine (Sigma-Aldrich), xanthine (Sigma-Aldrich), or adenine (Sigma-

Aldrich) were added exogenously to the medium (concentrations ranging from 0.01 – 1 mM). GMPS c-null cells were cultured in Tet (1 μg $ml^{-1\ daily}$) to maintain expression of the ectopic copy of the *gmps* gene plus appropriate antibiotics in either HMI-11 or HMI-19 media as indicated in the figure legends. *Tb*GMPS null cells were maintained by the addition of exogenous guanine (100 μM) to the HMI-19 culture medium. To determine the effects of loss of GMPS expression on *T. brucei* growth, cells were washed and plated in Tet (c-null) or guanine (null) free medium without antibiotics and cell growth rate was monitored over time. Cell density was determined by counting with a hemocytometer (Bright-Line). Cells number was plotted versus time and total cell numbers were calculated by multiplying cell density by the dilution factor [45] (also x volume?). Cell numbers below 10^4/ml cannot be quantitated (quantified?) by this method.

Cell growth effects of GMPS inhibitors

Growth inhibition by Acivicin and 6-diazo-5-oxo-L-norleucine (DON) (Sigma) (0.01 μM – 33 μM) was assessed using the CellTiter-Glo® Luminescent Cell Viability Assay (Promega). Cells were grown in 96 well CellStar plates (Greiner) with inhibitor in HMI-19 medium (200 μl) for 48 h prior to analysis. Aliquots (25 μl) of each condition were transferred to a LIA-plate (Greiner), the CellTiter-Glo reagent (50 μl) was added and luminescence was read after a 10 min incubation using a Synergy H1 plate reader at 27 °C. Data were collected in triplicate and were fitted by GraphPad Prism using the log(inhibitor) vs. response – variable slope (four parameters) equation.

Generation of the *gmps* conditional null cell line

The *gmps* conditional knock out cell line (c-null) was constructed using the fusion PCR method [46, 47]. First a Tet-regulated expression construct for *Leishmania major* GMPS (*Lm*GMPS) was generated by cloning the PCR amplified *L. major gmps* gene (primers 11 and 12 in a PCR reaction with *L. major* genomic DNA (a gift from Buddy Ullman)) into the pLew100v5 vector (gift from George Cross). The *L. major gmps* gene was used because of difficulties in cloning the *T. brucei gmps* gene into the pLew100v5 vector. The NotI (no space) linearized vector was transfected into SM cells and selected using phleomycin. Knockout constructs to replace the two alleles of the *gmps* gene with the hygromycin (*hyg*) and puromycin (*pac*) resistance genes were generated by fusion PCR. The *gmps* 5'and 3' UTRs were amplified from *T. brucei* SM genomic DNA using *gmps* specific primers (primers 1-4); the 5' UTR reverse primer included an overhang complementing the *hyg* or *pac* resistance gene and the 3'UTR the forward primer included an overlap to the resistance gene (primers are listed in Table 3.4). The *hyg* or *pac* resistance genes were also amplified by PCR (primer pairs 7/8 (*hyg*) or 15/16 (*pac*), Table 1) from plasmid pLew90 (gift from George A.M. Cross [44]) or pHD1437 (gift from Christine Clayton lab), respectively. Fragments were then used as template for fusion PCR with primers 5 and 6 (Table 3.4) targeting the internal regions of the 5' and 3' UTRs. The resulting fusion product (600 ng) containing the *hyg* selection marker was transfected into the SM cells containing the *Lm*GMPS Tet regulated expression construct in the presence of Tet and recombinants

(conditional single knockout line *gmps*(+/-)) were selected using hygromycin. PCR was performed to corroborate efficient allele replacement with the *hyg* resistance gene, using primers 1 and 8 (Table 3.4). The GMPS c-null cell line was created by transfection of the conditional single knockout cells with the fusion product containing the *pac* selection marker (above) and recombinants were selected with puromycin (0.1 μg/mL), in medium also containing hygromycin and Tet. PCR was performed to confirm that the resulting *Tb*GMPS c-null cell line had incorporated both selection markers (primers 5/16 and 5/8) and no longer contained a copy of the *T. brucei gmps* gene (primers 5/6). *T. brucei* BSF cells were cultured in HMI-11 medium throughout the selection process to isolate the *Tb*GMPS c-null cell line.

Generation of the *T. brucei gmps* null cell line

The *gmps* null cell line was created by replacing the two alleles of the *gmps* gene with the drug resistance markers for *hyg* and blasticidin (*bsd*). The *gmps* 5'and 3' UTRs, *hyg* and *bsd* genes (primers Table 3.4) were amplified as described above (the *bsd* resistance gene was amplified from pLew300 vector [92]). The resulting fusion PCR product containing *hyg* was transfected into SM cells grown in HMI-19 medium containing guanine (100 μM) and was selected using hygromycin to generate *gmps* single knockout cells. This line was then subsequently transfected with the *bsd* fusion PCR product and selected using blasticidn to generate the *gmps* null cell line. PCR was used to confirm that the two *gmps* alleles were replaced with the *hyg* and *bsd* resistance cassettes using primer pairs 5/8 and 5/26 and no longer contained a copy of the *T. brucei gmps* gene (primers 5/6) (Table 3.4).

In vivo viability analysis of the *T. brucei gmps* null cell line in mice

C57BL/6J were purchased from the Wakeland Laboratory (UTSW). Two groups of C57BL/6J mice (8 weeks old, $n = 4$) were infected intraperitoneally with 10^3 wild-type (SM) or *gmps* null *T. brucei* parasites. Before infection, these parasites were cultured in HMI-19 medium plus 100 μM guanine (without antibiotics) and washed three times with HMI-19 medium alone before injection. Mice were monitored every day for general appearance and behavior. Parasitemia was monitored daily from the third day post-infection onwards, collecting 1 μl of blood from the tail in a 1:150 dilution in medium and counting in a hemocytometer under a microscope. Both parasitemia and mice survival were monitored over a period of 30 days.

Quantitation of nucleotide pools in *T. brucei* BSF cells LC-MS/MS analysis

T. brucei SM and GMPS c-null cells (50 ml cultures) were grown in HMI-19 medium , in the presence or absence of Tet (1 μg/mL daily) to a density of 1.5 x 10^6 cells/mL. Cells were pelleted by centrifugation at 3000g and washed once with cold PBS. Washed cell pellets were suspended in 2 ml 65% methanol and frozen in liquid nitrogen. Cell metabolites were extracted by 10 cycles of freeze/thawing followed by centrifugation at 10,000 rpm for 10 min. Supernatant (1 ml) was collected, vacuum dried, and stored at -80°C. The supernatant was dried by vacuum dryer for 3 h, re-suspended in formic acid buffer (0.1% in HPLC grade water) and filtered through a 0.2 micron centrifuge filters (Grace Davison).

Nucleotide metabolite analysis was performed by LC-MS/MS on a Shimadzu Prominence LC20/SIL-20AC HPLC coupled to a ABSCIEX 3200 QTRAP triple quadrupole mass spectrometer as described [50]. Chromatographic separation was performed using a C18-based column with polar embedded groups (Synergi Fusion, 150 x 2.0 mm 4 μ, Phenomenex). Infusion quantitative optimization was performed to acquire optimal product ion mass for each metabolite. Multiple reaction monitoring (MRM) was used to detect and quantitate metabolites. The two most abundant daughter ions were used when possible and metabolite peak area was normalized to total ion content. Daughter ion pairs were as follows: GMP (364/152 and 364/135), GDP (443.9/152.1 and 443.9/135), GTP (521.9/78.9), AMP (348/136 and 348/119), ADP (428/136 and 428/119), ATP (508/136.2 and 508/410.1), XMP (364.9/97.1 and 364.9/152.9) and IMP (349/137). Data were plotted and analyzed (unpaired t-tests with equal SD) using GraphPad Prism.

Quantitation of ATP by a luciferease-based assay

GMPS cDKO cells were grown in HMI-19 media, in the presence or absence of Tet (1 μg/mL daily) to a density of 1.5-2.0 x 10^6 cells/mL. Cell numbers were quantitated by hemocytometer and a 2-fold serial dilution of cells from 3 x 10^4 – 1 x 10^6 cells/ml was made to demonstrate a linear relationship between cell number and luminescence. Aliquots of each (50 μl) were mixed with CellTiter-Glo reagent (50 μl) and luminescence was read after a 10 min incubation using a Synergy H1 plate reader at 27 °C. Luminescence values were

normalized per cell number and the data shown are for analysis of 500,000 cells. Data were collected in biological triplicate.

Molecular modeling and sequence alignment

The program PyMOL (*Pymol Molecular Graphics System* (2000) DeLano Scientific, San Carlos, CA) was used to generate all structure figures using coordinates for human (2VXO) and *E. coli (*1GPM) GMPS. Sequences were aligned using Clustal Omega (1.2.1) multiple sequence alignment software as described in Fig. 3.8.

RNA and DNA purification

Genomic DNA was isolated from 1×10^7 *T. brucei* cells using the DNAzol extraction method as recommended by the manufacture (Molecular Research Center, Inc). RNA was extracted from cells (~3×10^8) collected at different induction times and total RNA was extracted using TRIzol® (Invitrogen), according to manufacturer's protocol. Then, mRNA was purified from 250 μg total RNA using the Dynabeads ® mRNA purification kit (Invitrogen).

mRNA quantitation by RT PCR

Quantitative real-time PCR was performed using SYBR Green Mastermix (Bio-Rad). Cultures containing 5×10^7 cells, grown with or without tetracycline (1 μg/mL daily), were pelleted and washed in PBS once and suspended in 1 ml Trizol reagent (Invitrogen). Total

RNA was extracted according to the manufacturer's instructions followed by quantification via spectrophotometer (BioTek Hybrid Plate Reader). 5 μg total RNA was treated with 1 unit DNaseI (Invitrogen) and RT-PCR was performed (Invitrogen Superscript II RT-PCR Kit). *Lm*GMPS RNA abundance was quantified with primer pairs 21/22 or 23/24 respectively (Table 3.4) using iTaq SYBR Green Supermix with ROX (BioRad) in a reaction (20 μl) containing 50 ng RNA, 1X Supermix, and 7.5 pmols of each primer. The amplification conditions were: 95 °C for 15 s, 60 °C for 1 min, and data collection for 40 cycles. Relative gene abundance was calculated by the ΔΔCt method [93] using either DHODH or TERT [54] as the reference gene (primer pairs 21/22 or 23/24 respectively (Table 3.4)).

Western blot analysis

Parasites (~10^8) were harvested by centrifugation (3000 rpm, 10 min) and washed 3x with cold (4°C) phosphate-buffered saline (PBS) (10 mM Na_2HPO_4, 1.8 mM KH_2PO_4, 137 mM NaCl, 2.7 mM KCl, pH 7.4). Pellets were resuspended in protein lysis buffer (50 mM HEPES, pH 8.0, 100 mM NaCl, 5 mM β-mercaptoethanol, and protease inhibitor cocktail (as above)). Cells were lysed by three freeze/thaw cycles and clarified by high-speed centrifugation. Protein concentration was determined using the Bradford assay [88]. Protein (20 μg total protein per well), was separated by a 12% SDS-PAGE gel and transferred to a PVDF membrane (iBlot® Transfer Stack, PVDF, Invtirogen) using a dry transfer iBlot® Gel Transfer Device (Invitrogen) for 7 min. Membranes were blocked in 5% non-fat dry milk in Tris-buffered saline (TBS)(20 mM Tris-HCl pH 7.6, 137 mM NaCl, pH 7.6) 2 h at RT. Primary rabbit *Tb*GMPS polyclonal antibodies were generated by a commercial vendor

(COVANCE) from purified recombinant *Tb*GMPS (tag removed by the protease TEV as described [94]). Dilutions for primary antibodies in 5% milk in TBS-T (TBS plus 0.05% Tween) were α*Tb*GMPS – 1:2000. Secondary antibodies (anti-rabbit), were used at 1:10,000 dilution in 5% nonfat milk TBS-T. Dihydroorotate dehydrogenase levels were measured as a loading control using the previously described antibody (1:2500 dilution)[19]. Protein was detected by SuperSignal West Femto Chemiluminescent Substrate (Thermo scentific.) according to the manufacturer. Bands were visualized by ImageQuant LAS 4000 (GE).

Flow cytometery

For cell cycle examination, cells were grown to a density of 10^6 cells/mL in 20 ml HMI-11 medium, pelleted by centrifuged, resuspended in 70% ethanol and incubated at 4 °C overnight. Cells were washed using 10 ml of cold PBS, resuspended in 1 ml of PBS containing 10 μg/ml propidium iodide (PI) (Sigma), 10 μg/ml RNase A, and incubated at RT for 20 - 30 mins. Flow cytometry was performed with FACSCalibur (BD Biosciences) using the FL2-H and side-scatter detectors. A total of 10000 gated events were collected for each sample. Data was analyzed using software FlowJo (NIH).

DNA staining of trypanosomes

Cells were grown to a density of up to $1x10^6$cells/ml in HMI-12 medium, collected by centrifugation, washed in PBS and resuspended in 1 ml PBS. Cell suspension (0.2 – 0.3 ml) was placed on a cover slip for 20 min, the cover slip was then placed cell side up in a well of a 6-well plate, 1 ml 4% paraformaldehyde (PFM) (16% paraformaldehyde stock from

Electric Microscopy Sciences) was added and cells were incubated for 30 min at RT. PFM was removed by vacuum and the cover slip was washed with 1 ml of cold PBS 2 x, followed by a wash with PBS plus 0.1% triton X-100, and finally three 1 min washes with PBS. Cover slips were removed from the well and mounting medium (anti-fade, Invitrogen containing 4', 6-diamidino-2-phenylindole (DAPI)) (10 μl) was dropped onto the slide and the coverslip with cells was mounted on the slide. Cells were visualized using Deltavision Deconvolution, AppliedPrecision. NL.5 120 microscope. The differential interference contrast (DIC) and fluorescence field images were obtained at the same time. Images were visualized using the Image J software (NIH). For manual counting of nucleus and kinetoplastid content, 100 cells were counted for each condition.

Results

Recombinant expression and steady-state kinetic analysis of *Tb*GMPS

In order to demonstrate that the *T. brucei* gene annotated as GMPS encodes an active enzyme, recombinant *Tb*GMPS was expressed and purified from *E. coli* to evaluate its catalytic activity. *Tb*GMPS activity was detected using a pyrophosphate-coupled spectrophotometric assay. *Tb*GMPS catalyzed synthesis of GMP with an average k_{cat} of 4.7 s^{-1} (Table 3.2), which is comparable to the rate published for human GMPS [95]. Apparent K_m values were measured for each of the three substrates at fixed concentration of other substrates. $K_{m.app}$ values for XMP, glutamine and ATP were 8.8, 240, 200 μM, respectively, similar to those reported for other GMPS homologs (Table 3.2) [96, 97].

Acivicin, which is reported to be a broad-spectrum inhibitor of glutamine amidotransferases, was tested for inhibition of *Tb*GMPS. Acivicin is a glutamate analog and a covalent inhibitor of GMPS from other species [98-100]. Under the tested assay conditions, Acivicin inhibited *T. brucei* GMPS at mid-micromolar concentrations (apparent IC_{50} = 26 μM) (Table 3.3).

_Tb_GMPS is essential for growth of _T. brucei_ bloodstream form (BSF) cells.

To evaluate the essentiality of *Tb*GMPS in *T. brucei* we attempted to generate a *gmps* null cell line by knockout of both *gmps* alleles (*T. brucei* is a diploid organism) in BSF single marker (SM) cells. Parasites were grown in HMI-11 medium in the presence of guanine or guanosine (100 μM), which were expected to allow rescue of the *gmps* (-/-) knockout by supplementing GMP pools through the activity of HGPRT (Fig. 3.1). However, we were unable to generate a null cell line under these conditions suggesting that *Tb*GMPS is an essential enzyme. To further evaluate essentiality we generated a conditional null (c-null) cell line. Due to difficulties in cloning *T. brucei gmps* into the pLew100v5 expression vector in the sense orientation, the *Leishmania major gmps* gene was used to generate a Tet-regulated ectopic expression plasmid that was integrated into the genome of SM cells. Upon induction of *Lm*GMPS expression with Tet, both *T. brucei gmps* alleles could be replaced by selectable markers, leading to the generation of the *Tb*GMPS c-null *gmps* cells. The c-null cell line was validated by PCR analysis, demonstrating that the *gmps* gene had been removed from both original loci. Depletion of *Lm*GMPS from c-null cells by removal of Tet led to a severe attenuation of cell growth, which correlated with a loss in detectable *L. major gmps* transcript levels (Fig. 3.2A,B). Although very few cells were visible by day 4, cell growth resumed on

day 6. Analysis of the surviving cells by qPCR revealed re-expression of the *L. major gmps* transcript (Fig. 3.2B). Presumably, the escaped cells bypassed Tet-repression, a phenomenon that has been commonly observed in *T. brucei* regulated expression systems [68, 69, 101]. The finding that GMPS is essential differs from results obtained in a genome-wide RNAi screen where GMPS was not found to be essential [30], likely due to insufficient knockdown of GMPS by RNAi.

Supraphysiological concentrations of hypoxanthine impairs guanine rescue

We attempted to rescue the growth defect observed in the *Tb*GMPS c-null cells by the addition of exogenous guanine. Normal human plasma has been reported to contain less than 1 μM guanosine/guanine (Table 3.1), however, in standard *T. brucei* culture medium (HMI-11 medium), guanine concentrations up to 100 μM were not capable of fully rescuing growth (Fig. 3.2A). HMI-11 medium contains 1 mM hypoxanthine, significantly surpassing human plasma and CSF concentrations, which are reported to be on the order of 5 - 10 μM (Table 3.1). *T. brucei* BSFs possess two purine transporters, H2 and H3 and it was shown that both hypoxanthine and guanine compete for the H2 transporter and both bases are converted to nucleotides by a common enzyme (HGPRT) [16, 102]. To address the possibility that high concentrations of hypoxanthine were inhibiting transport and enzymatic conversion of guanine to GMP, hypoxanthine was removed from HMI-11 medium and we generated a new medium (designated HMI-19) that contained no added hypoxanthine or thymidine. However, this medium still contains 10% FBS, which is expected to lead to physiological levels of hypoxanthine (5 – 10 μM range), similar to that recently reported for a minimal *T. brucei*

culture medium (CMM) supplemented with 10% FBS but not with added hypoxanthine [103] (Table 3.1). The *gmps* c-null cells grew at similar rates in HMI-11 and HMI-19 media in the presence of Tet. Upon removal of Tet cell growth arrest was once again observed in HMI-19 medium, but exogenous guanine concentrations of 30 μM and 100 μM were now able to fully support growth in this medium, while 10 μM guanine remained insufficient (Fig. 3.2C). Titration of the effective guanine concentration that is required for rescue was performed, and showed that the effective dose of 50% activation (ED_{50}) is 20 (19 - 22) μM in HMI-19 medium (Fig. 3.2D). Additionally, adding back hypoxanthine recapitulates the growth defect observed with HMI-11 medium (Fig. 3.2D). Hypoxanthine concentrations exceeding 60 μM prevented rescue with 100 μM guanine, with an inhibitory ED_{50} = 100 (95 – 112) μM hypoxanthine (Fig. 3.2E).

GMPS null cells are auxotrophic for guanine and require supraphysiological levels for survival

With the knowledge that excessive hypoxanthine had prevented efficient guanine rescue of *gmps* knockdown, we were able to generate the null cell line using the newly formulated medium (HMI-19) supplemented with 100 μM guanine. Replacement of both *gmps* alleles by the selectable markers, *bsdR* and *hygR*, was confirmed by PCR. Western blot analysis for *Tb*GMPS further confirmed the complete absence of the protein (Fig. 3.3A). The ability to generate *gmps* null cells avoids the phenomenon of Tet control escape that we observed in the c-null cell line, allowing for a more robust analysis of the essentiality of *Tb*GMPS. Upon removal of exogenous guanine from the medium *gmps* null cells rapidly

stopped growing and complete death of the culture was observed by day 2-3 (Fig. 3.3A). We next supplemented cultures with a range of exogenous guanine concentrations (10 – 100 μM) to determine the minimum level needed to sustain growth (Fig. 3.3A). Guanine levels of 100 μM were required to fully rescue the growth defect caused by *Tb*GMPS knockout. Guanine at 10 μM showed minimal to no ability to support growth, while guanine levels of 30 μM provided partial rescue but cells still eventually died with a 3-4 day lag time compared to cells supplemented with 100 μM guanine. As observed with the c-null cells, xanthine, adenosine, or hypoxanthine at 100 μM were not capable of rescuing growth of the *gmps* null cells. These data show that guanine levels must be significantly higher than reported guanine plasma levels and ~20 fold higher than hypoxanthine levels before they are sufficient to support cell growth.

Cell cycle and morphologic analysis of c-null and null *GMPS* cells

To evaluate the effect of GMPS deficiency on the cell cycle, flow cytometry was performed. Cell cycle analysis of the GMPS null cells before (Fig. 3.4A) and 24 h after the removal of guanine (100 μM) (Fig. 3.4B) showed that loss of guanine led to a marked reduction (64%) in the fraction of cells in S-phase and an accumulation of cells in G2/M. These results are consistent with the requirement for guanine nucleotides for DNA synthesis. Similar results were also observed for the c-null cell line after Tet withdrawl (Fig. 3.4D and 3.4E) but the reduction in S-phase was less pronounced and the accumulation of cells in G2/M was greater. The finding of a more robust block of DNA synthesis in the null cell line after guanine was removed is consistent with the observation that the GMPS null cells die

more quickly than the c-null cells once the source of guanine nucleotides is removed. Cells were also examined by microscopy after DAPI staining, revealing significant morphological defects after either removal of guanine (null cells) or Tet (c-null cells). Null cells were badly misshapen, have missing or detached flagella and an abnormal texture just 24 h after guanine removal (Fig. 3.4C). A similar result was observed for the c-null cells 48 h after Tet withdrawl, where *Lm*GMPS knockdown resulted in short and enlarged cell bodies with absent or complex flagella configurations (Fig. 3.4F). DAPI staining was used to analyze the distribution of nuclei and kinetoplast in the c-null cells. An increase in 2K2N (14%) and 1K2N (30%) cellular bodies was observed consistent with arrest in the G2/M phase (Fig. 3.5).

GMPS is essential for virulence of *T. brucei* in mice

To address the question of whether *in vivo* host plasma levels are sufficient to bypass the metabolic block imposed by loss of *Tb*GMPS, we determined if *gmps* null cells were able to establish an infection in mice. Mice were injected with either *gmps* null or SM BSF (control) cells and the course of infection was monitored over a period of 30 days. All SM-infected mice developed detectable levels of parasitemia by day 3 post-infection, with all mice dying (or being euthanized) with hyperparasitemia by day 6 (median survival was 5.5 days post-infection) (Fig. 3.3B). In contrast, the *gmps* null infected mice never showed detectable levels of parasites in their blood and all animals survived until the end of the study (day 30 post-infection) (Figs. 3.3B,C). These data demonstrate that mouse plasma does not

contain sufficient levels of guanine or guanosine to support parasite growth in the absence of functional GMPS expression.

GMPS inhibitors block parasite growth.

To determine if the known GMPS inhibitors Acivicin and 6-diazo-5-oxo-L-norleucine (DON) also inhibited parasite growth we cultured wild-type parasites in their presence. Similar to Acivicin, DON has been reported to be a covalent inhibitor of GMPS [98-100]. Both compounds killed wild-type (SM) cells with an EC_{50} in the low micromolar range (1 – 3 μM)(Table 3.3). To determine if this killing was on target and caused by inhibition of *Tb*GMPS, we also evaluated these compounds on *gmps* null cells cultivated in the presence of 100 μM guanine. Both compounds also killed *gmps* null cells with similar dose response to the SM cells, demonstrating that for these compounds GMPS is not the primary target of cell killing. These compounds have also been shown to have off-target cell killing mechanisms in Leukemia L1210 cells [104] and *in C. albicans* [105].

GMPS knockdown leads to depletion of guanine and adenosine nucleotide pools.

To analyze the effects of *gmps* knockout on cell nucleotide pools, nucleotide levels were measured by LC-MS/MS analysis. In the absence of guanine supplementation, rapid death of *gmps* null cells prevented collection of sufficient quantities of cells for nucleotide analysis so the *gmps* c-null cell line was evaluated instead. The *gmps* c-null cells were grown ±Tet in HMI-19 medium for 2 days and cells were collected and processed for analysis. Attempts to collect cells past day 2 after Tet removal failed because cells lysed upon

centrifugation, indicating that by day 3 (-Tet) the cell integrity was already significantly compromised. Intracellular guanine nucleotide pools (GMP, GDP and GTP) were reduced 50 - 75% by day 2 (-Tet) relative to control (+Tet) cells consistent with loss of GMPS expression (Fig. 3.6). In addition AMP and ADP levels were reduced by 30 – 50%, respectively, and IMP decreased by 40% (Figs. 3.6 and 3.7). XMP levels increased by 22%, but this change did not reach statistical significance (Figs. 3.6 and 3.7C). ATP levels were also monitored, but due to the large number of ATP hydrolyzing enzymes in a cell, methods that require significant cell manipulation can result in erroneous results. To avoid this issue we used CellTiter-Glo assays to assess ATP levels as the reagent can be added directly to cell cultures reducing the error of the measurement. In this assay the level of luminescence is directly proportional to the amount of ATP that is present. We showed that the assay was linearly dependent on the number of cells and then we measured luminescence for a quantified number of cells (500,000) based on counting using a hemocytometer. We did not observe a signficant change in ATP pools after Tet removal (Fig. 3.7D).

Comparison of human and T. brucei GMPS binding sites.

We considered the potential for identification of species-specific inhibitors of *T. brucei* GMPS that will not inhibit the human enzyme. While an X-ray structure of *T. brucei* GMPS is not available, GMPS structures for both human and *E. coli* GMPS have been solved bound to various ligands (e.g. XMP, AMP and citrate). We aligned the amino acid sequences of *T. brucei* GMPS with the human and *E. coli* enzymes (Fig. 3.8) and then compared the residues in the various nucleotide and citrate binding sites (Figs. 3.9). Residues were

identified in all three binding sites that differ between the human and *T. brucei* GMPS suggesting it may be possible to identify species selective inhibitors.

Conclusions

Trypanosomatids including *T. brucei* are unable to synthesize purines *de novo* and rely on uptake and purine salvage pathways to acquire these essential nutrients. Because of the redundant nature of these salvage pathways, which support the interconversion of guanine and adenine nucleotide pools, it was thought that no single enzyme in the pathway would be essential for parasite growth. Herein we show that recombinant *T. brucei* GMPS efficiently catalyzes synthesis of GMP, and that *gmps* null bloodstream form parasites are auxotrophic for guanine. Importantly, we also show that the guanine concentrations required to support growth of the *gmps* null cell line *in vitro* (100 μM) significantly exceed, not only physiological levels of guanine in human plasma (guanine/guanosine human serum < 1 μM), but the levels of any salvageable nucleosides or bases in human plasma and CSF (Table 3.1). As a result, GMPS is essential for the infectivity of *T. brucei* in a mouse model and would be expected to be essential to sustain a human infection. The predominant purine bases and nucleosides available for salvage in both mammalian plasma and CSF are reported to be hypoxanthine and xanthine [106-108]. Thus despite the redundant pathway, the infective blood stage form of the parasite obtains purines primarily through salvage of hypoxanthine and xanthine via HGPRT and XPRT, leaving the parasite vulnerable to inhibition of key interconversion enzymes like GMPS. Taken together with the high druggability score for

GMPS (0.6) and species differences in the binding pocket, these data suggest that GMPS will be an excellent target for future drug discovery efforts against *T. brucei*.

The purine salvage pathway may offer significant promise for therapeutic intervention against a range of pathogenic protozoa and fungi enzymatic steps. In addition to our results showing that GMPS is essential in *T. brucei*, studies using RNAi-based gene knockdown have shown that both ADSS and ADSL knockdown led to attenuated virulence of *T. brucei* in mice [40]. The fact that parasites were not fully cleared in that study may be due to the leakiness of the RNAi system, in comparison to our GMPS study which characterized a null cell line. These data suggest that similarly to our findings with guanine, insufficient adenine may be present in serum to support parasite growth in the absence of ADSS and ADSL. Thus, the extracellular niche of *T. brucei* is likely to be a significant contributing factor to the vulnerability of the parasite to disruption of key interconversion enzymes required for the synthesis of GMP and AMP. In the pathogenic fungi *Candida albicans*, knockout of GMPS also led to guanine auxotrophy and to reduced virulence in a systemic candidiasis murine model where availability of plasma guanine was insufficient to support growth [109]. In *L. donovani*, ADSS and ADSL knockout cell lines showed reduced virulence [39] despite the fact that *Leishmania* species have access to intracellular purine pools. These results were ascribed to the presence of adenine aminohydrolase in *L. donovani*, which forces the parasite to rely on xanthine and hypoxanthine to supply required purines. While *T. brucei* lacks adenine aminohydrolase, apparently plasma adenine levels are insufficient to support normal growth. Thus despite initial dogma that the purine salvage pathway enzymes would not be essential, current data strongly supports the conclusion that

several enzymes in the pathway are essential in both *T. brucei* and *Leishmania,* findings which may likely extend to *T. cruzi* as well.

In *T. brucei*, several additional factors may also contribute to the observed insufficiency of plasma guanine pools to support growth and *in vivo* infectivity of *gmps* null cells. Firstly, *T. brucei* encodes guanine deaminase (Fig. 3.1A), which would contribute to depletion of any available environmental guanine and to the funneling of purine salvage through XMP. Secondly, the presence of GMPR may also contribute to depletion of any synthesized GMP leading first to formation of IMP and then to draining of guanine nucleotide pools into either adenine nucleotides via ADSS or into XMP via IMPDH (Fig. 3.1A). The "dead-end" accumulation of XMP would be the expected consequence of its continued synthesis (IMPDH and XPRT) in the absence of the degradative pathway (GMPS). In support, XMP levels were modestly increased after GMPS knockdown. Finally, competition between hypoxanthine and guanine for both uptake and for conversion to nucleotides by HGPRT may also play a role in preventing utilization of guanine given the significantly higher concentrations of hypoxanthine compared to guanine/guanosine in human plasma. Our data demonstrate that hypoxanthine competes with guanine, reducing or preventing the ability of guanine to rescue the cell growth defect of *gmps* c-null cells. Our studies also highlight the importance of evaluating knockout strains in physiologically relevant medium and they confirm prior results [103] that the high levels of hypoxanthine in standard HMI-11 medium are unnecessary to support growth. Excessive hypoxanthine levels were indeed detrimental to our ability to generate the *gmps* null cell line.

Metabolite analysis of purine nucleotide levels showed that the predominate effects of GMPS depletion were on the guanine and adenine nucleotide pools. Guanine nucleotide pools were uniformly depleted, a finding that would be a direct consequence of GMPS knockdown. AMP and ADP levels were also reduced. Additionally, we observed an increase in XMP pools, suggesting that some buildup of this dead-end product occurs as a consequence of the genetic block in degradation. It is important to note that we were only able to conduct nucleotide analysis relatively soon after Tet removal when *gmps* c-null cells were only just entering growth arrest. It is likely that changes in the nucleotide pools were more pronounced further into the growth curve (day 4 –Tet for the c-null cells) and in *gmps* null cells after guanine was removed. An unexplored question is whether or not *T. brucei* mounts an adaptive response to purine depletion as observed with *Leishmania* [110], which might contribute to the observed balance of adenine nucleotides relative to XMP and IMP after GMPS depletion.

In conclusion, we have demonstrated that despite having a redundant salvage pathway for the biosynthesis of guanine nucleotides, *T. brucei* parasites require GMPS activity for normal cell growth and infectivity *in vivo*. *T. brucei gmps* null cell lines are auxotrophic for guanine and levels of guanine required to restore growth significantly exceed physiological levels found in human extracellular fluids where parasites live. Our data suggest that similarly to *Leishmania*, the primary purine salvage route in *T. brucei* is through uptake and incorporation of hypoxanthine and xanthine into guanine and adenine nucleotides. GMPS is a highly druggable target and analysis of active site differences with human GMPS suggest that selective inhibitors of GMPS might be identified. Our results suggest that GMPS could

be an excellent target for future drug discovery efforts directed at controlling African sleeping sickness.

Figure 3.1. Purine salvage pathway in *T. brucei*. A. Overall pathway. GMPS, GMP synthase; GMPR, GMP reductase; GDA, guanine deaminase; IMPDH, inosine-5'-monophosphate dehydrogenase; ADSS, adenylosuccinate synthetase; AK adenosine kinase; AD, AMP deaminase; ADSL, adenylosuccinate lyase; NH, inosine-uridine (or non-specific) nucleoside hydrolase; HGPRT, hypoxanthine-guanine phosphoribosyltransferase; XPRT, xanthine phosphoribosyltransferase; APRT, adenine phosphoribosyltransferase. Druggability scores are shown in parenthesis and were obtained from tdrtargets.org. Scores of >0.6 (range 0 – 1) are considered to be a strong indication that a target is "druggable", e.g. likely to be capable of binding drug-like molecules with good affinity [41]. B. Enzymatic reaction catalyzed by GMPS. R5P, ribose 5'-phosphate.

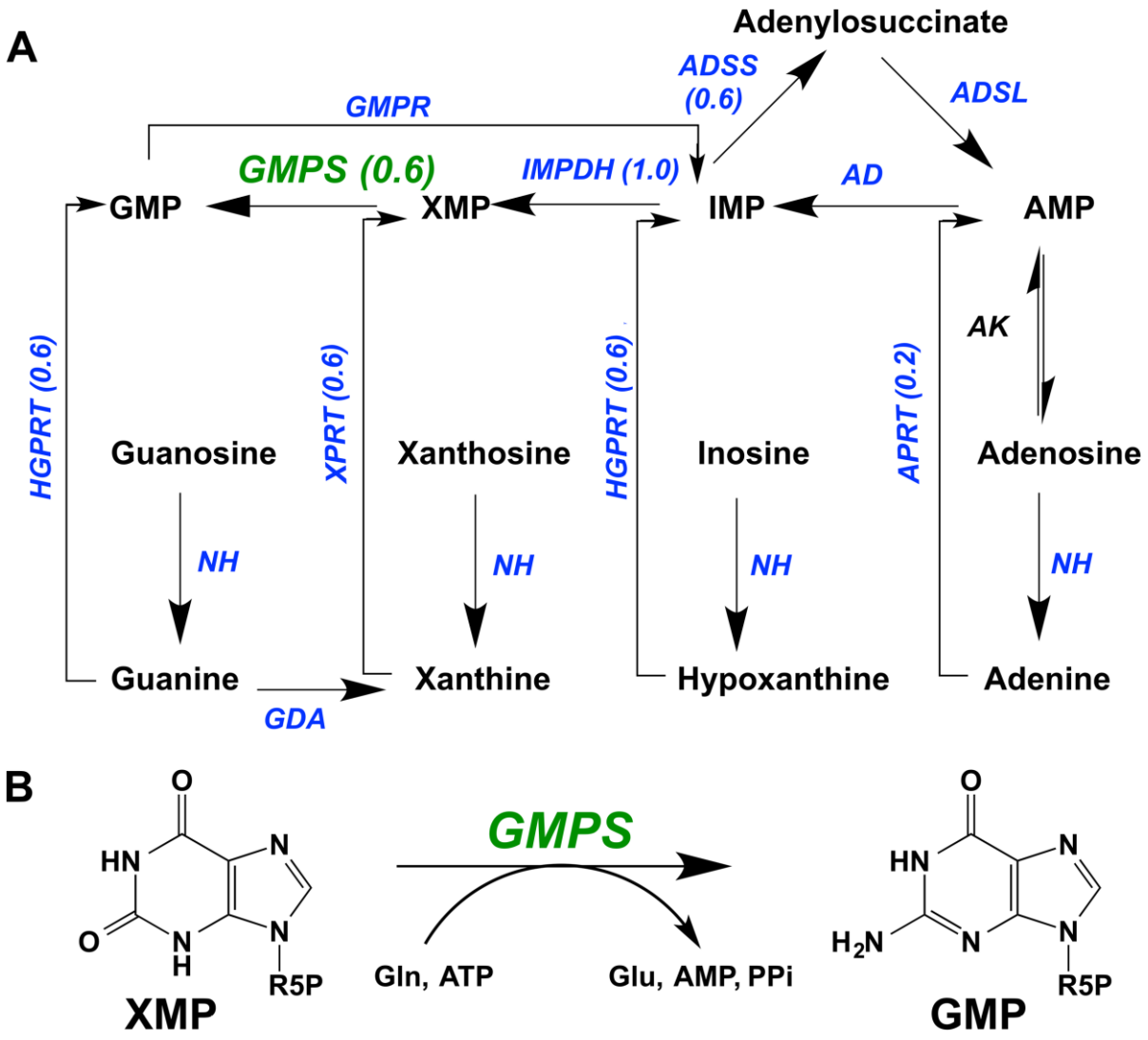

Figure 3.2. Effects of conditional GMPS knockdown (*gmps* c-null cells) on *T. brucei* bloodstream form cell growth. A. Analysis of the c-null cell line grown in HMI-11 medium in the presence or absence of added purine bases before (Control, day 0) or after withdrawal of Tet from the medium for the indicated time. B. Representative qPCR analysis of c-null cells. Cells were grown ± Tet for 0, 1 or 6 days in HMI-11. Expression levels of GMPS mRNA are reported relative to either the TERT or DHODH reference gene. C.

Analysis of the c-null cell line grown in HMI-19 medium in the presence or absence of added bases (concentration shown in μM) before (Control) or after withdrawal of Tet from the medium for the indicated time. D. Cell growth effects of guanine supplementation (0.8 – 100 μM) on c-null cells 4 days after Tet withdrawal for cells cultivated in either HMI-11 or HMI-19 medium. E. Cell growth effects of hypoxanthine supplementation (1.0 – 1000 μM) in HMI-19 medium in the presence or absence of guanine (100 μM) 4 days after Tet withdrawal. Total cell number is shown and represents cell number multiplied by the dilution factor relative to day zero. G, guanine, X, xanthine. All data represent the mean of three biological replicates. Qiong Li performed the qPCR analysis.

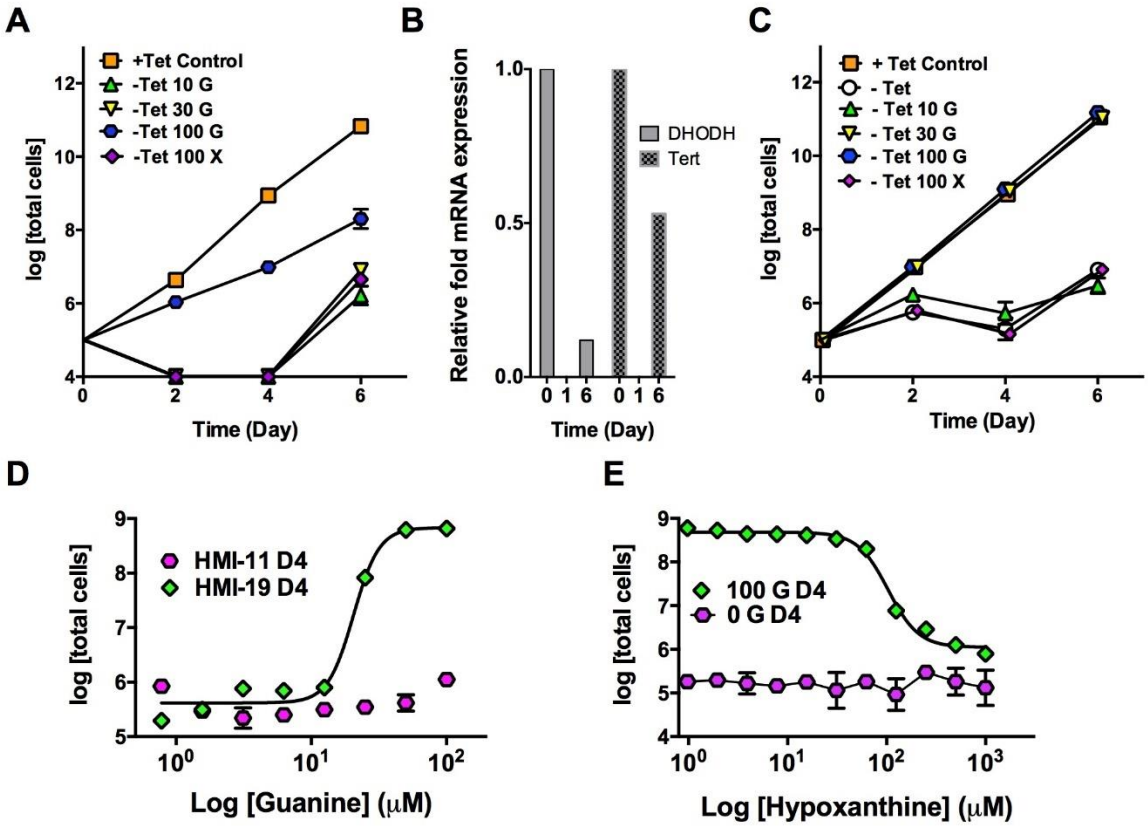

Figure 3.3. Effects of GMPS knockout on *in vitro* growth and viability in a mouse model of infection. A. GMPS null cells were grown in HMI-19 medium either in the absence or presence of supplementation with the indicated purine base (concentration is shown in μM) for control wild-type (WT) (green squares) and *gmps* null cells (white squares) cells. G, guanine, X, xanthine. A, adenine, H, hypoxanthine. Data represent the mean and standard deviation for three independent biological replicates. Inset: Western blot analysis (20 μg total protein/lane) of wild-type (WT) and *gmps* null cells grown in the presence of guanine (100 μM). Blots were probed with either *T. brucei* GMPS antibody or DHODH antibody as a loading control. B. Mice were intraperitoneally infected with 1000 WT (SM) control or *gmps* null parasites and parasitemia (parasites/mL of blood) assessed daily. Data represent the mean plus standard deviation for 4 mice per condition. C. Mouse survival curve versus days post-infection with either WT or *gmps* null cells. Median WT-infected mice survival is 5.5 days post-infection. Filipa Ferreira helped perform the *in vivo* mice studies.

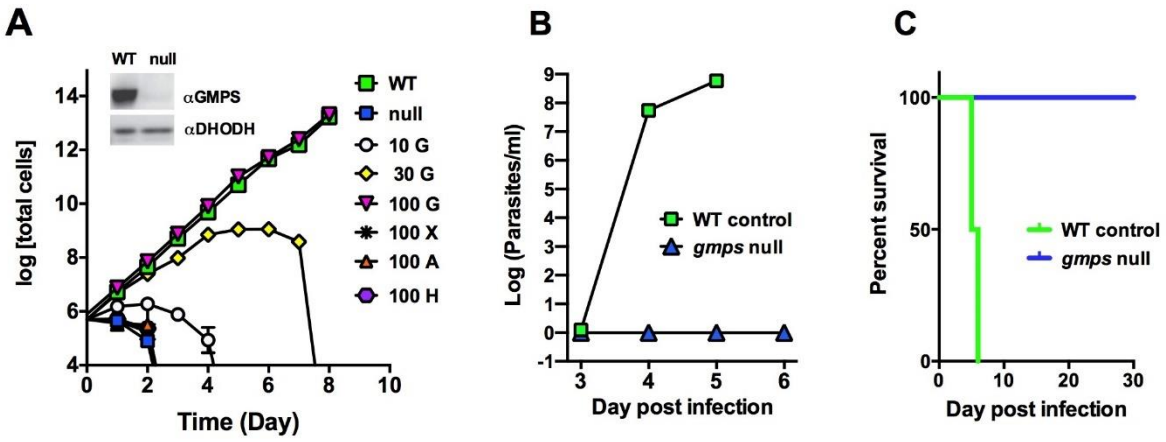

Figure 3.4. Morphology and cell cycle analysis of *T. brucei* blood form *gmps* null and c-null cells. A. Flow cytometry analysis of null cells grown with guanine (100 μM). B. Flow cytometry analysis of cells 24 h after guanine withdrawal. Cells were stained with propidium iodide (PI). PI fluorescence (FL3-Area) is plotted versus cell count. C. Images of representative cells before and 24 h after guanine withdrawal where panel 1 is an overlay of DAPI and DIC images, panel 2 is DAPI staining and panel 3 shows the DIC image. D. Flow cytometry analysis of cells prior to Tet withdrawal (day 0). E. Flow cytometry analysis of cells 48 h after Tet withdrawal. F. Images of representative cells before and 48 h after Tet withdrawal (2D). The cell cycle analysis was performed by Qiong Li.

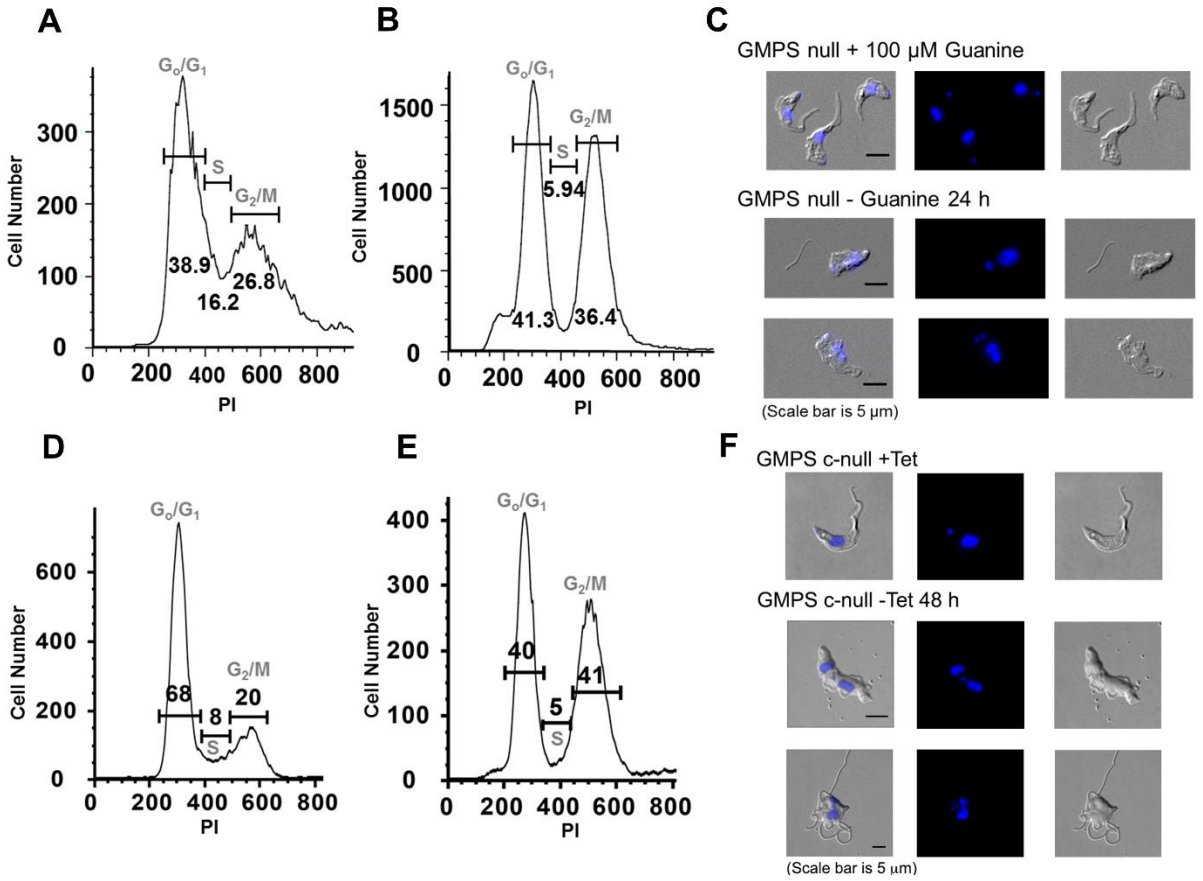
A
B
C
D
E
F
Cell Number
PI
G_o/G_1
S
G_2/M
38.9
16.2
26.8
5.94
41.3
36.4
GMPS null + 100 µM Guanine
GMPS null - Guanine 24 h
(Scale bar is 5 µm)
GMPS c-null +Tet
GMPS c-null -Tet 48 h
(Scale bar is 5 µm)
68
8
20
40
5
41

Figure 3.5. Cell cycle analysis of *T. brucei* blood form *gmps* c-null cells. Cells were grown ± Tet for 48 h, stained with DAPI and examined by fluorescence microscopy to score the number of kinetoplasts (K) and nuclei (N). 100 total cells were counted per condition. This analysis was performed by Qiong Li.

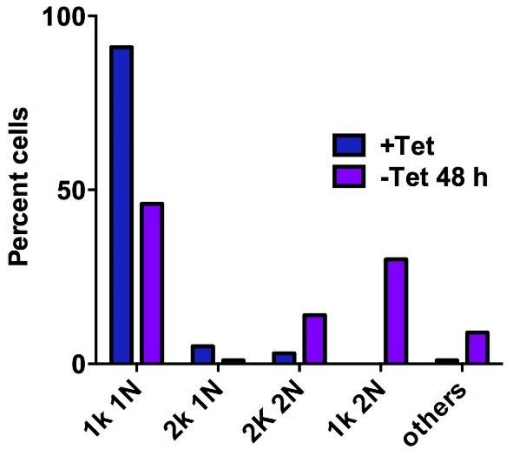

Figure 3.6. Nucleotide quantitation of the effects of GMPS knockdown in c-null cells. Intracellular levels of guanine nucleotides detected by LC-MS/MS for cells collected before and 2 days after Tet removal leading to loss of GMPS expression showing A) GMP and GDP levels, B) GTP levels for a representative data set. Relative ion abundance is shown. The data set includes three independent biological replicates collected on the same day. P values are displayed where * P<0.05, ** P<0.01, *** P <0.0005, **** P<0.0001 for one-tailed t-test. C. Ratio of -Tet/+Tet ion abundance is plotted for the indicated nucleotide. Data represent the mean of four - six independent biological replicates that were collected on three separate

dates. Error bars represent the standard deviation of the mean. MRMs to detect the indicated nucleotides were as follows: GMP (364/152), GDP (444/152), GTP (524/152), IMP (349/137), XMP (365/97), AMP (348/136), ADP (428/136). Jun Chen and Ben Tu collected the nucleotide quantitation data.

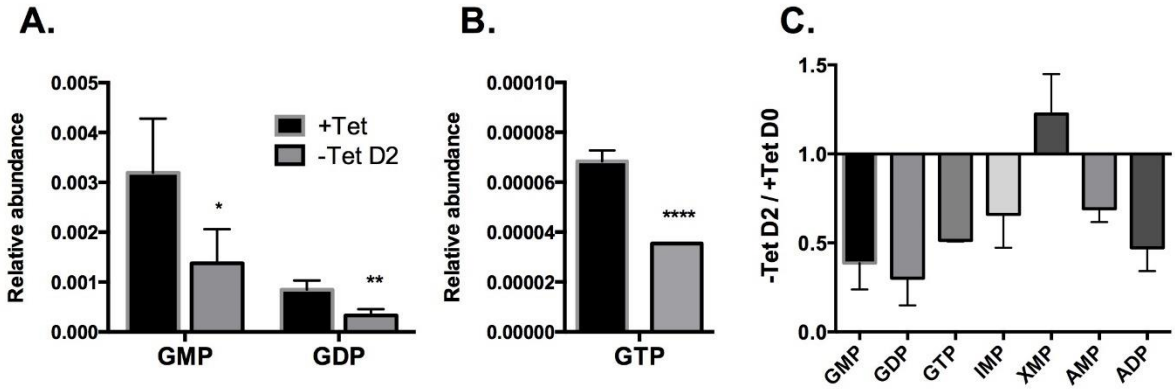

Figure 3.7. Intracellular levels of nucleotides detected by LC-MS/MS for cells collected before and 2 days after Tet removal leading to loss of GMPS expression. Relative ion abundance is shown for A) AMP, B) ADP and IMP and C) XMP. A representative data set for three independent biological replicates collected on the same day is displayed. Guanine nucleotide levels for the same sample set are shown in Fig. 3.6. P values are displayed where * P<0.05, ** P<0.01, *** P <0.0005, **** P<0.0001 for two-tailed t-test. GMP (364/152), GDP (444/152), GTP (524/152), IMP (349/137), XMP (365/97), AMP (348/136), ADP (428/136). D. ATP levels were measured by CellTiterGlo. Luminescence was measured for 500,000 cells where the cell number was determined by hemocytometer. The y-axis shows luminescence per cell. Jun Chen and Ben Tu collected the nucleotide quantitation data.

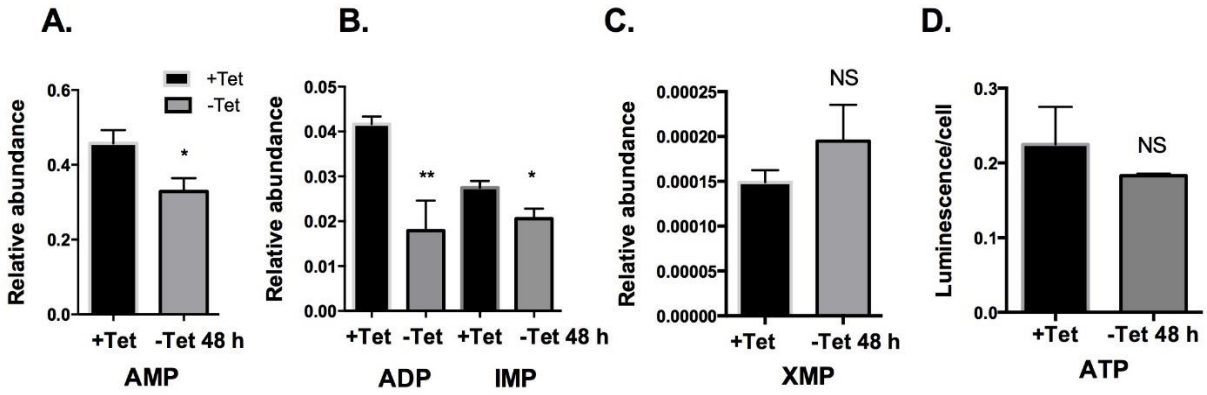

Figure 3.8. *T. brucei* GMPS aligned with human and *E. coli* GMPS. Sequences were aligned using Clustal Omega (1.2.1) multiple sequence alignment software. Genbank accession numbers were as follows: T. brucei (XP_845833), human (NP_003866) and E. coli (YP_490735). Residues within 4Å of XMP in the human x-ray structure (2VXO) are highlighted in green, residues within 4Å of the AMP binding-site based on the *E. coli* X-ray structure (1GPM) are in yellow and residues within 4Å of the citrate binding-site (presumed glutamate binding-site) based on the *E. coli* X-ray structure (1GPM) are shown in turquoise. Residues that differ in the ligand binding-sites between human and *T. brucei* GMPS are highlighted in pink. See Fig. 3.9 for structural alignment details. Jun Chen and Ben Tu collected the nucleotide quantitation data.

```
Ecoli        ------------------MTENIHKHRILILDFGSQYTQLVARRVRELGVYCELWAWDVT
Tbrucei      ----------------MSVQQEPVTECVVILDAGSQYGKVIDRKVRELRVESRVMPLDTP
Human        MALCNGDSKLENAGGDLKDGHHHYEGAVVILDAGAQYGKVIDRRVRELFVQSEIFPLETP 60

Ecoli        EAQIR-DFNPSGIILSGGPESTTEENSPRAPQYVFEAGVPVFGVCYGMQTMAMQLGGHVE
Tbrucei      TDILRSDPSIKGIIISGGPSSISDADAPSYNTDLFSVGKPLLGICYGVQLLTRAFGGKVG
Human        AFAIK-EQGFRAIIISGGPNSVYAEDAPWFDPAIFTIGKPVLGICYGMQMMNKVFGGTVH 119

Ecoli        ASNEREFGYAQVEVVNDSALVRGIEDALTADGKPLLDVWMSHGDKVTAIPSDFITVASTE
Tbrucei      CAGVREDGQDEITVDTNSPIFHGLSNK--------EKVLLTHGDSITEAGPHLKVTARSS
Human        KKSVREDGVFNISVDNTCSLFRGLQKE--------EVVLLTHGDSVDKVADGFKVVARS- 170

Ecoli        SCPFAIMANEEKRFYGVQFHPEVTHTRQGMRMLERFVRDICQCEALWTPAKIIDDAVARI
Tbrucei      AHIIAAVQHESLPLFGVQFHPEVELTENGVQILKNFL-TFCGCKFTFTMEDREEKALRLI
Human        GNIVAGIANESKKLYGAQFHPEVGLTENGKVILKNFLYDIAGCSGTFTVQNRELECIREI 230
```

```
Ecoli        REQVG-DDKVILGLSGGVDSSVTAMLLHRAIGK-NLTCVFVDNGLLRLNEAEQVLDMFGD
Tbrucei      RERTTQGQKVLCLASGGVDSTVCAVLLLKALGPERVVCTHIDHGFMRLNESQEVVAALR-
Human        KERVG-TSKVLVLLSGGVDSTVCTALLNRALNQEQVIAVHIDNGFMRKRESQSVEEALK- 288

Ecoli        HFGLNIVHVPAED-------------------RFLSALAGENDPEAKRKIIGRVFVEVF
Tbrucei      AAGVNVTLIDATKQFSEATTEFPAKRGKGA---YQTGKLCEAIDPEEKRVIIGNTFMSVC
Human        KLGIQVKVINAAHSFYNGTTTLPISDEDRTPRKRISKTLNMTTSPEEKRKIIGDTFVKIA 348

Ecoli        DEEALKL---EDVKWLAQGTIYPDVIESAA-SATGKAHVIKSHHNVGGLPKEMK--MGLV
Tbrucei      DAAVKDLNLDVNNLLLAQGTLRPDLIESGSAYASKVADAIKTHHNDTAVVRQLRAEGRII
Human        NEVIGEMNLKPEEVFLAQGTLRPDLIESASLVASGKAELIKTHHNDTELIRKLREEGKVI 408

Ecoli        EPLKELFKDEVRKIGLELGLPYDMLYRHPFPGPGLGVRVLGEVKKEYCDLLRRADAIFIE
Tbrucei      EPLCDYHKDEVRELGTRLGIPTHLVQRQPFPGPGLAIRVLCSDGSLFKDEHYARTEENVR
Human        EPLKDFHKDEVRILGRELGLPEELVSRHPFPGPGLAIRVICAEEPYICKDF-PETNNILK 467

Ecoli        ----------------------------ELRKADLYDKVSQAFTVFLPVRSVGVMGDGR
Tbrucei      -------------------AVCAGDERFELLKPLCKELRSLQPASCILPIRTVGVQGDGR
Human        IVADFSASVKKPHTLLQRVKACTTEEDQEKLMQ---ITSLHSLNAFLLPIKTVGVQGDCR 524

Ecoli        KYDWVVSLRAVETID-------------------------FM------------------
Tbrucei      TYAYAAALSIGRLPNKEEWNSLGRLALVIPKLTSNVNRIVFMFGPKRAEAPLKATKSSLV
Human        SYSYVCGISSK---DEPDWESLIFLARLIPRMCHNVNRVVYIFGPPVKEPPTDVTPTFLT 581

Ecoli        ------------TAHWAHLPYDFLGRVS---------------------------------
Tbrucei      PEVLDKLRLADDTVNRALIKYGLVRRLSQVPVVLLPIGFEEK-------GPFSVVIRPFI
Human        TGVLSTLRQADFEAHNILRESGYAGKISQMPVILTPLHFDRDPLQKQPSCQRSVVIRTFI 641

Ecoli        --------------------------NRIINEVNGISRVVYDISGKPPATIEWE
Tbrucei      TNDFMTGVPAAPGSADMPLEALKEIVETLQGFDFISRVMYDLTGKPPGTTEWE
Human        TSDFMTGIPATPGN-EIPVEVVLKMVTEIKKIPGISRIMYDLTSKPPGTTEWE 693
```

Figure 3.9. Structural alignment of human (2VXO) and *E. coli* (1GPM) GMPS. A. XMP and AMP binding-sites. The human and *E. coli* structures were superimposed in PyMol by including residues 218-602 human GMPS subunit A (purple) to residues 209 – 438 *E. coli* GMPS (turquoise) in the alignment (RMSD 1.17Å). XMP (green) is from human GMPS and AMP (yellow) is from *E. coli* GMPS. Human GMPS is a dimer and residues contributed from the opposite subunit B are shown in orange. B. Citrate binding-site. The human and *E. coli* structures were superimposed in PyMol by including residues 37 – 208 human subunit B (purple) to residues 19-202 *E. coli* (turquoise) in the alignment (RMSD 0.968). Residues within 4Å of the ligands (ball and stick) are displayed and the numbering is for the human

sequence. The nucleotide and citrate binding-sites could not be simultaneously aligned because of a large domain rotation. Residues that differ in the ligand binding-sites between human and *T. brucei* GMPS are highlighted in pink. Structural Alignment was performed by Margaret Phillips.

A.

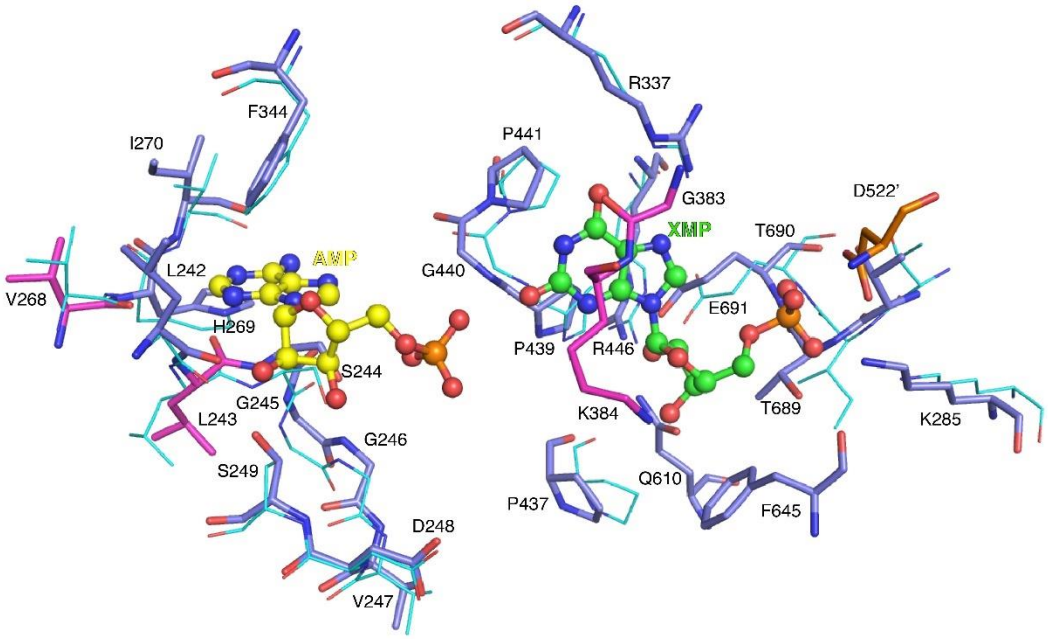

B.

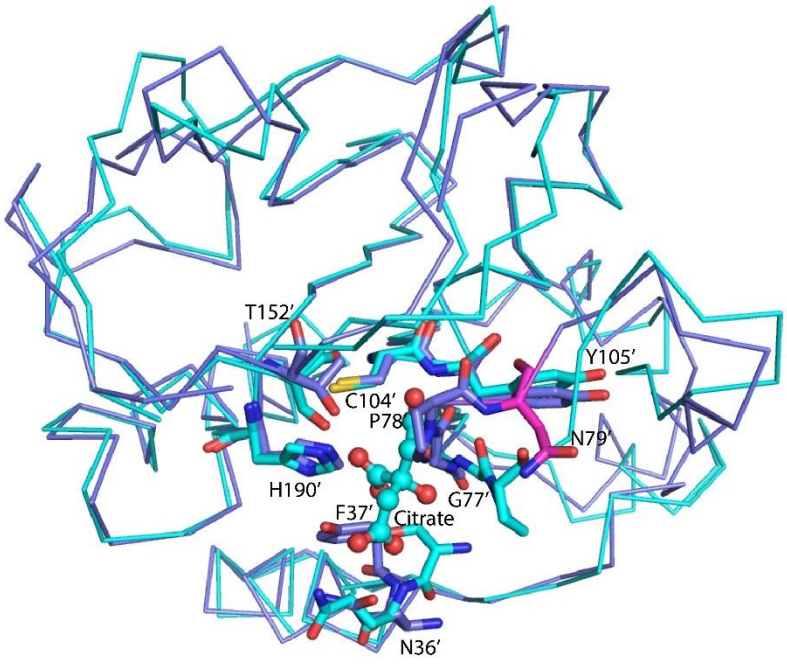

Table 3.1. *T. brucei* culture medium purine base and nucleoside concentrations in comparison to human plasma and CSF.

Nucleoside	HMI-11* -FCS	HMI-19* -FCS	CMM** +FCS	Human plasma***	Human CSF***
Hypoxanthine	1 mM	0	4.4 µM	8 µM	3.4 µM
Thymidine	0.16 mM	0	ND	0.2 µM	0.06 µM
Guanine	0	0	nd	ND	nd
Guanosine	0	0	nd	0.8 µM	nd
Inosine	0	0	nd	1.4 µM	0.62 µM
Xanthine	0	0	nd	1.4 µM	9 µM
Adenine	0	0	nd	0.5 µM	0 – 0.2
Adenosine	0	0	nd	1.0 µM	0 - 0.1

*Data represent concentrations prior to addition of 10% fetal bovine serum (FBS). ** Data were taken from [103] and were determined by LC/MS analysis after the addition of 10% FBS; *** data taken from www.hmdb.ca and are average values of reported data. Human

plasma purine base and nucleoside levels are also reported in [106-108]. ND, not detected; nd, not determined.

Table 3.2. Recombinant *T. brucei* GMPS steady state kinetic analysis.

	K_{mapp} (μM)			k_{cat} s^{-1}
	XMP	ATP	Glutamine	
T. brucei	8.8 ± 0.11	200 ± 21	240 ± 11	4.7 ± 0.07
*P. falciparum**	17	260	470	0.43
Human**	43	160	440	5.3

k_{cat} is the average value calculated for the three different substrate titration curves.

* data taken from [96]; ** data taken from [97]

Table 3.3. Inhibition of parasite growth and recombinant *Tb*GMPS by Acivicin and DON

	$IC_{50.App}$ *Tb*GMPS*	EC_{50} WT cells	EC_{50} *gmps* null cells
	μM		
Acivicin	26 (22 – 30)	1.3 (1.2 – 1.5)	1.8 (1.6 – 2.0)
DON	nd	2.6 (2.2 – 3.1)	3.0 (2.5 – 3.8)

*The time dependence of the enzyme inhibition was not evaluated and thus the IC_{50} values are apparent and dependent on the assay time. *T. brucei* BSF WT (SM) and GMPS null cells were grown in the presence of 100 μM guanine in HMI-19 medium. Error in parenthesis represents the standard error of the fit for triplicate data. nd, not determined.

Table 3.4. Cloning primers. List of cloning primers and corresponding sequences (5'-3') used throughout the study. The primer names contain information regarding their target and functions.

#	Primer name	Primers sequence (5' to 3')
1	GMPS 5' UTR forward	TGCACTGTCACAGCTCCCT
2	GMPS 5' UTR reverse(HYG)	GGTGAGTTCAGGCTTTTTTCATCCGTTTCTGAAGCTTATCC
3	GMPS 3' UTR forward(HYG)	GTCCGAGGGCAAAGGAATAGGCGTTATGTATGATCTCACGGG
4	GMPS 3' UTR reverse	CCCTTTCCCCCGCATCACA
5	GMPS fusion forward	CGTTGTAATTCAGCGGCGC
6	GMPS fusion reverse	TTCCTTCAGCCTCCCTCCGC
7	HYG forward	ATGAAAAAGCCTGAACTCACC
8	HYG reverse	CTATTCCTTTGCCCTCGGAC
9	GMPS RNAi forward	CCACAATGATACGGCAGTTG
10	GMPS RNAi reverse	AGCACCTCAGGGACAAGAGA
11	Lm GMPS forward	CCCAAGCTT ATGTCTCATGAAGGCGCTCC
12	Lm GMPS reverse	GCGGGATCC CTACTCCCATTCAGTGGTGCC
13	GMPS 5' UTR reverse (PAC)	CGTGGGCTTGTACTCGGTCATCCGTTTCTGAAGCTTATCC
14	GMPS 3' UTR forward (PAC)	CGCAAGCCCGGTGCCTGAGCGTTATGTATGATCTCACGGG
15	PAC forward	ATGACCGAGTACAAGCCCAC
16	PAC reverse	TCAGGCACCGGGCTTGCGGGTC
17	Splice leader	CGCTATTATTAGAACAGTTTCTGTACTATATTG
18	GMPS mapping reverse	CACGCCATAACAAATACCCAGC
19	*Lm* GMPS RT forward	GCACAGAAAGCCACACTGTC
20	*Lm* GMPS RT Reverse	GCCGTCTTGGGAATCTCCTT
21	TERT RT forward	GAGCGTGTGACTTCCGAAGG,
22	TERT RT reverse	AGGAACTGTCACGGAGTTTGC
23	DHODH RT forward	GCGAATGTGAATGCCTTTT
24	DHODH RT reverse	CAGAGCAGTGCCGACTTGTA
25	BSD forward	ATGGCCAAGCCTTTGTCTCAA
26	BSD reverse	TTAGCCCTCCCACACATAACCA

CHAPTER FOUR

GENETIC VALIDATION OF ADENYLOSUCCINATE LYASE ESSENTIALITY AND KINETIC CHARACTERIZATION

Introduction

Trypanosoma brucei is an extracellular human pathogen that causes Human African Trypanosomiasis. In contrast to the pyrimidine pathway, trypanosomes are incapable of synthesizing purine nucleotides *de novo*, instead relying entirely on the salvage of nucleosides/nucleobases from the host. As a consequence, there exists a network of salvage and interconversion enzymes to accommodate nucleotide biosynthesis from any single purine precursor. A key enzyme, adenylosuccinate lyase (ADSL), which converts adenylosuccinate to fumarate and AMP, serves as a metabolic bridge to hypoxanthine, xanthine, and guanine salvage. Generation of a conditional null cell line revealed that ADSL is essential for growth despite the presence of alternative metabolic routes to AMP synthesis. In the absence of ADSL, the parasite is restricted to the salvage of adenine and adenosine to supplement AMP pools. Attempts to restore growth with adenine or adenosine supplementation were unsucessful, suggesting that cell death is occurring due to the dead-end buildup of adenylosuccinate. Recombinant ADSL was expressed and purified from *E. coli* for kinetic characterization. The measured k_{cat} and K_m were found to be very similar to ADSL from *Leishmania donovani*, a closely related parasitic protozoan. Structural modeling of the published *T. brucei* and human proteins reveal unique differences in the active sites that could be exploited to develop trypanosome specific ADSL inhibitors.

Materials and Methods

Gene accession *numbers*

The following genes were obtained from TriTrypDB: ADSL (Tb927.9.7550), ADSS (Tb927.11.3650), GMP reductase (Tb927.2080), GMP synthase (Tb927.7.2100)Adenosine kinase (Tb927.6.2300), Inosine 5'-monophosphate dehydrogenase (Tb927.10.16120), AMP deaminase 1 (Tb927.11.3850), AMP deaminase 2 (Tb927.9.9740), AMP deaminase 3 (Tb927.9.7180), AMP deaminase 4 (Tb297.11.15750), TERT (Tb927.11.10190).

T. brucei in vitro growth

Bloodform SM *T. brucei* was cultured in HMI-19 media as described in chapters 2 and 3. *ADSL* c-null cells were grown in 2.5 µg/mL G418, 2.5 µg/mL blasticidin, 2.5 µg/mL phleomycin, and 1.0 µg/mL hygromycin. To induce expression of the ectopic *Tb*ADSL, 1 µg/mL Tet was added daily. Tet-free conditions were obtained by washing cells (20 mL HMI-19 x 3) prior to beginning the growth analysis. For purine rescue experiments, 100 mM stock solutions of sterile filtered adenine and adenosine were added to media at the concentrations described. The growth rates were evaluated using the methods described in chapter 2.

Transfection of *T. brucei*

Transfection of cells with either the NotI linearized pLew100v5-phleo containing the N-terminal FLAG-tag *Tb*ADSL or PCR product were performed as described in chapter 2.

Generation of *T. brucei TK* conditional null cell lines

The *ADSL* c-null cells were obtained by utilizing the PCR fusion method previously described (Table 4.1). SM cells were transfected with a PCR product containing the hygromycin resistance gene flanked by the 5' and 3' UTRs of *ADSL*. PCR amplification from genomic DNA allowed for creation of the N-terminal FLAG-tag ADSL. The forward primer contained a HindIII restriction site followed by the FLAG sequence, the reverse primer incorporated a BamHI restriction site. The HindIII and BamHI digested PCR product containing the FLAG-tag ADSL was ligated into the linearized pLew100v5 vector. Cells containing allelic replacement of the first ADSL copy were further transfected with pLew100v5-phleo containing the Tet regulated N-terminal FLAG-tagged ADSL. Expression of the ectopic copy was induced 48 h prior to replacement of the last allele with a blasticidin resistance marker. PCR primers flanking the 5' and 3' UTRs were used to verify that both copies of *ADSL* were replaced.

RNA and DNA purification

As described in chapter 2.

Western blot analysis

As described in chapter 2.

Quantitation of mRNA by qPCR

RNA extraction and cDNA synthesis was performed as described in chapters 2 and 3. *ADSL* c-null cells were washed of Tet and harvested at a 48 h time point. Each qPCR analysis was performed in triplicate.

Cloning and expression of T. brucei ADSL

The DNA sequence for the *T. brucei* ADSL was obtained from TriTryDB (Tb927.9.7550). PCR was used to generate flanking BsaI and XbaI restriction sites that allowed for cloning into the pE-SUMO(KAN) vector (LifeSensors, Malvern, PA) and expression as a N-terminal His_6-SUMO fusion protein (Table 4.1). The *Tb*ADSL pE-SUMO vector was transformed into BL21 cells. Cells were cultured in 4L LB-KAN (50 μg/mL) media at 37°C until OD_{600} 0.7, then induced with 1 mM IPTG (Isopropyl β-D-1-thiogalactopyranoside) for 3 h. Cells were collected by centrifugation and suspended in buffer A (50 mM NaH_2PO_4 pH 8.0, 300 mM NaCl, 10 mM imidazole) supplemented with 2 mM PMSF (phenylmethane sulfonyl fluoride) and a protease inhibitor cocktail (1 mg/mL leupeptin, 2 mg/mL antipain, 10 mg/mL benzamidine, 1 mg/mL pepstatin, 1 mg/mL chymostatin). Cells were lysed by cell disruptor and the cell debris removed by centrifugation. Supernatant was applied to a HisTrap HP column (GE Healthcare) and washed with buffer A. The His_6-SUMO *Tb*ADSL fusion was eluted with buffer B (50 mM NaH_2PO_4 pH 8.0, 300 mM NaCl, 250 mM imidazole). Fractions were analyzed by SDS-

PAGE and those containing *Tb*ADSL were pooled, concentrated (10 kDa MWCO Millipore) and dialyzed against buffer A. The His_6-Sumo tag was removed by overnight incubation at 4^{o}C with His_6-tagged Ubiquitin-like-specific protease 1 (ULP1) as described [65]. After incubation the mixture was applied to a second HisTrap HP column and cleaved *Tb*ADSL was collected in the flow-through, while His_6-tagged ULP-1 and impurities were retained on the resin. The flow through was concentrated for further purification by Gel Filtration chromatography on a SuperDex 200 Prep Grade column (GE Healthcare) using buffer A. Protein concentration was determined by Bradford Assay (Bio-Rad).

ADSL kinetic characterization

A continuous spectrophotometric assay was used to measure the activity of recombinant *Tb*ADSL by monitoring the decrease of adenylosuccinate at 282 nM using a Beckman spectrophotometer using quartz cuvettes. A steady state kinetic analysis was performed by collected data over 5 minutes in reactions (1 mL) containing 20 mM HEPES (pH 7.0), 1 µg enzyme, and 0 – 150 µM adenylosuccinate (ε = 16,430 $M^{-1}cm^{-1}$). The collected triplicate data was fitted to the Michalis-Menton equation ($Y = V_{max}*X/(K_m+X)$) using GraphPad Prism to determine K_m and k_{cat}.

Results

ADSL is essential for growth in culture

To evaluate the essentiality of ADSL, attempts were made to generate an *ADSL* null cell line. Allelic replacement of a single *ADSL* allele with a selectable marker was obtained and repeated attempts to replace the last allele were unsuccessful, suggesting essentiality. As an alternative approach, we set out to generate an *ADSL* conditional null cell line (c-null), allowing us to deplete ADSL in the background of a null cell line. The single allelic replacement was transfected with a pLew100v5 vector containing an N-terminal FLAG-tag ADSL under tetracycline (Tet) regulation. The addition of Tet to growth medium induced expression of the ectopic FLAG-tagged ADSL, permitting replacement of the remaining allele. To confirm that the ADSL locus has been replaced by the hygromycin and blasticidin resistance markers, genomic DNA was extracted the ADSL c-null cell line and analyzed for integration of the resistance markers (Fig. 4.1A). Primers flanking the 5' and 3' *ADSL* UTRs were used for PCR amplification, confirming that the both alleles have been replaced. To evaluate the effect of ADSL depletion on cell growth, Tet was removed from the growth medium. Western blot analysis 48 h after the removal of Tet coincided with depletion of the FLAG-tagged ADSL and a rapid arrest of cell growth (Fig. 4.2A). qPCR analysis 48 h after the removal of Tet mirrored the western blot results, demonstrating excellent regulation of the ectopic ADSL (Fig. 4.1B). On day 4, parasites begin to reemerge despite the absence of Tet in the growth media, suggesting the loss of regulation of the ectopic copy. This is a common phenomenon that has been observed with numerous c-null cell lines (Chapters 2 and 3).

Adenine and adenosine are unable to rescue ADSL depleted cells

To circumvent the lethality of ADSL depletion, we attempted to rescue growth phenotype with adenine or adenosine supplementation. Based on the current annotation of *T. brucei* purine pathway, there are two major routes to AMP formation. In the case of ADSL depleted cells, the only possible route to AMP nucleotides is through the salvage of adenine by APRT or by the phosphorylation of adenosine by adenosine kinase (Fig. 4.1). Previous studies demonstrate that the parasite possesses two adenosine transport systems, P1 and P2[111]. The P2 system has been shown to also mediate the transport of adenine. These two systems also facilitate the uptake of melarsoprol and pentamidine, and the loss of P2 has been associated with drug resistance and treatment failure[112]. To evaluate the potential of these two purines in restoring the growth of ADSL depleted cells, concentrations up to 100 μM of adenine and adenosine were added to the growth media following the removal of Tet. We found that concentrations as low as 10 μM adenine resulted in a slight initial rescue of the growth phenotype (Fig. 4.2B). However, this trend does not continue past 48 h after removal of Tet as the cells eventually enter growth arrest. In contrast, no concentration of adenosine had any effect on cell growth (Fig. 4.2C). It is known that fetal bovine serum (FBS) contains large quantities of adenosine deaminase[113]. The presence of this enzyme, which is absent in *T. brucei*, would result in the conversion of adenosine to inosine, subverting the possibility of adenosine restoring AMP pools. Although the FBS is heat inactivated prior to formulation of the growth media, it is possible that residual adenosine deaminase activity is present. The inability of adenine or adenosine to restore the growth of ADSL depleted cells suggests that

there could be an alternative mechanism mediating cell death that is independent of AMP pools.

qPCR reveals no significant changes in the expression of purine enzymes

To gain further mechanistic insight into the lethality of ADSL depletion we performed a qPCR analysis on various genes in the purine pathway. Although it is well known that trypanosomes lack transcriptional regulation, there exists mechanisms that regulate mRNA decay[114]. ADSL c-null cells were collected 48 h after the removal of Tet and the expression of a subset of purine genes were analyzed (Fig. 4.3). As expect, ADSL expression was virtually undetectable, while the expression of the majority of genes analyzed were not significantly changed. We observed a slight increase in ADSS and AMP deaminase 1 (AMPD1), which could suggest increased flux towards adenylosuccinate formation. The lack of any significant changes in mRNA levels related to these purine genes does not preclude the possibility of changes at the level of protein.

Recombinant ADSL is capable of catalyzing the formation of AMP and fumarate

To date, there has been no kinetic characterization performed on the *T. brucei* ADSL (*Tb*ADSL) to demonstrate activity. The putative *Tb*ADSL was cloned into the pE-SUMO (KAN) vector for expression as an N-terminal His_6-SUMO-TbADSL fusion in *E. coli*. After the first Ni-NTA affinity column, the His6-SUMO tag was cleaved and second subtracting Ni-NTA affinity column permitted isolation of tag-free *Tb*ADSL. Further purification by a preparatory size exclusion column yielded high purity *Tb*ADSL that was used for kinetic

characterization. To measure *Tb*ADSL activity, adenylosuccinate was continuously monitored at 282 nm as it was converted to AMP and fumarate. *Tb*ADSL catalyzed the formation of AMP with a k_{cat} of 1640 min^{-1}, nearly identical to the published k_{cat} of 1680 min^{-1} for *Leishmania donovani* ADSL (*Lm*ADSL)[39] (Fig. 4.4) . Titration of the substrate adenylosuccinate revealed an apparent Km of 22 µM, also very similar to the reported value of 24 µM for *Lm*ADSL.

There are unique differences between the *T. brucei* and human ADSL active sites

Structural and biochemical characterization of the human ADSL has provided insight into the identity catalytic residues as well as those mediating substrate binding[115]. An amino acid sequence analysis of the trypanosome enzyme reveals high conservation among key residues (Fig. 4.5). Although the vast majority are retained within the trypanosome counterpart, differences in residues composing the active site could provide the basis for developing species specific inhibitors. Using the available *Tb*ADSL crystal structure, a structural alignment of the trypanosome and human active sites was generated. Further analysis of the active site residues within 5 Å of the substrate exposed 5 amino acid differences between the trypanosome and human structures (Fig. 4.6).

Conclusions

The lack of a *de novo* route has made the purine pathway an attractive target for therapeutic intervention. Until recently, the prospect of identifying a single purine enzyme that would be essential for parasite viability remained a major questions due to the redundant

nature of the pathway. Our approach of strategically depleting key interconversion enzymes reveals that this redundancy can be overcome (Chapter 3). In this work, we demonstrate that *Tb*ADSL is an active enzyme that is capable of catalyzing the formation of AMP. Through the use of a *ADSL* c-null we genetically validate that ADSL is required for viability in culture despite the availability of alternative routes to AMP formation. Purine rescue experiments were performed to address the possibility that the ADSL depleted cells require increased amounts of adenine or adenosine for viability. Concentrations of both purines up to 100 μM were unable to reverse the growth phenotype. To gain further insight into the consequences of ADSL depletion, we performed a qPCR analysis of genes in the purine pathway. We determined that at the level of transcription there were no major changes. We also assess the feasibility of developing a species selective ADSL inhibitor by performing a structural alignment of the *Tb*ADSL and *Hs*ADLS active sites using the previously solved crystal structures. The active site differences suggest that it may be possible to selectively target *Tb*ADSL by a chemical inhibitor.

Our prior work demonstrates that strategic inhibition of key metabolic routes exploits a major vulnerability related the parasites nutrient limited extracellular niche. In the case of guanosine-5'-monophosphate synthase (GMPS), the metabolic block imposed by GMPS depletion forces the parasite to rely solely on guanine to maintain GMP pools. To remain viable, the parasite requires a concentrations of guanine (>100 μM) that far exceeds physiological levels found in human blood (< 1 μM). As for ADSL depletion, no amount appears to rescue the growth phenotype. Although no *in vivo* studies were performed, we expect that *ADSL* c-null cells will be rendered avirulent in mice upon ADSL depletion.

Previously published RNAi experiments in mice demonstrate that ADSL knockdown reduces virulence[40]. However, the inability of these mice to fully clear the parasites may be the result of insufficient ADSL knockdown. In further support, depletion of ADSL in *Leishmania donovani* significantly reduces the parasite's ability to infect mice [39].

The inability of adenine or adenosine to rescue *ADSL* c-null cells has some interesting implications. In *L. donovani* promastigotes, it was only possible to rescue ADSL depleted cells with adenine or adenosine in the presence of an adenine aminohydrolase inhibitor. This enzyme is not present in mammals and is unique to *Leishmania*. It catalyzes the conversion of adenine to hypoxanthine, preventing the salvage of adenine into AMP pools by APRT [116]. It is believed that Trypanosomes do not possess this enzyme, therefore this metabolic route should not compete with the salvage of adenine. However, it is possible that this activity may exist in the parasite and could be competing for the salvage of adenine. There has been reports that *T. brucei* and *T. cruzi* possess adenosine aminohydrolase activity[117]. This activity may explain why adenosine had no effect in delaying the onset of growth arrest in ADSL depleted cells. An alternative explanation for the inability of adenine or adenosine to rescue could be that in the absence of ADSL there is a lethal dead end buildup of adenylosuccinate. This phenomenon was observed when ADSL was depleted in *Leishmania donovani*, where the resulting dead-end accumulation of adenylosuccinate presumably caused the depletion of guanylate nucleotides [39]. Perhaps even in the presence of salvageable adenine/adenosine the irreversible accumulation of adenylossucinate is toxic or leads to an imbalance of purine nucleotides. It is conceivable that an *ADSS* null cell line

would circumvent the accumulation of adenylosuccinate and remain viable if cultured in media supplemented with adenine or adenosine.

In conclusions, our study genetically validates ADSL as a potential drug target in *T. brucei*. We provide the first kinetic characterization of the trypanosome enzyme, demonstrating that it is capable of catalyzing the conversion of adenylosuccinate into AMP. Although there exists an alternative route to AMP formation through the extracellular salvage of adenine or adenosine, no amount is capable of restoring parasite viability. These results suggest an alternative mechanism mediating cell death. As consequence, it is unlikely that physiological concentrations of these purines in human plasma will be capable of supporting an infection. Furthermore, if ADSL essentiality extents to the closely related intracellular trypanosomatid *T. cruzi*, higher intracellular levels of purines will also be unable to support growth. Structural analysis of the *T. brucei* and human active sites reveal unique differences that could be exploited to develop inhibitors selectively targeting the trypanosome enzyme. This study demonstrates that ADSL is an excellent target for the development of drugs to treat HAT.

Figure 4.1 Endogenous ADSL expression has been replaced with Tet regulated *Tb*ADSL. A. PCR amplification of the *ADSL* locus using primers flanking the selectable markers and *ADSL* 5' and 3' UTRs. The selectable markers were amplified from *ADSL* c-null genomic DNA. The *ADSL* locus was amplified from genomic DNA extracted from *ADSL* c-null and SM cells. B. qPCR analysis comparing mRNA expression levels of *Tb*ADSL to the

TERT control ±Tet for 24 h. Error bars represent standard error of the mean (SEM) for triplicate data.

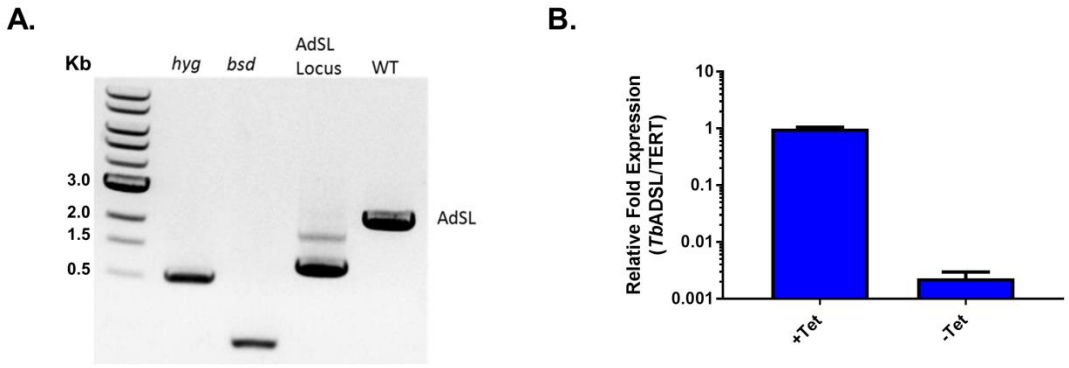

Figure 4.2. ADSL is essential for growth in vitro and cannot be rescued with adenine and adenosine supplementation. A. Growth analysis of *ADSL* c-null cells ±Tet. Expression of ectopic FLAG-tagged *Tb*ADSL is under Tet control, thus removal of Tet leads to loss of *Tb*ADSL expression. Cells were grown in HMI-19 medium and growth was monitored for the indicated days. Error bars represent standard deviation (SD) for triplicate biological replicates. Inset shows western blot analysis of FLAG-tagged *Tb*ADSL expression ±Tet for 48h. *Tb*BiP was detected as a loading control. B-C. Growth analysis of *ADSL* c-cells supplemented with (B) adenine (μM) or (C) adenosine (μM) (±Tet). Error bars represent SD for triplicate biological replicates.

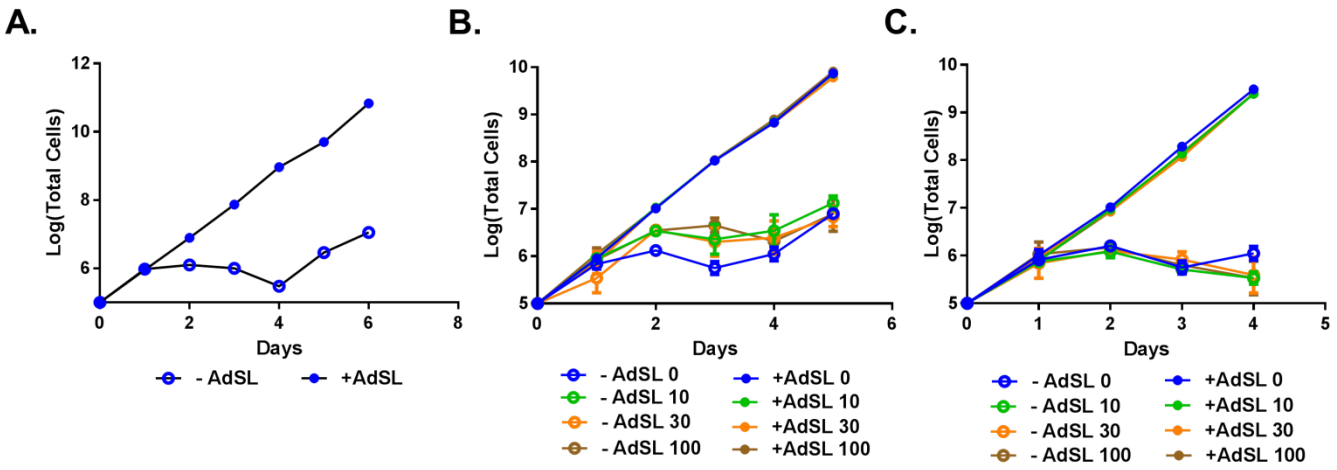

Figure 4.3 qPCR analysis of purine genes reveals no significant changes in mRNA abundance upon *Tb*ADSL depletion. The relative expression of the following purine genes were measured 48 h post ADSL depletion (±Tet): ADSL, adenylosuccinate synthase (ADSS), GMP reductase (GMPR), IMP dehydrogenase (IMPDH), adenosine kinase 1(AK1), AMP deaminase 1-4 (AMPD), GMP synthase (GMPS), adenine phosphoribosyltransferase 1-2 (APRT). TERT was used as a reference gene and error bars represent standard error of the mean (SEM) for triplicate data.

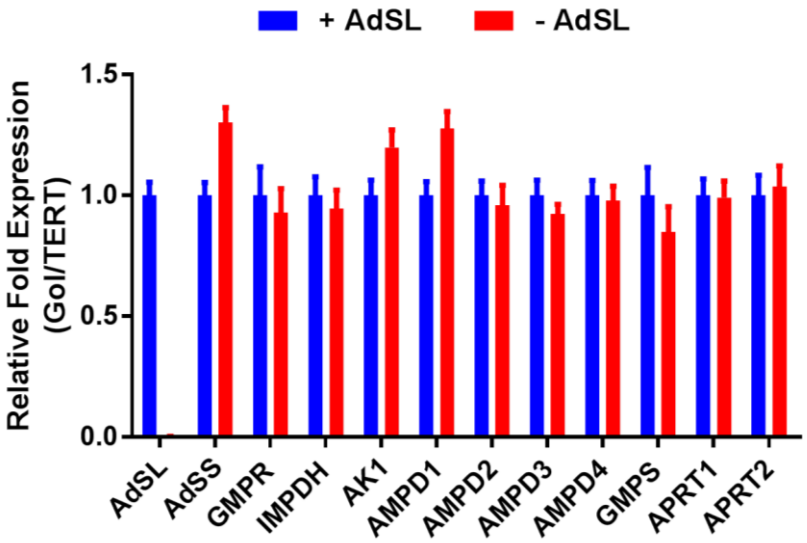

Figure 4.4. Steady-state kinetic analysis of *T. brucei* ADSL. A spectrophotometric assay is used to monitor depletion of the substrate adenylosuccinate by the purified recombinant enzyme. The calculated *Tb*ADSL K_m and k_{cat} are compared to the *Leishmania donovani* ADSL.

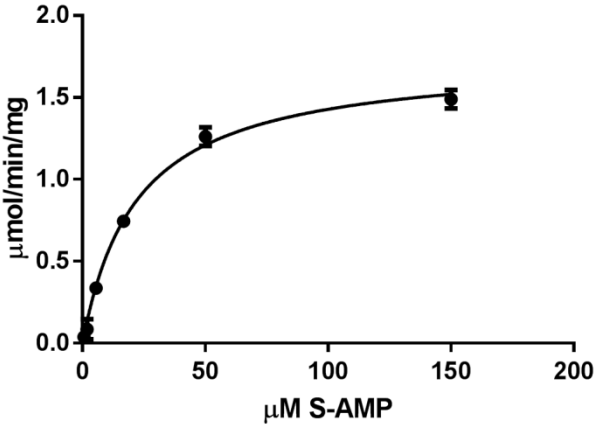

	TbAdSL	LmAdSL
k_{cat} (min^{-1})	1640 ± 40.24	1680
k_m (µM)	22.06 ± 1.7	24

Figure 4.5. Amino acid sequence alignment (Clustal Omega version 1.2.2) of ADSLs from select species (UniProt Entry). Saccharomyces cerevisiae (Sc-Q05911), Human (Hs – P30566), Mus muscaris (Mm – P54822), E. coli (Ec – P0AB89), T. brucei (Tb – Q38EJ2), Leishmania donovani (Ld – A7LBL3). Amino acids colored red and green represent catalytic residues and substrate binding sites based on the human structure, respectively.

```
ScADSL      --------------------------MPDYDNYTTPLSSRYASKEM--SATFSLRNRFST   32
HsADSL      -----------MA---------AGGDHGSPDSYRSPLASRYASPEM--CFVFSDRYKFRT   38
MmADSL      -----------MA---------ASGDPGSAESYRSPLAARYASREM--CFLFSDRYKFQT   38
EcADSL      ------------------------MELSSLTAVSPVDGRYGDKVSALRGIFSEYG-LLK   34
TbADSL      -----------MEKGSPSDLNGVDYSVDNPLFALSPLDGRYKRQTKALRAFFSEYG-FFR   48
LdADSL      MSLPSAEEAAAPAVTTTAHKAPAEISQDSPLYSLSPLDGRYKRDTTPLRAYFSEYA-LFK   59
                                      .    :*: .**         **    :

ScADSL      WR----KLWLNL--AIAEKELGLTVVTDEAIEQMRKHVE-ITD-DEIAKASAQEAIVRHD   84
HsADSL      WR----QLWLWL--AEAEQTLGLPIT-DEQIQEMKSNLE-NID---FKMAAEEEKRLRHD   87
MmADSL      WR----QLWLWL--AEAEQTLGLPIT-DEQIQEMKSNLN-NID---FQMAAEEEKRLRHD   87
EcADSL      FRVQVEVRWLQKLAAHAA-IKEVPAFAADAIGYLD-AIVASFSEEDAARIKTIERTTNHD   92
TbADSL      YRVLVEVEYFTALCKDVPTIVPLRSVTDEQLQKLRKITLDCFSVSSAEEIKRLERVTNHD  108
LdADSL      YRVQVEVLYFEALCKEVPAITQLRGVTDAQLGELRATTFENFAVDDAKIIKGIEAVTNHD  119
            :*      ::      .     :       :  :                   *   .**

ScADSL      VMAHVHTFGET----C--PAAAGIIHLGATSCFVTDNADLIFIRDAYD-IIIPKLVNVIN  137
HsADSL      VMAHVHTFGHC----C--PKAAGIIHLGATSCYVGDNTDLIILRNALD-LLLPKLARVIS  140
MmADSL      VMAHVHTFGHC----C--PKAAGIIHLGATSCYVGDNTDLIILRNAFD-LLLPKLARVIS  140
EcADSL      VKAVEYFLKEKVAEIPELHAVSEFIHFACTSEDINNLSHALMLKTARDEVILPYWRQLID  152
TbADSL      IKAVEYFIKERMDT-CGLSHVTEFVHFGLTSQDINNTAIPMMIRDAIVTLYLPALDGIIG  167
LdADSL      IKAVEYYLKDKMSA-CGLEAEKEFIHFGLTSQDINNTSIPMLLRDALHHHYIPTLDQLIA  178
            : *  : : .             ::*:. **  : : :  :::: *     :*    :*

ScADSL      RLAKFAMEYKDLPVLGWTHFQPAQLTTLGKRATLWIQELLWDLRNFERARNDIGLRGVKG  197
HsADSL      RLADFAKERASLPTLGFTHFQPAQLTTVGKRCCLWIQDLCMDLQNLKRVRDDLRFRGVKG  200
MmADSL      RLADFAKDRADLPTLGFTHFQPAQLTTVGKRCCLWIQDLCMDLQNLKRVRDELRFRGVKG  200
EcADSL      GIKDLAVQYRDIPLLSRTHGQPATPSTIGKEMANVAYRMERQYRQLNQVEILGKINGAVG  212
TbADSL      SLTSKLV-DWDVPMLARTHGQPASPTNLAKEFVVWIERLREQRRQLCEVPTTGKFGGATG  226
LdADSL      LLKSKLP-EWDVPMLARTHGQPASPTNLAKEFMVWIERLEEQRTMLLSIPNTGKFGGATG  237
             : .      .:* *. ** ***  :.:.*.       :  :   :        : *. *

ScADSL      TTGTQASFLALFHGNHDKVEALDERVTELLGFDKVYPVTGQTYSRKID-IDVLAPL----  252
HsADSL      TTGTQASFLQLFEGDDHKVEQLDKMVTEKAGFKRAFIITGQTYTRKVD-IEVLSVL----  255
MmADSL      TTGTQASFLQLFEGDHQKVEQLDKMVTEKAGFKRAFIITGQTYTRKVD-IEVLSVL----  255
EcADSL      ---NYNAHIAAYPEVDWH-QFSEEFVT-SLGIQW------NPYTTQIEPHDYIAELFDCV  261
TbADSL      ---NFNAHLVAYPSVNWR-AFADMFLAKYLGLKR------QQATTQIENYDHLAALCDAC  276
LdADSL      ---NFNAHLCAYPGVNWL-DFGELFLSKYLGLRR------QRYTTQIEHYDNLAAICDAC  287
               .  :.:  :   .      :  ::   *:        :  : :::  : :: :

ScADSL      SSFAATAHKMATDIRLLANLKEVEEPFEKSQIGSSAMAYKRNPMRCERVCSLA---RHLG  309
HsADSL      ASLGASVHKICTDIRLLANLKEMEEPFEKQQIGSSAMPYKRNPMRSERCCSLA---RHLM  312
MmADSL      ASLGASVHKICTDIRLLANLKEMEEPFEKQQIGSSAMPYKRNPMRSEHCCSLA---RHLM  312
EcADSL      ARFNTILIDFDRDVWGYIALNHFKQKTIAGEIGSSTMPHKVNPIDFENSEGNLGLSNAVL  321
TbADSL      ARLHVILIDMCRDVWQYISMGFFKQKVKEGEVGSSTMPHKVNPIDFENAEGNLALSNALL  336
LdADSL      ARLHTILMDLAKDVWQYISLGYFDQKVRAGEVGSSAMPHKVNPIDFENAEGNLGMSNAVL  347
            : : .   .:  *:     :  ..:     ::***:* :* **:  *.  .     . :

ScADSL      SLFSDAVQTASVQWFERTLDDSAIRR-ISLPSAFLTADILLSTLLNISSGLVVYPKVIER  368
HsADSL      TLVMDPLQTASVQWFERTLDDSANRR-ICLAEAFLTADTILNTLQNISEGLVVYPKVIER  371
MmADSL      ALTMDPLQTASVQWFERTLDDSANRR-ICLAEAFLTADTILNTLQNISEGLVVYPKVIER  371
EcADSL      QHLAS---KLPVSRWQRDLTDSTVLRNLGVGIGYA--LIAYQSTLKGVSKLEVNRDHLLD  376
TbADSL      NFFAS---KLPISRLQRDLTDSTVLRNLGVPIGHA--CVAFASISQGLEKLMISRETISR  391
LdADSL      GFLSA---KLPISRLQRDLTDSTVLRNLGVPLSHA--LIAFASLRRGIDKLLLNKDVIAS  402
                    .  :.  :* * **:  * : :  ..        :  .  . * :  . :

ScADSL      RIKGELPFMATENIIMAMVEKNASRQEVHERIRVLSHQAAAVVKEEGGENDLIERVKRDE  428
HsADSL      RIRQELPFMATENIIMAMVKAGGSRQDCHEKIRVLSQQAASVVKQEGGDNDLIERIQVDA  431
MmADSL      RIRQELPFMATENIIMAMVKAGGSRQDCHEKIRVLSQQAAAVVKQEGGDNDLIERIRADA  431
EcADSL      ELDHNWEVLA-EPIQTVMRRYG--IEKPYEKLKELTRGKR--VDAEGMK-QFIDGLA---  427
TbADSL      ELSSNWAVVA-EGIQTVLRREC--YPKPYETLKKLTQGNTD-VTEEQVR-NFINGLT---  443
LdADSL      DLEGNWAVVA-EGIQTVLRREG--YPKPYEALKDLTRGNAH-VTEETVH-RFVQQLE---  454
             :  :  .:* * *  .: .      . :* :: *::     *  *     ::: :
```

Figure 4.6. Structural alignment of T. brucei (4EFC) and human (2VD6) ADSL. The *T. brucei* and human structures were superimposed in PyMol by including residues 12-466 of T. *brucei* (green) ADSL to residues 5 – 471of the human ADSL (turquoise) in the alignment (RMSD 1.17Å). Residues within 5Å of the ligand (S-AMP, ball and stick) that differ between human and *T. brucei* ADSL are displayed and numbered according to the *T. brucei* sequence.

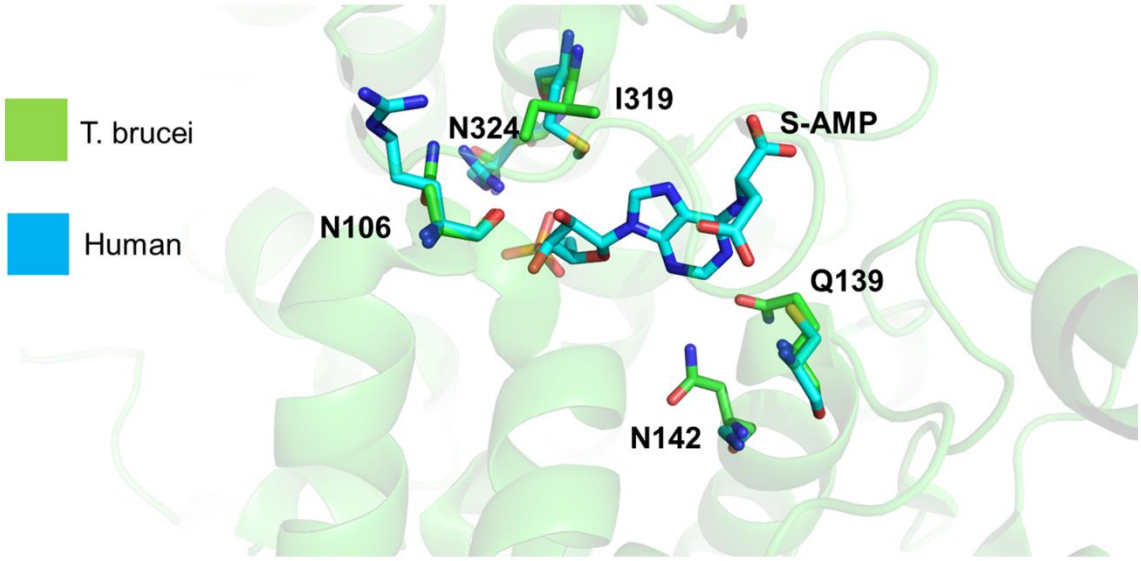

Table 4.1. Cloning primers. List of cloning primers and corresponding sequences (5'-3') used throughout the study. The primer names contain information regarding their target and functions.

#	Primer name	Sequence (5' to 3')
1	ADSL 5' UTR forward	gccagttgcattagcgtagctgt
2	ADSL 3' UTR reverse	gggagggctcaaaagaatcggtgg
3	ADSL 5' UTR reverse (HYG)	ggtgagttcaggctttttcatcctttctttttgttttttg
4	ADSL 3' UTR forward (HYG)	agttccttgtagtccttggtccgagggcaaaggaatag
5	ADSL 5' UTR reverse (BSD)	ttgagacaaaggcttggccatcctttctttttgttttttg
6	ADSL 3' UTR forward (BSD)	agttccttgtagtccttgtggttatgtgtgggagggctaa
7	ADSL fusion forward	ggg agg gct caa aag aat cgg tgg
8	ADSL fusion reverse	gga agg cag gag gga agg gac atc
9	HYG forward	atgaaaaagcctgaactcacc
10	HYG reverse	cta ttc ctt tgc cct cgg ac
11	BSD forward	atggccaagcctttgtctcaa
12	BSD reverse	tta gcc ctc cca cac ata acc a
13	ADSL HindIII NT-FLAG forward	taaaattcacaagcttatggactacaaagacgacgacgacaaagagaagggttcaccatccgac
14	ADSL BamHI reverse	gtt cct cgc ttc agt gct aaa taa gga tcc tgc cca ttt a
15	ADSL Sumo forward	gctaggtctcaaggtgagaagggttcaccatccgac
16	ADSL Sumo reverse	tag ctc tag att att tag cac tga agc gag gaa c
17	ADSL qPCR forward	gcatgtgttgcgtttgcttc
18	ADSL qPCR reverse	cgcagaactgtttgaatgcc
19	ADSS qPCR forward	tcaatgatgaggggttctc
20	ADSS qPCR reverse	tccacaccatcagcattctc
21	AMPD1 qPCR forward	aggatcgggtcttcacaatg
22	AMPD1 qPCR reverse	tgctcattacgtgcctcaag
23	AMPD2 qPCR forward	agtttgcttcgtgacttgcg
24	AMPD2 qPCR reverse	aacgaatgcgcatgtccaag
25	AMPD3 qPCR forward	agggaaaagaaccgcaaacg
26	AMPD3 qPCR reverse	agtgttgtgtcgacttgcac
27	AMPD4 qPCR forward	acgcaacgctgatgaagttg
28	AMPD4 qPCR reverse	ttttgctttaccgcgtcagg
29	GMPR qPCR forward	accttgtattgccgatggtg
30	GMPR qPCR reverse	gttccagcgagcatatttcc
31	AK1 qPCR forward	cggtttcacgttgacagttg
32	AK1 qPCR reverse	aaaagtccatccacctcacg
33	IMPDH qPCR forward	atcagcggcattcttgtcac
34	IMPDH qPCR reverse	tattttcgcgccgtgtcatg
35	GMPS qPCR forward	ttgttatggcgtgcagttgc
36	GMPS qPCR reverse	tgcgtgagaagcacctttc
37	APRT1 qPCR forward	cacttgtggaggttttgccg
38	APRT1 qPCR reverse	atacccgccacttccacaag
39	APRT2 qPCR forward	acttcacgctggcagatacc
40	APRT2 qPCR reverse	gcggggagagtttgaagtga

CHAPTER FIVE

PERSPECTIVES

Pyrimidine metabolism, specifically the pathway related to thymidylate biosynthesis, has been proven to be druggable and is the foundation of many therapies. Perhaps the most well-known is methotrexate, which is used to treat cancer and autoimmune diseases by competitively inhibiting dihydrofolate reductase (DHFR)[118]. In *T. brucei*, this enzyme is expressed as a fusion with thymidylate synthase (DHFR-TS) and is responsible for reducing dihydrofolate to tetrahydrofolate. Methenylation of tetrahydrofolate permits the methylation of dUMP to form dTMP. Inhibition of DHFR ultimately interferes with the synthesis of thymidylates and results in the toxic build-up of dUTP[119]. The antifolates methotrexate and raltitrexed were reported to have nanomolar potency against the parasite in culture [120]. However, the effectiveness of these drugs are highly susceptible to extracellular folate concentrations. Thymidine kinase has also been the focus of many revolutionary antiviral drug therapies. For example, the most well-known are the class of nucleoside analogues that function as a prodrug to selectively target herpes simplex virus (HSV-1) and varicella-zoster virus (VZV). These subversive compounds exploit the viral TK's broad substrate specificity to incorporate these chain terminating analogues into DNA[121]. In fact, our data demonstrates that *T. brucei* has some degree of sensitivity to 50 µg/mL of ganciclovir, however a more detailed titration needs to be performed (Fig. 2.6 C). Kinetic characterization of *Tb*TK revealed that the enzyme has a less strict substrate preference compared to the human TK, explaining its sensitivity to ganciclovir [28]. Historically, there is great precedent for developing drugs that target enzymes in the pyrimidine pathway, especially TK.

The pyrimidine pathway in Trypanosomes could be viewed as one of the most well studied pathways. It could be argued that drawing upon an abundance of previous work in

higher eukaryotes and recent genomic data from the sequencing and annotation of the reference genome that a near complete picture of pyrimidine metabolism has been obtained. First glance of the current data would support this. The canonical genes related to the *de novo* biosynthesis of pyrimidine precursor UMP is present. The pathway possesses the highly conserved ribonucleotide-reductase to catalyze the formation of deoxynucleotides, functioning on both branches of the pathway ensuring the synthesis of dTTP and dCTP. The presence of dihydrofolate-thymidylate synthase provides a route linking folate metabolism to the conversion of uracil nucleotides into thymine nucleotides. In the case of cytosine nucleotides, CTP synthase fulfills the rate limiting function of linking UTP to the formation of CTP.

In addition to a fully functional *de novo* route, there is an abundance of pyrimidine salvage enzymes. These seemingly redundant enzymes serve the role of salvaging preformed nucleosides and nucleobases from the host, presumably reducing the metabolic costs related to the biosynthesis of nucleotides. These enzymes directly supplement thymine nucleotide pools which represent the most metabolically expensive molecules to synthesize. TK allows for the phosphorylation of thymidine or deoxyuridine into dTMP and dUMP, respectively. Cytidine deaminase salvages available deoxycytidine into deoxyuridine, contributing to dUMP formation. Upstream in the pathway uracil phosphoribosyltransferase, in conjunction with a high affinity uracil transporter, provides the salvaged materials to feed both branches of the pathway by converting uracil to UMP. Despite the utility of these enzymes, it was clear that trypanosomes are not pyrimidine auxotrophs. In contrast to purine requirements, the parasite is capable of growth in pyrimidine-free conditions. Based on these observations,

it was presumed that these salvage enzymes are expendable and had no significant role in pyrimidine metabolism.

The discovery of this novel metabolic route linking cytosine and thymine nucleotide pools changes our understanding of flux through the pyrimidine pathway. It is not the bifurcated linear system we imagined, where the nucleotide precursors split into their respective dTTP and dCTP branches of the pathway. Instead, there is a dynamic interplay of substrate cycling where monophosphate nucleotides can be interconverted by pyrimidine salvage enzymes to provide another layer of regulation and balance between nucleotide pools. The existence of such a metabolic bridge is not unprecedented as eukaryotes and prokaryotes possess the enzymes capable of converting deoxycytidylates into deoxythymidylate nucleotides. It is likely that this metabolic link functions to balance between thymine and cytosine nucleotide pools, to effectively bypass the irreversible commitment of pyrimidine precursors to one particular nucleotide. The ability to interconvert between the pools offers a degree of metabolic flexibility that would prove advantageous in situations where there is a demand for one particular precursor without having to compromise one particular branch of the pathway.

The discovery of TK's essential role in *T. brucei* pyrimidine metabolism has profound implications. In addition to advancing our understanding of nucleotide metabolism in trypanosomes, it exposes a major vulnerability among kinetoplastids that could be exploited to develop a drug that targets multiple pathogens. Thus far, we have observed one other major method of linking deoxycytidylate nucleotides to deoxythymidylate nucleotides via dCMP/dCTP deaminase. This discovery describes a second method of performing the

same function, but instead utilizing pyrimidine salvage enzymes. These two different metabolic arrangements represent a redundancy that converges on dUMP pools. Humans have the second method of generating dUMP via the 5'-nucleotidase, CDA, and TK. Due to the presence of both routes, the significance of this second route has never been realized because any depletion of either DCTD or TK individually would likely have no effect. In *T. brucei*, the lack of DCTD leaves only one route linking deoxycytidine nucleotides to dUMP. This explains why severing the remaining link, by depletion of TK or CDA, is lethal to these parasites. I suspect that the same arrangement observed in other kinetoplastids makes them vulnerable to TK inhibition. Although CDA inhibition is lethal, variabilities in the availability of dUrd and dThd may allow cells to overcome inhibition. The development of a pan TK inhibitor would revolutionize the treatment of HAT, Chagas disease, and Leishmaniasis.

Based on our bioinformatics analysis, it is probable that we have identified one of the many 5'-nucleotidases in *T. brucei*. I suspect that there are several enzymes possessing overlapping activity that have roles in multiple physiological processes. I predict that if the YfbR homologue is the sole enzyme catalyzing the formation of deoxycytidine then knockout cells will be rendered pyrimidine auxotrophs similar to the *CDA* null. Alternatively, severing this metabolic link from the deoxycytidylate and deoxythymidylate pools might prevent the dead end accumulation of nucleosides, potentially preventing the irreversible draining of deoxycytidylate pools. We have described one potential role of nucleotidases in the pyrimidine pathway, yet our data demonstrates activity on multiple purines. It is likely that these nucleotidases will have some function in balancing the purine pathway.

During our bioinformatics analysis I noticed that the *T. brucei* 5'-nucleotidase has a human homologue: HD domain-containing protein 2 (HDDC2). There is very little known about HDDC2 with regard to catalytic activity but based on sequence similarity (48%) and conservation of key residues, it may have 5'-nucleotidase activity. It was also identified as forming a complex with HIV integrase in a high-throughput pulldown experiment. HIV integrase is known to possess nuclease activity, allowing for integration of viral DNA into host DNA. During this process it is believed to recruit other cellular enzymes to assist with the later steps in the integration mechanism [122]. It is not immediately clear what function HDDC2 might have in this process, but perhaps it has a role in degrading RNA following reverse transcription of the viral genome prior to incorporation by HIV integrase.

In addition to the pyrimidine pathway, my work in the purine pathway has uncovered two additional drug targets. Both GMPS and ADSL occupy unique positions within the purine pathway where the precursors from multiple salvage routes converge. I demonstrate that inhibition of these key enzymes interferes with the parasite's ability to synthesize purine nucleotides. The depletion of GMPS and its effects on guanine nucleotide pools were expected based on prior knowledge of the purine pathway. Of particular interest are the effects of ADSL depletion on the purine pathway. In theory, the availability of adenine should circumvent the inability to generate AMP from adenylosuccinate. These results suggest that even with AMP pools being maintained, the depletion of ADSL is causing cell death by some alternative mechanism. I speculate that the irreversible dead-end formation of adenylosuccinate may be the cause of cell death. This implies that there is unregulated flux through the ADSS/ADSL pathway that likely supplies the majority of precursors for AMP

synthesis. A more detailed analysis of this phenomenon alongside an *ADSS* null cell line will provide a greater understanding of this phenomenon.

To summarize, my work in the *T. brucei* pyrimidine and purine pathways has led to the identification and characterization of numerous essential genes that could provide the foundation for multiple drug development projects. In addition to drug target validation, my work has uncovered a novel metabolic link in the pyrimidine pathway that has advanced our understanding of parasite nucleotide metabolism. I also purified and characterized the first 5'-nucleotidase in Trypanosomes and identified numerous other candidates with similar activity. I believe the unique features I have identified within the *T. brucei* pyrimidine pathway will likely extend to other kinetoplastids, providing an opportunity to target multiple human pathogens with a single drug.

REFRENCES

1. Simarro, P.P., et al., *The human African trypanosomiasis control and surveillance programme of the World Health Organization 2000-2009: the way forward.* PLoS Negl Trop Dis, 2011. **5**(2): p. e1007.
2. Jamonneau, V., et al., *Untreated human infections by Trypanosoma brucei gambiense are not 100% fatal.* PLoS Negl Trop Dis, 2012. **6**(6): p. e1691.
3. Simarro, P.P., et al., *Estimating and mapping the population at risk of sleeping sickness.* PLoS Negl Trop Dis, 2012. **6**(10): p. e1859.
4. Checchi, F., et al., *Estimates of the duration of the early and late stage of gambiense sleeping sickness.* BMC Infect Dis, 2008. **8**: p. 16.
5. Odiit, M., F. Kansiime, and J.C. Enyaru, *Duration of symptoms and case fatality of sleeping sickness caused by Trypanosoma brucei rhodesiense in Tororo, Uganda.* East Afr Med J, 1997. **74**(12): p. 792-5.
6. Rudenko, G., *African trypanosomes: the genome and adaptations for immune evasion.* Essays Biochem, 2011. **51**: p. 47-62.
7. Hertz-Fowler, C., et al., *Telomeric expression sites are highly conserved in Trypanosoma brucei.* PLoS One, 2008. **3**(10): p. e3527.
8. Navarro, M., X. Penate, and D. Landeira, *Nuclear architecture underlying gene expression in Trypanosoma brucei.* Trends Microbiol, 2007. **15**(6): p. 263-70.
9. Yun, O., et al., *NECT is next: implementing the new drug combination therapy for Trypanosoma brucei gambiense sleeping sickness.* PLoS Negl Trop Dis, 2010. **4**(5): p. e720.
10. Legros, D., et al., *Risk factors for treatment failure after melarsoprol for Trypanosoma brucei gambiense trypanosomiasis in Uganda.* Trans R Soc Trop Med Hyg, 1999. **93**(4): p. 439-42.
11. Hammond, D.J. and W.E. Gutteridge, *UMP synthesis in the kinetoplastida.* Biochim Biophys Acta, 1982. **718**(1): p. 1-10.
12. Hammond, D.J. and W.E. Gutteridge, *Purine and pyrimidine metabolism in the Trypanosomatidae.* Mol Biochem Parasitol, 1984. **13**(3): p. 243-61.
13. Berg, M., et al., *Inhibitors of the purine salvage pathway: a valuable approach for antiprotozoal chemotherapy?* Current medicinal chemistry, 2010. **17**(23): p. 2456-81.
14. Li, Q., et al., *GMP synthase is essential for viability and infectivity of Trypanosoma brucei despite a redundant purine salvage pathway.* Mol Microbiol, 2015. **97**(5): p. 1006-20.
15. Ali, J.A., et al., *Pyrimidine salvage in Trypanosoma brucei bloodstream forms and the trypanocidal action of halogenated pyrimidines.* Mol Pharmacol, 2013. **83**(2): p. 439-53.

16. de Koning, H.P., D.J. Bridges, and R.J. Burchmore, *Purine and pyrimidine transport in pathogenic protozoa: from biology to therapy.* FEMS Microbiol Rev, 2005. **29**(5): p. 987-1020.
17. El-Sayed, N.M., et al., *Comparative genomics of trypanosomatid parasitic protozoa.* Science, 2005. **309**(5733): p. 404-9.
18. Ali, J.A., et al., *Pyrimidine biosynthesis is not an essential function for Trypanosoma brucei bloodstream forms.* PLoS One, 2013. **8**(3): p. e58034.
19. Arakaki, T.L., et al., *Characterization of Trypanosoma brucei dihydroorotate dehydrogenase as a possible drug target; structural, kinetic and RNAi studies.* Mol Microbiol, 2008. **68**(1): p. 37-50.
20. Ong, H.B., et al., *Trypanosoma brucei (UMP synthase null mutants) are avirulent in mice, but recover virulence upon prolonged culture in vitro while retaining pyrimidine auxotrophy.* Mol Microbiol, 2013. **90**(2): p. 443-55.
21. de Saint Vincent, B.R., M. Dechamps, and G. Buttin, *The modulation of the thymidine triphosphate pool of Chinese hamster cells by dCMP deaminase and UDP reductase. Thymidine auxotrophy induced by CTP in dCMP deaminase-deficient lines.* J Biol Chem, 1980. **255**(1): p. 162-7.
22. Weinberg, G., B. Ullman, and D.W. Martin, Jr., *Mutator phenotypes in mammalian cell mutants with distinct biochemical defects and abnormal deoxyribonucleoside triphosphate pools.* Proc Natl Acad Sci U S A, 1981. **78**(4): p. 2447-51.
23. Castillo-Acosta, V.M., et al., *Pyrimidine requirements in deoxyuridine triphosphate nucleotidohydrolase deficient Trypanosoma brucei mutants.* Mol Biochem Parasitol, 2013. **187**(1): p. 9-13.
24. Larson, E.T., et al., *The crystal structure and activity of a putative trypanosomal nucleoside phosphorylase reveal it to be a homodimeric uridine phosphorylase.* J Mol Biol, 2010. **396**(5): p. 1244-59.
25. Berk, A.J. and D.A. Clayton, *A genetically distinct thymidine kinase in mammalian mitochondria. Exclusive labeling of mitochondrial deoxyribonucleic acid.* J Biol Chem, 1973. **248**(8): p. 2722-9.
26. Lee, L.S. and Y. Cheng, *Human deoxythymidine kinase II: substrate specificity and kinetic behavior of the cytoplasmic and mitochondrial isozymes derived from blast cells of acute myelocytic leukemia.* Biochemistry, 1976. **15**(17): p. 3686-90.
27. Wang, L., et al., *Human thymidine kinase 2: molecular cloning and characterisation of the enzyme activity with antiviral and cytostatic nucleoside substrates.* FEBS Lett, 1999. **443**(2): p. 170-4.
28. Ranjbarian, F., et al., *Trypanosoma brucei thymidine kinase is tandem protein consisting of two homologous parts, which together enable efficient substrate binding.* J Biol Chem, 2012. **287**(21): p. 17628-36.
29. Valente, M., et al., *Cell cycle regulation and novel structural features of thymidine kinase, an essential enzyme in Trypanosoma brucei.* Mol Microbiol, 2016.

30. Alsford, S., et al., *High-throughput phenotyping using parallel sequencing of RNA interference targets in the African trypanosome.* Genome Res, 2011. **21**(6): p. 915-24.
31. Berens, R.L., E.C. Krug, and J.J. Marr, *Purine and pyrimidine metabolism*, in *Biochemistry of Parasitic Organisms and its Molecular Foundations* J.J. Marr and M. Muller, Editors. 1995, Academic Press: New York. p. pp 89–117.
32. Boitz, J.M., et al., *Purine salvage in Leishmania: complex or simple by design?* Trends Parasitol, 2012. **28**(8): p. 345-52.
33. Zhao, H., et al., *The purinosome, a multi-protein complex involved in the de novo biosynthesis of purines in humans.* Chem Commun, 2013. **49**(40): p. 4444-52.
34. Landfear, S.M., *Nutrient transport and pathogenesis in selected parasitic protozoa.* Eukaryot Cell, 2011. **10**(4): p. 483-93.
35. Ortiz, D., et al., *Two novel nucleobase/pentamidine transporters from Trypanosoma brucei.* Mol Biochem Parasitol, 2009. **163**(2): p. 67-76.
36. Landfear, S.M., et al., *Nucleoside and nucleobase transporters in parasitic protozoa.* Eukaryot Cell, 2004. **3**(2): p. 245-54.
37. Boitz, J.M. and B. Ullman, *Leishmania donovani singly deficient in HGPRT, APRT or XPRT are viable in vitro and within mammalian macrophages.* Mol Biochem Parasitol, 2006. **148**(1): p. 24-30.
38. Boitz, J.M. and B. Ullman, *A conditional mutant deficient in hypoxanthine-guanine phosphoribosyltransferase and xanthine phosphoribosyltransferase validates the purine salvage pathway of Leishmania donovani.* J Biol Chem, 2006. **281**(23): p. 16084-9.
39. Boitz, J.M., et al., *Adenylosuccinate synthetase and adenylosuccinate lyase deficiencies trigger growth and infectivity deficits in Leishmania donovani.* J Biol Chem, 2013. **288**(13): p. 8977-90.
40. Mony, B.M., et al., *Genome-wide dissection of the quorum sensing signalling pathway in Trypanosoma brucei.* Nature, 2014. **505**(7485): p. 681-5.
41. Aguero, F., et al., *Genomic-scale prioritization of drug targets: the TDR Targets database.* Nat Rev Drug Discov, 2008. **7**(11): p. 900-7.
42. Berriman, M., et al., *The genome of the African trypanosome Trypanosoma brucei.* Science, 2005. **309**(5733): p. 416-22.
43. Ginger, M.L., et al., *Intracellular positioning of isoforms explains an unusually large adenylate kinase gene family in the parasite Trypanosoma brucei.* J Biol Chem, 2005. **280**(12): p. 11781-9.
44. Wirtz, E., et al., *A tightly regulated inducible expression system for conditional gene knock-outs and dominant-negative genetics in T. brucei.* Mol Biochem Parasitol, 1999. **99**: p. 89-101.
45. Wang, Z., et al., *Inhibition of Trypanosoma brucei gene expression by RNA interference using an integratable vector with opposing T7 promoters.* J Biol Chem, 2000. **275**(51): p. 40174-9.
46. Nguyen, S., et al., *Allosteric activation of trypanosomatid deoxyhypusine synthase by a catalytically dead paralog.* J Biol Chem, 2013. **288**(21): p. 15256-67.

47. Merritt, C. and K. Stuart, *Identification of essential and non-essential protein kinases by a fusion PCR method for efficient production of transgenic Trypanosoma brucei.* Mol Biochem Parasitol, 2013. **190**(1): p. 44-9.
48. Kalidas, S., Q. Li, and M.A. Phillips, *A Gateway(R) compatible vector for gene silencing in bloodstream form Trypanosoma brucei.* Mol Biochem Parasitol, 2011. **178**(1-2): p. 51-5.
49. Mullen, A.R., et al., *Oxidation of alpha-ketoglutarate is required for reductive carboxylation in cancer cells with mitochondrial defects.* Cell Rep, 2014. **7**(5): p. 1679-90.
50. Tu, B.P., et al., *Cyclic changes in metabolic state during the life of a yeast cell.* Proc Natl Acad Sci USA, 2007. **104**(43): p. 16886-91.
51. Ferraro, P., et al., *Quantitation of cellular deoxynucleoside triphosphates.* Nucleic Acids Res, 2010. **38**(6): p. e85.
52. Sherman, P.A. and J.A. Fyfe, *Enzymatic assay for deoxyribonucleoside triphosphates using synthetic oligonucleotides as template primers.* Anal Biochem, 1989. **180**(2): p. 222-6.
53. Tomiya, N., et al., *Determination of nucleotides and sugar nucleotides involved in protein glycosylation by high-performance anion-exchange chromatography: sugar nucleotide contents in cultured insect cells and mammalian cells.* Anal Biochem, 2001. **293**(1): p. 129-37.
54. Brenndorfer, M. and M. Boshart, *Selection of reference genes for mRNA quantification in Trypanosoma brucei.* Mol Biochem Parasitol, 2010. **172**(1): p. 52-5.
55. Pfaffl, M.W., *A new mathematical model for relative quantification in real-time RT-PCR.* Nucleic Acids Res, 2001. **29**(9): p. e45.
56. Trindade, S., et al., *Trypanosoma brucei Parasites Occupy and Functionally Adapt to the Adipose Tissue in Mice.* Cell Host Microbe, 2016. **19**(6): p. 837-48.
57. Kanehisa, M., et al., *KEGG as a reference resource for gene and protein annotation.* Nucleic Acids Res, 2016. **44**(D1): p. D457-62.
58. Kanehisa, M. and S. Goto, *KEGG: kyoto encyclopedia of genes and genomes.* Nucleic Acids Res, 2000. **28**(1): p. 27-30.
59. UniProt, C., *UniProt: a hub for protein information.* Nucleic Acids Res, 2015. **43**(Database issue): p. D204-12.
60. Finn, R.D., et al., *The Pfam protein families database: towards a more sustainable future.* Nucleic Acids Res, 2016. **44**(D1): p. D279-85.
61. Altschul, S.F., et al., *Gapped BLAST and PSI-BLAST: a new generation of protein database search programs.* Nucleic Acids Res, 1997. **25**(17): p. 3389-402.
62. Marchler-Bauer, A., et al., *CDD: NCBI's conserved domain database.* Nucleic Acids Res, 2015. **43**(Database issue): p. D222-6.
63. Hildebrand, A., et al., *Fast and accurate automatic structure prediction with HHpred.* Proteins, 2009. **77 Suppl 9**: p. 128-32.
64. Soding, J., A. Biegert, and A.N. Lupas, *The HHpred interactive server for protein homology detection and structure prediction.* Nucleic Acids Res, 2005. **33**(Web Server issue): p. W244-8.

65. Velez, N., C.A. Brautigam, and M.A. Phillips, *Trypanosoma brucei S-adenosylmethionine decarboxylase N terminus is essential for allosteric activation by the regulatory subunit prozyme.* J Biol Chem, 2013. **288**(7): p. 5232-40.
66. Proudfoot, M., et al., *General enzymatic screens identify three new nucleotidases in Escherichia coli. Biochemical characterization of SurE, YfbR, and YjjG.* J Biol Chem, 2004. **279**(52): p. 54687-94.
67. Leonard, M., et al., *Robust colorimetric assays for dynamin's basal and stimulated GTPase activities.* Methods Enzymol, 2005. **404**: p. 490-503.
68. Pratt, C., S. Nguyen, and M.A. Phillips, *Genetic validation of Trypanosoma brucei glutathione synthetase as an essential enzyme.* Eukaryot Cell, 2014. **13**(5): p. 614-24.
69. Krieger, S., et al., *Trypanosomes lacking trypanothione reductase are avirulent and show increased sensitivity to oxidative stress.* Mol Microbiol, 2000. **35**(3): p. 542-52.
70. Pilger, B.D., et al., *Substrate diversity of herpes simplex virus thymidine kinase. Impact Of the kinematics of the enzyme.* J Biol Chem, 1999. **274**(45): p. 31967-73.
71. Sharma, S., et al., *Purine Analogues as Kinase Inhibitors: A Review.* Recent Pat Anticancer Drug Discov, 2015. **10**(3): p. 308-41.
72. Welin, M., et al., *Structures of thymidine kinase 1 of human and mycoplasmic origin.* Proc Natl Acad Sci U S A, 2004. **101**(52): p. 17970-5.
73. Posch, M., C. Hauser, and C. Seiser, *Substrate binding is a prerequisite for stabilisation of mouse thymidine kinase in proliferating fibroblasts.* J Mol Biol, 2000. **300**(3): p. 493-502.
74. Zylka, M.J., et al., *Prostatic acid phosphatase is an ectonucleotidase and suppresses pain by generating adenosine.* Neuron, 2008. **60**(1): p. 111-22.
75. Knapp, K., et al., *Crystal structure of the human ecto-5'-nucleotidase (CD73): insights into the regulation of purinergic signaling.* Structure, 2012. **20**(12): p. 2161-73.
76. Zimmerman, M.D., et al., *Structural insight into the mechanism of substrate specificity and catalytic activity of an HD-domain phosphohydrolase: the 5'-deoxyribonucleotidase YfbR from Escherichia coli.* J Mol Biol, 2008. **378**(1): p. 215-26.
77. Kuznetsova, E., et al., *Functional Diversity of Haloacid Dehalogenase Superfamily Phosphatases from Saccharomyces cerevisiae: BIOCHEMICAL, STRUCTURAL, AND EVOLUTIONARY INSIGHTS.* J Biol Chem, 2015. **290**(30): p. 18678-98.
78. Sanchez, A., et al., *Replication fork collapse and genome instability in a deoxycytidylate deaminase mutant.* Mol Cell Biol, 2012. **32**(21): p. 4445-54.
79. Creek, D.J., et al., *Probing the metabolic network in bloodstream-form Trypanosoma brucei using untargeted metabolomics with stable isotope labelled glucose.* PLoS Pathog, 2015. **11**(3): p. e1004689.
80. Bianchi, V. and J. Spychala, *Mammalian 5'-nucleotidases.* J Biol Chem, 2003. **278**(47): p. 46195-8.

81. Skladanowski, A.C., *The role of soluble 5'-nucleotidases in the conversion of nucleotide analogs: metabolic and therapeutic aspects.* Curr Med Chem, 2013. **20**(34): p. 4249-59.
82. Hunsucker, S.A., B.S. Mitchell, and J. Spychala, *The 5'-nucleotidases as regulators of nucleotide and drug metabolism.* Pharmacol Ther, 2005. **107**(1): p. 1-30.
83. Lal, P.B., et al., *The redundant aminotransferases in lysine and arginine synthesis and the extent of aminotransferase redundancy in Escherichia coli.* Mol Microbiol, 2014. **94**(4): p. 843-56.
84. Thiel, M., et al., *Involvement of a Leishmania thymidine kinase in flagellum formation, promastigote shape and growth as well as virulence.* Mol Biochem Parasitol, 2008. **158**(2): p. 152-62.
85. Vinayak, S., et al., *Genetic modification of the diarrhoeal pathogen Cryptosporidium parvum.* Nature, 2015. **523**(7561): p. 477-80.
86. Chen, Y.L., S. Eriksson, and Z.F. Chang, *Regulation and functional contribution of thymidine kinase 1 in repair of DNA damage.* J Biol Chem, 2010. **285**(35): p. 27327-35.
87. Deng, X., et al., *Structural plasticity of malaria dihydroorotate dehydrogenase allows selective binding of diverse chemical scaffolds.* J Biol Chem, 2009. **284**(39): p. 26999-7009.
88. Bradford, M.M., *A rapid and sensitive method for the quantitation of microgram quantities of protein utilizing the principle of protein-dye binding.* Anal Biochem, 1976. **72**: p. 248-54.
89. Smyth, D.A. and C.C. Black, *Measurement of the pyrophosphate content of plant tissues.* Plant physiology, 1984. **75**(3): p. 862-4.
90. Hirumi, H. and K. Hirumi, *Continuous cultivation of Trypanosoma brucei blood stream forms in a medium containing a low concentration of serum protein without feeder cell layers.* J Parasitol, 1989. **75**(6): p. 985-9.
91. Burkard, G., C.M. Fragoso, and I. Roditi, *Highly efficient stable transformation of bloodstream forms of Trypanosoma brucei.* Mol Biochem Parasitol, 2007. **153**(2): p. 220-3.
92. Willert, E.K. and M.A. Phillips, *Regulated expression of an essential allosteric activator of polyamine biosynthesis in African trypanosomes.* PLoS Pathog, 2008. **4**(10): p. e1000183.
93. Winer, J., et al., *Development and validation of real-time quantitative reverse transcriptase-polymerase chain reaction for monitoring gene expression in cardiac myocytes in vitro.* Anal Biochem, 1999. **270**(1): p. 41-9.
94. Grishin, N.V., et al., *Crystallization and preliminary X-ray studies of ornithine decarboxylase from Trypanosoma brucei.* Proteins, 1996. **24**(2): p. 272-3.
95. Nakamura, J. and L. Lou, *Biochemical characterization of human GMP synthetase.* J Biol Chem, 1995. **270**(13): p. 7347-53.
96. Bhat, J.Y., B.G. Shastri, and H. Balaram, *Kinetic and biochemical characterization of Plasmodium falciparum GMP synthetase.* Biochem J, 2008. **409**(1): p. 263-73.

97. Lou, L., et al., *High-level production from a baculovirus expression system and biochemical characterization of human GMP synthetase.* Protein Expr Purif, 1995. **6**(4): p. 487-95.
98. Nakamura, J., et al., *The glutamine hydrolysis function of human GMP synthetase. Identification of an essential active site cysteine.* J Biol Chem, 1995. **270**(40): p. 23450-5.
99. Chittur, S.V., et al., *Mechanism for acivicin inactivation of triad glutamine amidotransferases.* Biochemistry, 2001. **40**(4): p. 876-87.
100. Patel, N., H.S. Moyed, and J.F. Kane, *Xanthosine-5'-phosphate amidotransferase from Escherichia coli.* J Biol Chem, 1975. **250**(7): p. 2609-13.
101. Roper, J.R., et al., *Galactose metabolism is essential for the African sleeping sickness parasite Trypanosoma brucei.* Proc Natl Acad Sci USA, 2002. **99**(9): p. 5884-9.
102. de Koning, H.P. and S.M. Jarvis, *Purine nucleobase transport in bloodstream forms of Trypanosoma brucei is mediated by two novel transporters.* Mol Biochem Parasitol, 1997. **89**(2): p. 245-58.
103. Creek, D.J., et al., *Metabolomics guides rational development of a simplified cell culture medium for drug screening against Trypanosoma brucei.* Antimicrob Agents Chemother, 2013. **57**(6): p. 2768-79.
104. Lyons, S.D., M.E. Sant, and R.I. Christopherson, *Cytotoxic mechanisms of glutamine antagonists in mouse L1210 leukemia.* J Biol Chem, 1990. **265**(19): p. 11377-81.
105. Rodriguez-Suarez, R., et al., *Mechanism-of-action determination of GMP synthase inhibitors and target validation in Candida albicans and Aspergillus fumigatus.* Chem Biol, 2007. **14**(10): p. 1163-75.
106. Boulieu, R., et al., *Hypoxanthine and xanthine levels determined by high-performance liquid chromatography in plasma, erythrocyte, and urine samples from healthy subjects: the problem of hypoxanthine level evolution as a function of time.* Anal Biochem, 1983. **129**(2): p. 398-404.
107. Hartwick, R.A., A.M. Krstulovic, and P.R. Brown, *Identification and quantitation of nucleosides, bases and other UV-absorbing compounds in serum, using reversed-phase high-performance liquid chromatography. II. Evaluation of human sera.* J Chromatogr, 1979. **186**: p. 659-76.
108. Slowiaczek, P. and M.H. Tattersall, *The determination of purine levels in human and mouse plasma.* Anal Biochem, 1982. **125**(1): p. 6-12.
109. Jiang, L., et al., *Functional characterization and virulence study of ADE8 and GUA1 genes involved in the de novo purine biosynthesis in Candida albicans.* FEMS Yeast Res, 2010. **10**(2): p. 199-208.
110. Martin, J.L., et al., *Metabolic reprogramming during purine stress in the protozoan pathogen Leishmania donovani.* PLoS pathogens, 2014. **10**(2): p. e1003938.
111. Geiser, F., et al., *Molecular pharmacology of adenosine transport in Trypanosoma brucei: P1/P2 revisited.* Mol Pharmacol, 2005. **68**(3): p. 589-95.

112. Carter, N.S. and A.H. Fairlamb, *Arsenical-resistant trypanosomes lack an unusual adenosine transporter.* Nature, 1993. **361**(6408): p. 173-6.
113. Thompson, L.F., et al., *Purine metabolism in cultured human fibroblasts derived from patients deficient in hypoxanthine phosphoribosyltransferase, purine nucleoside phosphorylase, or adenosine deaminase.* Proc Natl Acad Sci U S A, 1978. **75**(8): p. 3722-6.
114. Fadda, A., et al., *Transcriptome-wide analysis of trypanosome mRNA decay reveals complex degradation kinetics and suggests a role for co-transcriptional degradation in determining mRNA levels.* Mol Microbiol, 2014. **94**(2): p. 307-26.
115. Ray, S.P., et al., *Structural and biochemical characterization of human adenylosuccinate lyase (ADSL) and the R303C ADSL deficiency-associated mutation.* Biochemistry, 2012. **51**(33): p. 6701-13.
116. Boitz, J.M., et al., *Adenine aminohydrolase from Leishmania donovani: unique enzyme in parasite purine metabolism.* J Biol Chem, 2012. **287**(10): p. 7626-39.
117. Davies, M.J., A.M. Ross, and W.E. Gutteridge, *The enzymes of purine salvage in Trypanosoma cruzi, Trypanosoma brucei and Leishmania mexicana.* Parasitology, 1983. **87 (Pt 2)**: p. 211-7.
118. Rajagopalan, P.T., et al., *Interaction of dihydrofolate reductase with methotrexate: ensemble and single-molecule kinetics.* Proc Natl Acad Sci U S A, 2002. **99**(21): p. 13481-6.
119. McIntosh, E.M. and R.H. Haynes, *dUTP pyrophosphatase as a potential target for chemotherapeutic drug development.* Acta Biochim Pol, 1997. **44**(2): p. 159-71.
120. Sienkiewicz, N., et al., *Chemical and genetic validation of dihydrofolate reductase-thymidylate synthase as a drug target in African trypanosomes.* Mol Microbiol, 2008. **69**(2): p. 520-33.
121. De Clercq, E. and H.J. Field, *Antiviral prodrugs - the development of successful prodrug strategies for antiviral chemotherapy.* Br J Pharmacol, 2006. **147**(1): p. 1-11.
122. Brin, E., et al., *Modeling the late steps in HIV-1 retroviral integrase-catalyzed DNA integration.* J Biol Chem, 2000. **275**(50): p. 39287-95.